

Surrogate-Assisted Model Methods for Maximum Compression
Capacity Predictions of Concrete-Filled Stainless-Steel Tubular
Columns



A Thesis Submitted in Partial Fulfillment of the Requirements
for the Degree of Master of Engineering in Civil Engineering
Department of Civil Engineering
Faculty Of Engineering
Chulalongkorn University
Academic Year 2023

ระเบียบวิธีการจำลองแบบใช้ตัวแทนสำหรับการทำนายความสามารถในการรับแรงอัดสูงสุดของ
เสาท่อสแตนเลสสตีลที่เติมคอนกรีต



วิทยานิพนธ์นี้เป็นส่วนหนึ่งของการศึกษาตามหลักสูตรปริญญาวิศวกรรมศาสตรมหาบัณฑิต
สาขาวิชาวิศวกรรมโยธา ภาควิชาวิศวกรรมโยธา
คณะวิศวกรรมศาสตร์ จุฬาลงกรณ์มหาวิทยาลัย
ปีการศึกษา 2566

Thesis Title	Surrogate-Assisted Model Methods for Maximum Compression Capacity Predictions of Concrete-Filled Stainless-Steel Tubular Columns
By	Mr. Ly Ith
Field of Study	Civil Engineering
Thesis Advisor	Associate Professor SAWEKCHAI TANGARAMVONG, Ph.D

Accepted by the FACULTY OF ENGINEERING, Chulalongkorn University
in Partial Fulfillment of the Requirement for the Master of Engineering

----- Dean of the FACULTY OF
ENGINEERING

(Professor SUPOT TEACHAVORASINSKUN, D.Eng.)

THESIS COMMITTEE

----- Chairman

(Associate Professor PITCHA JONGVIVATSAKUL,
Ph.D.)

----- Thesis Advisor

(Associate Professor SAWEKCHAI
TANGARAMVONG, Ph.D)

----- External Examiner

(Associate Professor Ganchai Tanapornraweekit, Ph.D.)

จุฬาลงกรณ์มหาวิทยาลัย

CHULALONGKORN UNIVERSITY

ลี อิด : ระเบียบวิธีการจำลองแบบใช้ตัวแทนสำหรับการทำนายความสามารถในการรับแรงอัดสูงสุดของเสาท่อสแตนเลสโดยอาศัยตัวแบบที่ได้มีการเรียนรู้ของเครื่องคอมพิวเตอร์ (Surrogate-Assisted Model Methods for Maximum Compression Capacity Predictions of Concrete-Filled Stainless-Steel Tubular Columns) อ.ที่ปรึกษาหลัก : เสาวกษัย ตั้งอร่ามวงศ์

งานวิจัยฉบับนี้ศึกษาการพยากรณ์ความแข็งแรงตามแนวแกนของห่อเสาเหล็กสแตนเลส ซึ่งมีคุณค่าเดิมอยู่ภายใน (CFSST) โดยใช้เทคนิคการเรียนรู้ของเครื่องคอมพิวเตอร์ (machine learning) ระดับสูง ได้แก่ Gaussian Process Regression (GPR) และ Extreme Gradient Boosting (XGBoost) โดยนำเข้าชุดฐานข้อมูลมากกว่า 100 รายการ ซึ่งมาจากการทดสอบจริง โดยมีชุดข้อมูลเพียงไม่กี่รายการที่ถูกจำแนกเป็นเสายาว หรือเสาที่มีความสูงชั้นสูด ทำให้เกิดข้อจำกัดทางความแม่นยำในการทำนาย เพื่อแก้ไขปัญหาที่เกิดขึ้น วิทยานิพนธ์ฉบับนี้นำเสนอวิธีการแบบจำลองทางคณิตศาสตร์โดยระเบียบวิธีไฟโนต์โอลิเมนต์ (FEM) เพื่อสร้างชุดข้อมูลเพิ่มเติมสำหรับเสาที่มีความยาวและสูงชั้นสูด นอกจากนี้ ผลลัพธ์ที่ได้จากแบบจำลองทางคณิตศาสตร์ ถูกนำมาทดสอบกับมาตรฐานที่ได้รับการยอมรับอย่าง AISC (American Institute of Steel Construction) และ Eurocode 4 เพื่อแสดงศักยภาพของอัลกอริทึมการเรียนรู้ของเครื่องที่สามารถเข้าแทนที่ข้อกำหนดแบบดั้งเดิมได้



จุฬาลงกรณ์มหาวิทยาลัย
CHULALONGKORN UNIVERSITY

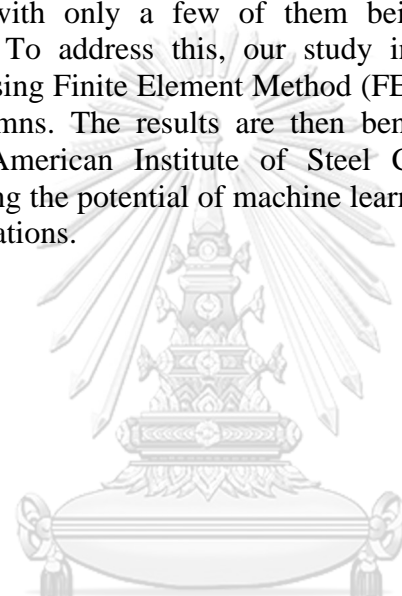
สาขาวิชา	วิศวกรรมโยธา	ลายมือชื่อนิสิต
ปีการศึกษา	2566	ลายมือชื่อ อ.ที่ปรึกษาหลัก

6472074921 : MAJOR CIVIL ENGINEERING

KEYWORD: Concrete-filled stainless steel tubular columns (CFSST); Columns
D: axial compressive strength prediction; Gaussian process regression
(GPR); Xtreme-Gradient Boost (XGBoost)

Ly Ith : Surrogate-Assisted Model Methods for Maximum Compression
Capacity Predictions of Concrete-Filled Stainless-Steel Tubular Columns.
Advisor: Assoc. Prof. SAWEKCHAI TANGARAMVONG, Ph.D

This work explores the prediction of axial strength of circular concrete-filled stainless-steel tubular (CFSST) columns, employing advanced machine learning techniques, including Gaussian Process Regression (GPR) and Extreme Gradient Boosting (XGBoost). The dataset comprises over 100 columns from experimental tests, with only a few of them being long or slender, limiting prediction accuracy. To address this, our study introduces a robust numerical modeling approach using Finite Element Method (FEM) to generate additional data points for long columns. The results are then benchmarked against established standards such as American Institute of Steel Construction (AISC) and the Eurocode 4, illustrating the potential of machine learning algorithms to supplant the conventional specifications.



จุฬาลงกรณ์มหาวิทยาลัย

CHULALONGKORN UNIVERSITY

Field of Study: Civil Engineering

Student's Signature

Academic Year: 2023

Advisor's Signature

ACKNOWLEDGEMENTS

The author would like to genuinely acknowledge Associate. Professor. Dr. Sawekchai Tangaramvong for his vigorous and enormous supervision across the whole work along with Dr. Rut Su for revising, editing and providing various comments as well as all the solutions clearing all the obstacles encountered so far, without whom, this work would not come into reality. Extended gratitude to the Chulalongkorn University's Graduate Scholarship Programme for ASEAN or Non-ASEAN Countries is also expressed for granting the author this marvelous opportunity to learn and conduct the research.



Ly Ith

TABLE OF CONTENTS

	Page
ABSTRACT (THAI)	iii
ABSTRACT (ENGLISH).....	iv
ACKNOWLEDGEMENTS.....	v
TABLE OF CONTENTS	vi
LIST OF TABLES	ix
LIST OF FIGURES	x
CHAPTER 1 INTRODUCTION	1
1.1 BACKGROUND AND MOTIVATION	1
1.2 RESEARCH OBJECTIVE	2
1.3 SCOPE OF RESEARCH	3
1.4 RESEARCH SIGNIFICANT AND INNOVATIVE	3
1.5 RESEARCH DESIGN AND METHODOLOGY	3
CHAPTER 2 LITERATURE REVIEW.....	5
2.1 GENERAL.....	5
2.2 EXPERIMENTAL CFSST COLUMN DATA.....	6
2.3 IMPLEMENTATION OF MACHINE LEARNING IN STRUCTURAL ENGINEERING	15
CHAPTER 3 METHODOLOGY	18
3.1 GENERAL.....	18
3.2 MATERIALS CONSTITUTIVE LAW	19
3.2.1 GENERAL	19
3.2.2 STAINLESS STEEL	19
3.2.3 CONFINED CONCRETE.....	24
3.2.3.1 CONCRETE DAMAGED PLASTICITY	24
3.2.3.2 STRESS-STRAIN RELATIONSHIP IN COMPRESSION.....	25
3.2.3.3 STRESS-STRAIN RELATIONSHIP IN TENSION.....	27

3.3 FINITE ELEMENT MODELING	28
3.3.1 INITIAL LOCAL GEOMETRIC IMPERFECTION	28
3.3.2 INITIAL GLOBAL GEOMETRIC IMPERFECTION	30
3.3.3 MODELING PROPERTIES	32
3.3.4 LOADING TYPE	34
3.3.5 CFSST COLUMN AXIAL STRENGTH DETERMINATION	36
3.3.6 VERIFICATION OF THE FINITE-ELEMENT MODEL	38
3.3.7 SIMULATED CFSST COLUMN DATA	42
3.4 MACHINE LEARNING ALGORITHMS	43
3.4.1 GENERAL	43
3.4.2 MACHINE LEARNING TRAINING PROCESS	48
3.4.3 STATISTICAL ACCURACY MEASUREMENT PARAMETERS	50
3.5 CFSST COLUMN AXIAL STRENGTH DETERMINATION FROM STANDARD SPECIFICATIONS	51
3.5.1 EUROCODE 4	51
3.5.1.1 GENERAL	51
3.5.1.2 MATERIAL PROPERTY	52
3.5.1.3 LIMITATIONS AND ASSUMPTIONS	53
3.5.1.4 LOCAL BUCKLING EFFECT	54
3.5.1.5 NOMINAL AXIAL COMPRESSIVE STRENGTH.....	56
3.5.2 ANSI/AISC 360-22	59
3.5.2.1 GENERAL	59
3.5.2.2 LIMITATIONS	60
3.5.2.3 SECTION CLASSIFICATION FOR LOCAL BUCKLING EFFECT	60
3.5.2.4 NOMINAL AXIAL COMPRESSIVE STRENGTH.....	61
CHAPTER 4 RESULTS AND DISCUSSIONS	65
4.1 PREDICTED STRENGTHS OF EACH PREDICTIVE METHOD	65
4.2 VISUALIZATION OF THE PREDICTIVE MODELS	71
4.3 ASSESSMENT AND THE PREFERRED PREDICTIVE METHODS.....	76

CHAPTER 5 CONCLUSIONS	77
APPENDIX A SIMULATED CFSST COLUMNS DATA	79
APPENDIX B STANDARD SPECIFICATIONS PREDICTED COLUMN STRENGTHS	109
REFERENCES	123
VITA	127



LIST OF TABLES

	Page
Table 2.1 Collected experimental axial compressive strength of CFSST columns	12
Table 3.1 Parameters for concrete stress-strain curve.....	26
Table 3.2 Initial local imperfection.....	29
Table 3.3 CFSST stub column curve type using confinement factor.....	38
Table 3.4 Comparison of FEM models against the experimental programs.....	40
Table 3.5 Comparison of the FEM models against the numerical programs.....	42
Table 3.6 CFSST columns data from combined experimental and simulations	43
Table 3.7 Pros and Cons of Gaussian Process Regression (GPR) and Extreme-Gradient Boost (XGBoost)	44
Table 3.8 Training input parameters of each machine learning model	49
Table 3.9 Machine learning model input parameters statistical properties.....	50
Table 3.10 Limiting Width-to-Thickness Ratios for Compression Steel Elements in Composite Members Subjected to Axial Compression	61
Table 4.1 Axial compressive strength predictions of CFSST columns.....	65
Table 4.2 Machine learning predictive model statistical parameters	70

LIST OF FIGURES

	Page
Figure 1.1 Applications of stainless steel: (a) appliances (b) structural steel tube	1
Figure 2.1 Column sections	6
Figure 2.2 Failure shape of CFSST stub columns: (a) rectangular section, (b) circular section (Uy et al. 2011)	7
Figure 2.3 Typical axial load versus axial strain curve of stub columns (Uy et al. 2011)	7
Figure 2.4 Fig. 12 of Ellobody & Ghazy [8].....	8
Figure 2.5 Slender column specimens after testing: (a) circular sections (b) rectangular sections (Uy et al. 2011)	10
Figure 2.6 Measurement setup for initial global geometric imperfection (He et al. 2021)	10
Figure 2.7 Slender CFSST columns failure mode: (a) experimental (b) numerical (He et al. 2021)	11
Figure 2.8 Various structures whose responses were predicted using ML approaches: (a) CFST columns (Nguyen et al. 2023), (b) Semi-rigid steel structures (Truong et al. 2022), (c) Circular CFSST column (Tran et al. 2023)	16
Figure 3.1 Flowchart of the research work	18
Figure 3.2 Stress strain diagram of low-carbon steel (Tao et al. 2013 [2]).....	19
Figure 3.3 Typical nominal stress-strain curve of stainless-steel versus the basic Ramberg-Osgood equation	20
Figure 3.4 Nominal versus true stress-strain curve (austenitic or duplex alloy)	23
Figure 3.5 Stress-strain curve of confined and unconfined-concrete (Tao et al. 2013 [2]).....	26
Figure 3.6 Typical confined-concrete stress-strain curve	28
Figure 3.7 Assumed local imperfection for square section (Tao et al. 2011 [25]).....	29
Figure 3.8 First eigen buckling mode of CFSST stub columns: (a) rectangular section (b) circular section	30
Figure 3.9 First eigen buckling mode of slender column	31
Figure 3.10 Keywords modification for initial imperfection.....	31

Figure 3.11 Typical sectional-mesh view: (a) circular section (b) rectangular section	32
Figure 3.12 Column ends conditions (pin-ended).....	33
Figure 3.13 Corner regions of rectangular steel tube.....	34
Figure 3.14 CFSST stub column loading curve.....	35
Figure 3.15 Increment size of stub columns nonlinear analysis	35
Figure 3.16 Typical mid-height displacement versus axial force curve	37
Figure 3.17 Flowchart of column axial strength determination from simulations and experimental tests.....	38
Figure 3.18 CFSST stub columns failure mode: (a) rectangular section (b) circular section	39
Figure 3.19 CFSST slender column failure mode: (a) rectangular section (b) circular column.....	39
Figure 3.20 Verification of the FEM models: (a) stub columns, (b) slender columns (c) combined stub and slender columns	41
Figure 3.21 Verification of the FEM models against the numerical program	42
Figure 3.22 Multivariate normal distribution (Wang 2020 [34])	45
Figure 3.23 Gaussian Process Regression: (a) K-fold cross validation, (b) comparison between prediction and confident intervals of a function.....	46
Figure 3.24 XGBoost (a) decision tree (b) grid search for optimal hyperparameters .	48
Figure 3.25 Normal distribution of column properties.....	50
Figure 4.1 Rectangular stub column model charts results	72
Figure 4.2 Circular stub column model charts results	73
Figure 4.3 Slender rectangular column model charts results	74
Figure 4.4 Slender circular column model charts results.....	75

CHAPTER 1

INTRODUCTION

1.1 BACKGROUND AND MOTIVATION

Apart from the fact that stainless steel is 3-5 times more expensive than low-carbon steel, it possesses plenty of high-quality properties such as higher ductility, great resistance against corrosion and extreme heat. More importantly, its smooth and bright shining surface makes it more suitable for our daily life uses such as appliances, water bottles, etc. With all these benefits, it would be a splendid idea to use the stainless steel as a structural member, especially when combining with infilled-concrete, resulting in higher resistance structural member with relatively smaller cross section comparing to the conventional reinforced-concrete or infilled-concrete structures with low-carbon steel. In the last few decades, the use of concrete in combination with structural steel as structural members has attracted many designers' interests around the world due to its numerous advantages. This can be seen in many civil infrastructures, especially buildings where concrete is cast inside structural steel to form composite columns.



Figure 1.1 Applications of stainless steel: (a) appliances (b) structural steel tube

The design of composite structures can be very challenging since many factors have to be taken into consideration such as, confinement effect, local buckling, global buckling, initial geometric imperfection due to significant large size of the members' cross-section or length. Many design standards have developed formulas to estimate the axial strength capacity of concrete filled steel tubular columns subjected to combined axial compression and bending. However, these provisions are applicable

only to certain limited conditions of either material properties (strength of concrete and steel) or geometric conditions (slenderness ratio) due to the fact that they are developed merely from the experimental data and there are not enough tests of high strength materials. In addition, the structural steel type is that of low-carbon steel with well-defined mechanical properties, well-defined yield, and ultimate stress. The mechanical property of stainless-steel is almost completely different from that of conventional structural steel since it has no specific yield point resulting in the adoption of 0.2% proof stress, $\sigma_{0.2}$, as the yield stress.

In the era of technology, the revolution of artificial intelligence has seen lots of improvement making our daily lives much easier and more convenient in an incredible way that we, sometimes, do not even notice that many applications around us usually involve the algorithms of artificial intelligence. An obvious example is the video suggestions based on our watched histories in Youtube, Netflix, etc. The algorithm was trained to predict what the user might favor based on various parameters which could be age, gender, music genre, etc. However, the protocol in training and testing those types of machine learning might be way more complicated than we could ever imagine since it was not our expertise. On the other hand, the machine learning algorithms that the author attempts to use in this work are to perform regressions only.

Due to the lack of standard provision for stainless-steel and popularity of machine learning in predicting the response of structural members, we decided to overcome this problem by performing machine learning algorithms to evaluate the axial compressive strength of concrete-filled stainless-steel tubular columns considering both stub and slender columns of circular and rectangular sections.

1.2 RESEARCH OBJECTIVE

The research objective includes:

- (1) to train the machine learning models capable of predicting the axial compressive strength of concrete-filled stainless-steel tubular columns of both rectangular and circular sections

- (2) to validate the predicted strength from machine learning models with those from the standard specifications including Eurocode 4 (EC4), American Institute of Steel Construction (ANSI/AISC 360-22)

1.3 SCOPE OF RESEARCH

- (1) collect the column data from the literature for using as training and testing sets of the machine learning models
- (2) Simulate more column data using ABAQUS if those collected from the literature could not provide satisfactory result
- (3) investigate the accuracy of a model trained with respect to only one group of sectional shape or column length (short or slender)
- (4) assess the accuracy of standard specifications over CFSST columns axial strength prediction even though the formulations are of low-carbon steel instead of stainless steel
- (5) validate the results from the machine learning models with those from standard specifications

1.4 RESEARCH SIGNIFICANT AND INNOVATIVE

The research focuses mainly on developing predictive models for axial compressive strength of CFSST in lieu of conventional standard specifications methods. The author expects to develop a quick and versatile machine learning model capable of predicting the axial strength of CFSST columns that would require less computational time with relatively reasonable accuracy.

1.5 RESEARCH DESIGN AND METHODOLOGY

(1) Column data

A total of 183 column data were collected from the literatures, 12 of which were of long or slender columns. An additional 930 column data were obtained from finite-element modeling analysis using ABAQUS. This amount remains tentative since more column data will be simulated if needed.

(2) Finite-element modeling

The two stage compressive stress-strain relationship based on modified Ramberg Osgood equations was used to model the behavior of stainless steel [1] while the confined concrete stress-strain relationship [2] was used for the concrete behavior. To model the global buckling behavior of slender columns, the analysis must consist of two steps to account for this effect. The first step is the linear buckling analysis using the perturbation buckle analysis available in ABAQUS. The column buckling shape and eigen buckling load are then inputted into the second step analysis using Static, Riks step.

(3) Machine learning

Our primary goal is to develop one model with respect to one section type or column length. Two machine learning algorithms are chosen to perform here including the Gaussian Process Regression (GPR) and Extreme-Gradient Boost (XGBoost). The data are split into training and testing sets composed of 80% and 20% of the total column data, respectively.

(4) Standard Specification Estimation

The specifications for low-carbon structural steel were utilized to estimate the nominal axial compressive strength of CFST columns with stainless steel. The Eurocode 4 transform the effective steel tube area into equivalent steel tube thickness to account for the effect of local buckling, while the AISC 360-22 classified the section into three categories which are “Compact”, “Noncompact” and “Slender-element” composite sections.

CHAPTER 2

LITERATURE REVIEW

2.1 GENERAL

To develop a model capable of making predictions, substantial data must be gathered through any means including collecting from literature, laboratory experiments, or numerical simulation. The data will be then split into training and testing sets. Since performing the column compressive tests are very costly and time consuming, only those collected from the literature and generated from the simulations will be used here. CFSST column data collection from various experimental programs was the most important aspect of the literature review, plus some applications of machine learning algorithms in the field of structural engineering.

Nomenclature

CFSST	concrete-filled stainless-steel tubular
f_c'	concrete compressive strength
f_y	yield strength of low-carbon steel
$\sigma_{0.2}$	0.2% proof stress of stainless-steel
$\sigma_{0.2,c}$	0.2% proof stress of corner region
$\sigma_{0.2,v}$	0.2% proof stress of virgin material
$\sigma_{0.01}$	0.01% proof stress of stainless-steel
σ_{t0}	ultimate concrete tensile stress
B	width (rectangular section)
D	depth (circular section)
A_e	effective steel tube area
A_s	steel tube area
ρ	local buckling effect reduction factor
t	steel tube thickness
ξ_c	confinement factor
E_c	concrete initial modulus of elasticity
E_s	modulus of elasticity of steel
P_u	ultimate axial compressive force
P_n	nominal axial compressive strength
P_{cr}	elastic critical buckling force
f_r	modulus of rupture

ε_{cr}	cracking strain
λ	lightweight concrete factor
σ_p	proof stress corresponding to the plastic strain
n	strain hardening exponent
σ_{true}	true stress
ε_{true}	true strain
σ_{nom}	nominal stress
ε_{nom}	nominal strain

2.2 EXPERIMENTAL CFSST COLUMN DATA

Many researchers have performed experimental tests on concrete-filled stainless-steel tubular columns to investigate the behavior as well as the axial compressive strength capacity [13] - [14]. A total of 84 columns data were collected from numerous experimental programs while only 12 of which were of long or slender columns owing to the fact that constructing column samples for testing requires lots of resources which are not cost-effective.

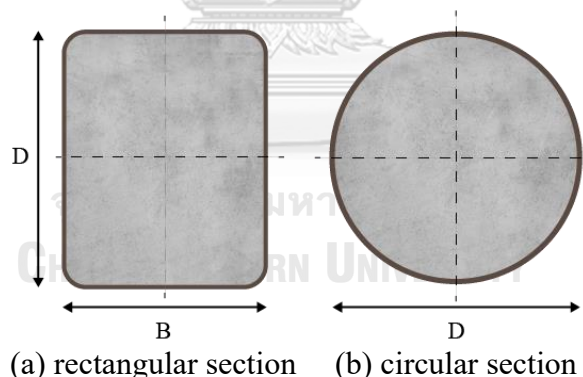


Figure 2.1 Column sections

Uy et al. 2011 [10] performed compressive tests on CFSST columns samples with both stub and slender columns with circular and rectangular cross section. Two exact samples labeled with "A" and "B" were made for each stub column specimen to ensure each sample accuracy and to account for any potential imperfection such as material properties, section's dimension, etc. Hence, the average between the two specimens is deemed to be the axial strength of that corresponding specimen. The

method of constructing two exact samples for each specimen was also done by Liao et al. 2019 [5], Guo et al. 2019 [9] and Han et al. 2022 [12].

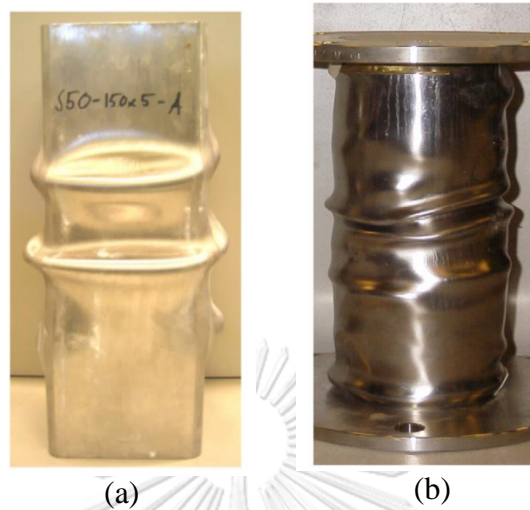


Figure 2.2 Failure shape of CFSST stub columns: (a) rectangular section, (b) circular section (Uy et al. 2011)

The study found that stub column failure modes were governed by local buckling with the axial strength defined as the load corresponding to 1% ultimate axial strain even though they still have the potential to undergo larger axial force as depicted by the ascending branch of “Type A” axial force versus axial strain curve (Figure 2.3), since the column deformed shapes were already too obvious to be seen with naked eyes thereby not suitable for its aesthetic criteria. The strength for “Type B” or “Type C” curve column, on the other hand, was defined as the instant load when the maximum or the first peak load was reached.

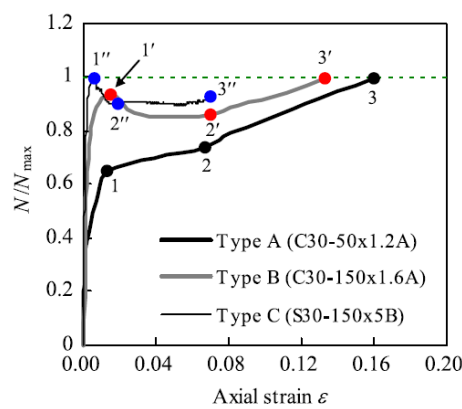


Figure 2.3 Typical axial load versus axial strain curve of stub columns (Uy et al. 2011)

The methodology of defining the strength as the first peak load instead of the load corresponding to the 1% ultimate axial strain was due to the fact that the latter load was less than the former one; therefore, this method is adopted in the current work. There was no consensus on the ultimate axial strain limit for the stub column axial strength definition, which led to different arbitrary definitions from researcher to researcher. Dai et al. [13], Li et al. [15] and Li et al. [16] lifted the limit to 5% axial strain while Ellobody & Ghazy [8] didn't mention its specific value but it could be seen from Fig. 12 of their work in which the first peak load of specimen C2 was corresponded to axial strain greater than 2%.

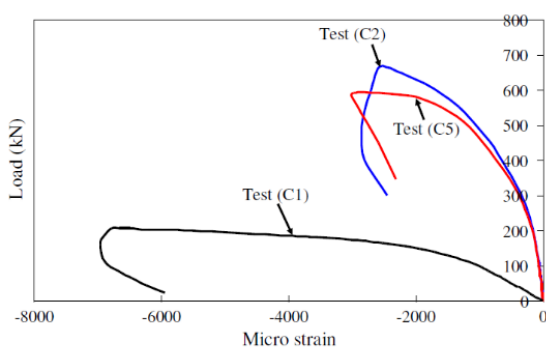


Fig. 12. Load versus average strain curves for hollow and concrete-filled stainless steel circular tubular stub columns (C1, C2 and C5).

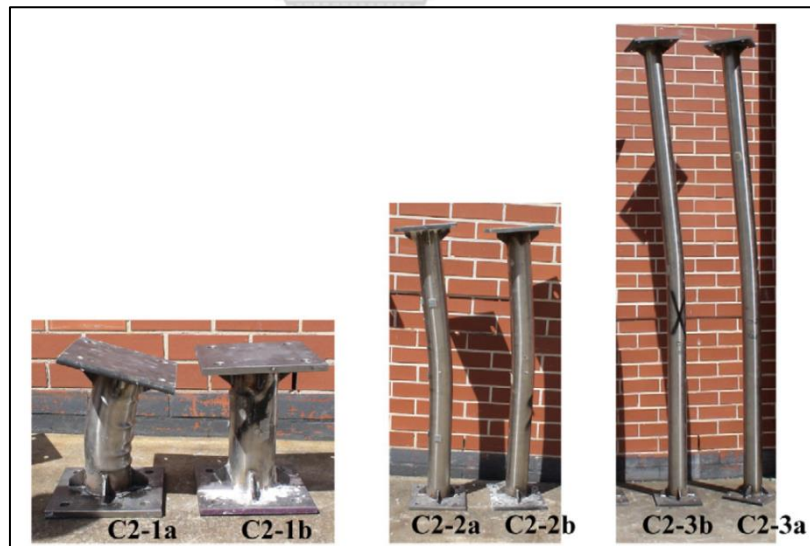
Figure 2.4 Fig. 12 of Ellobody & Ghazy [8]

To avoid global buckling effect in case of stub columns, almost all specimens' length was prepared to be triple the section depth (Figure 2.1). As of the author current research, the only study of CFSST stub columns with slenderness ratio greater than three was that of Yu et al. 2013 [14]. In their study, 17 circular column specimens were constructed with various slenderness ratio values including 3, 3.5 and the maximum of 4. Therefore, slenderness ratio limit of 4 was adopted as the threshold to distinguish stub and slender columns apart with those satisfying Eq. (2.1) are treated as stub columns. Most of the collected stub column specimens' ends were constructed to ensure pin-ended conditions except that of Dai et al. 2020 [13] with pinned and fixed ended conditions at the top and bottom of the specimen, respectively. Nevertheless, differences in support conditions between these specimens will be accounted for later in the machine learning process since the column effective length is used instead of the original length.

$$\frac{L_e}{D} \leq 4 \quad (2.1)$$

Push-out loading tests were applied on some specimens as done by Tao et al. 2016 [17] and Han et al. 2022 [12] to study the bond behavior between the core concrete and the steel tube. Since we are dealing only with columns subjected to axial compression (where core concrete and steel tube were loaded simultaneously), columns data corresponding to push-out loadings are not concerned and only those subjected to axial compression are considered.

The slender column specimens tested by Uy et al. [10] were constructed in a manner that no initial global imperfection occurred. The study found that the mid-height lateral deflection was not obvious before the peak load was obtained with the deflection not being perfectly symmetrical owing to random distribution of global imperfection (Figure 2.5). Due to the absence of the steel tube corner radius in case of square or rectangular sections in the literature, it is assumed to be the same to the tube thickness for modeling purpose only and was ignored in sectional properties calculations. Hence, the actual cross-sectional areas from the literatures were ignored.



(a)

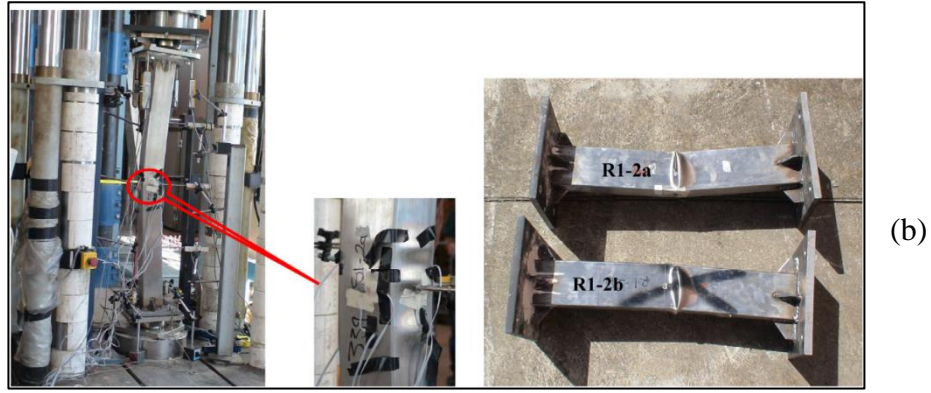


Figure 2.5 Slender column specimens after testing: (a) circular sections (b) rectangular sections (Uy et al. 2011)

Since the initial geometric imperfection tends to be inevitable and slender columns in the actual structures are prone to this phenomenon; therefore, those slender columns data from Uy et al. [10] are not included in the machine learning process since we attempt to predict the strength of columns with presumed initial imperfection. This can be seen as done by He et al. 2021 [11] where the initial global imperfection was measured along the columns by rotating the column's cross section every 60 degree, then the maximum value recorded was selected.

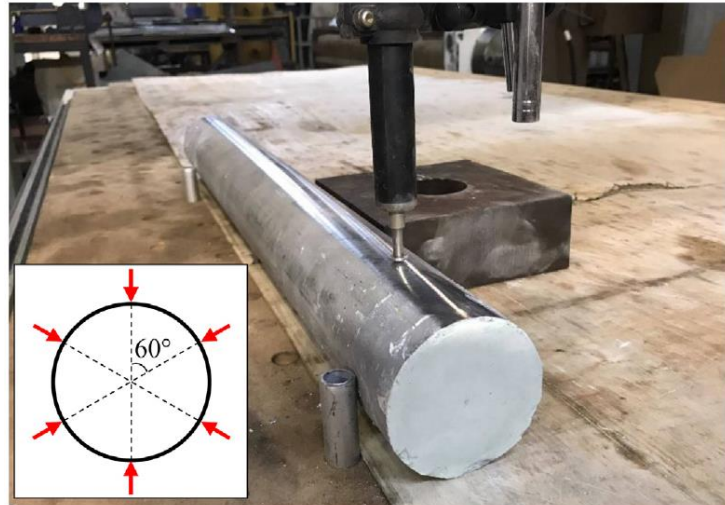


Figure 2.6 Measurement setup for initial global geometric imperfection (He et al. 2021)

Three initial global geometric imperfection value in the experimental program of He et al. 2021 [11] including $\omega_g + e_0$, $\frac{L_e}{300}$, $\frac{L_e}{1000}$ were used in the simulation for verification while the last one yielded the best results compared to the experimental

tests. Keep in mind that their columns were formed using recycled aggregates and a small reduction in columns' strength was also pointed out compared to those with normal aggregates. The portion of recycled aggregates in each column sample could be referred to from its sample name. For instance, sample "D89-L1200-R35" indicated column sample with section diameter, effective length and recycled aggregate percentage of, 89mm, 1200mm and 35%, respectively, while "D89-L1200-R0" referred to column with 100% natural aggregate.

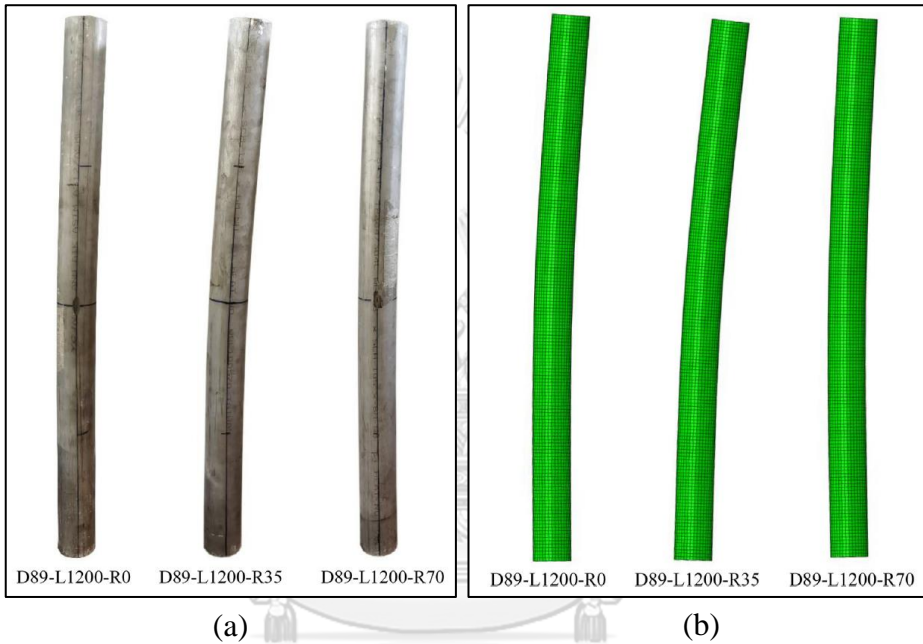


Figure 2.7 Slender CFSST columns failure mode: (a) experimental (b) numerical (He et al. 2021)

It is worth mentioning that material properties used in the tests of each author were not all the same. Liao et al. 2019 [5] used sea sand instead of river or lake sand while Li et al. 2016 [15] used sea water and sea sand to cast the concrete core with Li et al. 2018 [16] also used these materials to study the axial compression tests on concrete-filled double-skin stainless steel circular tubes. Additionally, several researchers used recycled aggregate instead of the normal one either completely or proportionally ([6], [7], [11] and [12]). To ensure the consistency of columns data during the machine learning process, these experimental data not completely containing conventional materials will be omitted. Note that only the experimental column data (and not the numerical ones) were concerned and collected to be used in the machine learning process. With all details regarding the experimental program of

CFSST columns, the author has opted to collect only those constrained to the following criteria:

- Columns subjected to axial compression (push-out loading types are omitted)
- Slender columns with initial imperfection of L/1000
- Columns made of conventional materials (natural aggregate, river or lake sand...)
- Normal weight concrete (greater than 2160kg / m³)
- Experimental data (not the numerical data)

Table 2.1 Collected experimental axial compressive strength of CFSST columns

Nº	Literature name	B	D	t	L _e	f _{c'}	σ _{0.2}	P _u	Refs.
1	SHS100X100X2-C30	100.2	101.6	2.2	300	30	385	534	[3]
2	SHS100X100X2-C60	101.3	99.3	2	300	53	385	687	
3	SHS100X100X2-C100	99.8	101.0	2.2	300	74	385	836	
4	SHS100X100X5-C30	99.9	100.6	5	300	30	458	1410	
5	SHS100X100X5-C60	100.5	99.9	4.9	300	53	458	1488	
6	SHS100X100X5-C100	100.6	99.9	4.9	300	74	458	1559	
7	CHS104X2-C30	-	104.0	2	300	31	412	699	
8	CHS104X2-C60	-	104.0	2	300	49	412	901	
9	CHS104X2-C100	-	104.0	2	300	65	412	1133	
10	CHS114X6-C30	-	114.3	6.02	300	31	266	1593	
11	CHS114X6-C60	-	114.3	6.02	300	49	266	1648	
12	CHS114X6-C100	-	114.3	6.02	300	65	266	1674	
13	A1	-	300.0	8	900	34	248	6134	[4]
14	A2	-	300.0	10	900	34	242	7076	
15	A3	-	300.0	12	900	34	249	8088	
16	A4	-	300.0	8	900	37.7	248	5601	
17	A5	-	300.0	10	900	37.7	242	6848	
18	A6	-	300.0	12	900	37.7	249	8230	
19	A7	-	300.0	8	900	40.5	248	6171	
20	A8	-	300.0	10	900	40.5	242	7193	
21	A9	-	300.0	12	900	40.5	249	8432	
22	D1	-	325.0	8	975	36.6	544	10190	
23	D2	-	325.0	10	975	36.6	542	11032	

Table 2.1 Collected experimental axial compressive strength of CFSST columns

Nº	Literature name	B	D	t	L _e	f _{c'}	σ _{0.2}	P _u	Refs.
24	D3	-	325.0	12	975	36.6	542	12926	
25	D4	-	325.0	8	975	42.5	544	10304	
26	D5	-	325.0	10	975	42.5	542	10260	
27	D6	-	325.0	12	975	42.5	542	13499	
28	D7	-	325.0	8	975	45.7	544	10533	
29	D8	-	325.0	10	975	45.7	542	13240	
30	D9	-	325.0	12	975	45.7	542	13265	
31	C-3-L-RS	-	159	2.88	480	37.4	383.9	1293	
32	C-3-H-RS	-	159	2.88	480	43.7	383.9	1332	
33	C-4-L-RS	-	159	3.8	480	37.4	400.7	1625	
34	C-5-L-RS	-	159	4.5	480	37.4	401	1672	
35	S-3-L-RS	160	160	2.88	480	37.4	446.2	1498	
36	S-3-H-RS	160	160	2.88	480	43.7	446.2	1559	
37	S-4-L-RS	160	160	3.9	480	37.4	414.5	1985	
38	S-5-L-RS	160	160	4.8	480	37.4	431.9	2068	
39	CS-0	-	168.9	2.86	510	41.2	339.6	1708	
40	RS-0	97.1	200.7	3.96	600	41.2	301.5	1423	
41	C-S-N	-	120	1.77	360	53.9	286.7	823	
42	S-S-N	120	120	1.77	360	53.9	286.7	923	
43	C2	-	100	2	300	42	324	667	
44	CFSST-D125	-	125	1.3	375	54.5	496	1137	
45	CFSST-D150	-	150	1.65	445	54.5	493	1680	
46	CFSST-D180	-	180	1.7	540	54.5	493	2181	
47	C20-50×1.2	-	50.8	1.2	150	20	291	109	
48	C30-50×1.2	-	50.8	1.2	150	30	291	132	
49	C20-50×1.6	-	50.8	1.6	150	20	298	136	
50	C30-50×1.6	-	50.8	1.6	150	30	298	165	
51	C20-100×1.6	-	101.6	1.6	300	20	320	424	
52	C30-100×1.6	-	101.6	1.6	300	30	320	477	
53	C20-127x1.6	-	127	1.6	400	20	274	675	
54	C30-127x1.6	-	127	1.6	400	30	274	746	
55	C20-150x1.6	-	152.4	1.6	450	20	279	809	
56	C30-150x1.6	-	152.4	1.6	450	30	279	897	
57	C20x200x2.0	-	203.2	2	500	20	259	1384	
58	C30-200x2.0	-	203.2	2	500	30	259	1536	

Table 2.1 Collected experimental axial compressive strength of CFSST columns

Nº	Literature name	B	D	t	L _e	f _{c'}	σ _{0.2}	P _u	Refs.
59	S20-50x2	51	51	1.81	150	21.5	353	239	[11]
60	S30-50x2	51	51	1.81	150	34.9	353	271	
61	S20-50x3	51	51	2.85	150	21.5	440	361	
62	S30-50x3	51	51	2.85	150	34.9	440	394	
63	S20-100x3	100	100	2.85	300	21.5	358	711	
64	S30-100x3	100	100	2.85	300	34.9	358	754	
65	S20-100x5	101	101	5.05	300	21.5	435	1350	
66	S30-100x5	101	101	5.05	300	34.9	435	1448	
67	S20-150x3	152	152	2.85	450	21.5	268	1049	
68	S30-150x3	152	152	2.85	450	34.9	268	1142	
69	S20-150x5	150	150	4.8	450	21.5	340	1801	
70	S30-150x5	150	150	4.8	450	34.9	340	1962	
71	D89-L700-R0	-	88.75	2.81	811	67.5	303.9	525	[11]
72	D89-L700-R35	-	88.68	2.84	812	58.5	303.9	504	
73	D89-L700-R70	-	88.87	2.82	811	52.4	303.9	481	
74	D89-L1200-R0	-	88.58	2.76	1312	67.5	303.9	498	
75	D89-L1200-R35	-	88.79	2.86	1312	58.5	303.9	429	
76	D89-L1200-R70	-	88.8	2.78	1311	52.4	303.9	424	
77	D101-L700-R0	-	101.17	2.85	812	67.5	271.8	737	
78	D101-L700-R35	-	101.45	2.86	810	58.5	271.8	670	
79	D101-L700-R70	-	101.52	2.86	811	52.4	271.8	639	
80	D101-L1200-R0	-	101.22	2.86	1310	67.5	271.8	575	
81	D101-L1200-R35	-	101.29	2.86	1311	58.5	271.8	555	
82	D101-L1200-R70	-	101.41	2.85	1311	52.4	271.8	540	
83	SC200-R0-5	-	201.8	4.98	605.4	53.1	293.1	2923	[12]
84	SS200-R0-5	201	201	4.98	603	53.1	293.1	3164	

If the prescribed constraints were to be lifted, the actual collected column data would go from 84 to more than 200. Blindly combining columns data of inconsistent properties might result in “trash-in, trash-out” phenomenon during machine learning process and current author firmly believes in quality over quantity, which led to only this much column data being collected. This compilation shall be deemed enough for initial evaluation of the machine learning algorithm (discussed later in the following sections) especially for stub columns since the majority of them are of stub columns

while only a few are of long or slender columns. This clearly provides prior knowledge that the prediction model to be trained using only the data from the literatures would not be able to attain highly accurate predictions for slender columns.

2.3 IMPLEMENTATION OF MACHINE LEARNING IN STRUCTURAL ENGINEERING

It is not a completely new idea to implement machine learning algorithms into civil engineering applications. Several researchers have employed and concluded that the use of machine learning in predicting the responses of structural members not only yield acceptable results, superior prediction capacity over uncertainty, but also enable us to estimate the output parameters outside the inputs periphery which is the main reason in the implementation of this method. Naser et al. 2021 [18] evaluated the structural response of concrete-filled steel tubular columns made of low-carbon steel using GA (Genetic Algorithms) and GEP (Gene Expression Programming) with a total of 3103 tests data. For a given problem, GEP can develop a macro that can be run using MATLAB software, while GA is capable of deriving a formula to be substituted into by hand calculation using Excel spreadsheet. Truong et al. 2022 [19] developed the model for the assessment of semi-rigid steel structures using 12 machine learning algorithms including, three Linear Regression (Linear, Lasso and Ridge), Support Vector Machine (SVM), Deep Learning (DL) and seven tree-based ensemble algorithms (RF, GTB, Adaboost, Hist, XGBoost, LightGBM and CatBoost). Among these, the XGBoost method turned out to be the most accurate and robust approach and was therefore recommended as the efficient machine learning method for the prediction of load-carrying capacity of semi-rigid steel structures considered. Xu et al. 2021 [20] proposed one for cold-formed stainless-steel tubular columns but not the concrete-filled one.

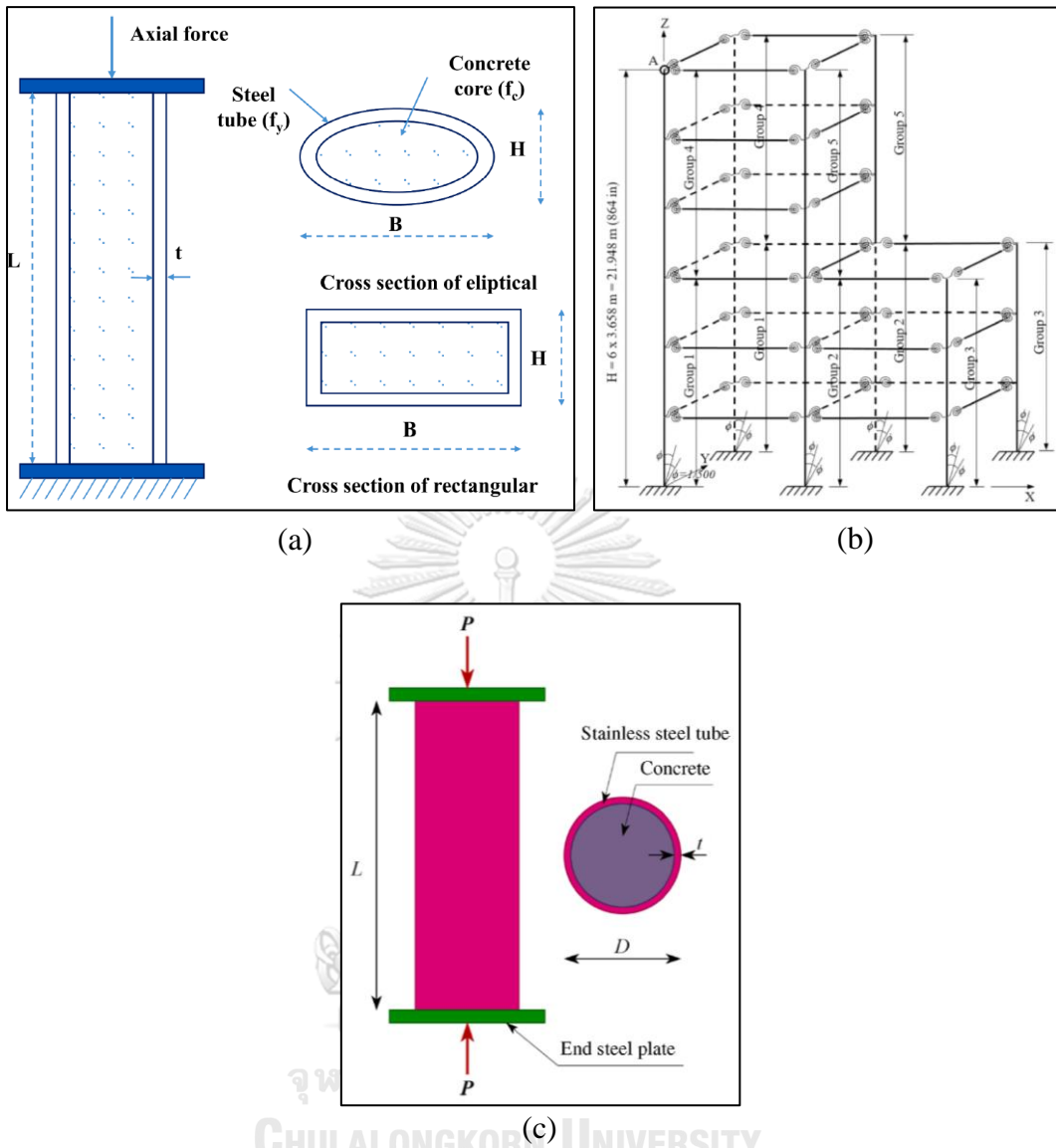


Figure 2.8 Various structures whose responses were predicted using ML approaches: (a) CFST columns (Nguyen et al. 2023), (b) Semi-rigid steel structures (Truong et al. 2022), (c) Circular CFSST column (Tran et al. 2023)

Nguyen et al. 2023 [21] also utilized machine learning algorithms to predict the ultimate axial load of CFST (concrete-filled steel tubular) columns using a unified model for different cross-sections including elliptical and rectangular section instead of one model for one unique section type. It was done by modified the input space using the concrete radius of gyration instead of literal section dimension. Xu et al. 2021 [20] proposed one for cold-formed stainless-steel tubular columns but not the concrete-filled one. Tran et al. 2023 [22] recently utilized six machine learning

algorithms including Decision Tree (DT), Random Forest (RF), K-Nearest Neighbors (KNN), Adaptive Boosting (AdaBoost), Gradient Boosting Regression Tree (GBRT), and Extreme Gradient Boosting (XGBoost) to predict the axial strength of circular concrete-filled stainless-steel tubular column using 142 tests data. The results were then validated against standard specifications such as Eurocode 4, AISC 3610-16, ACI 318-19, etc. Regardless of the splendid results, their work merely revolved around circular section only. With that and the fact that no work has ever been carried out to investigate the accuracy of machine learning model for both circular and rectangular sections of CFSST columns, they serve as the main motives for the current work.



CHAPTER 3

METHODOLOGY

3.1 GENERAL

To develop a surrogate model for standard specifications, we must first collect substantial column data. It can be done either by collecting from the literature or numerical simulations if those collected from the literature could not provide satisfied results. Figure 3.1 outlines main steps of the research work, we can see that it quite revolves around gathering and simulating the column data as much as possible if the desired results still could not be attained as mentioned previously.

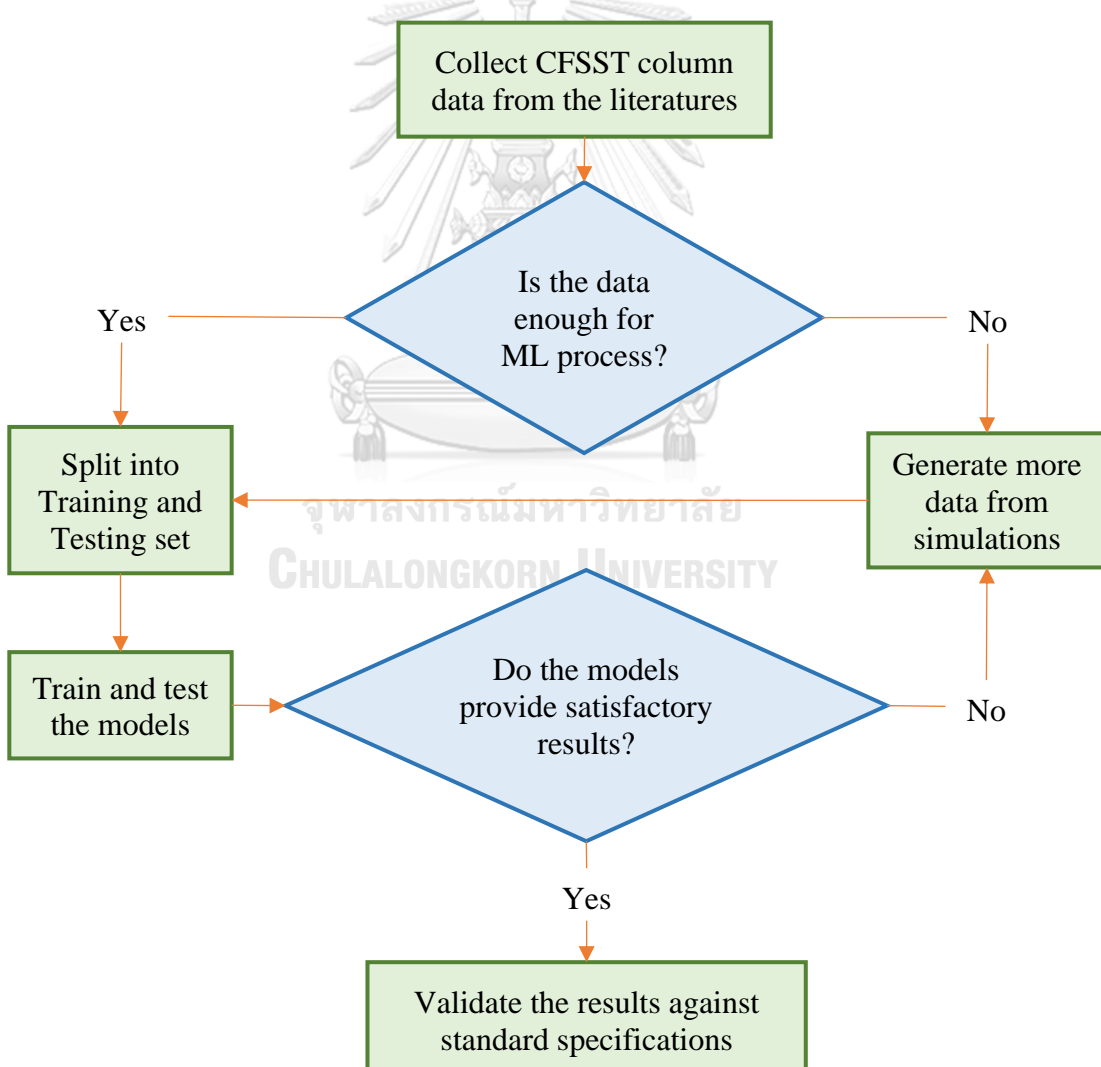


Figure 3.1 Flowchart of the research work

3.2 MATERIALS CONSTITUTIVE LAW

3.2.1 GENERAL

To capture the behavior of CFSST columns, proper stress-strain relationships for both stainless steel and confined-concrete must be well-prepared first since we aim to perform the nonlinear analysis to get the post-buckling behavior of both stub and slender columns. The modified stress-strain model for uniaxial confined concrete under compression proposed by Samani & Attard 2012 [23] and the simplified two-stage stress-strain model of stainless steel from Fernando et al. 2020 [1] are preferred by the current author (over the complicated three-stage model) to represent the materials behavior in the simulations.

3.2.2 STAINLESS STEEL

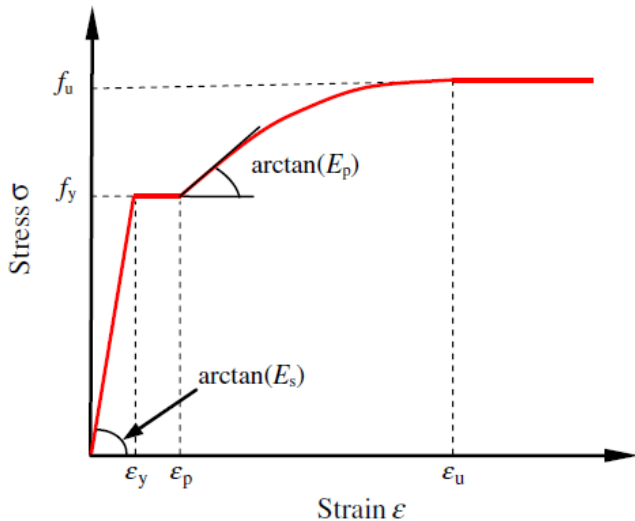


Figure 3.2 Stress strain diagram of low-carbon steel (Tao et al. 2013 [2])

The stress-strain diagram of conventional structural steel is shown in Figure 3.2. The material exhibits linear elastic behavior when the strain is less than or equal to the yield strain, then undergoes no changes in stress when the strain is between the yield strain and plastic strain with the ultimate tensile strength f_u and corresponding ultimate strain ϵ_u . However, the stress strain diagram of stainless-steel shows no specific yield point. The offset yield stress method is used where a straight line parallel to the initial slope of the curve is offset by 0.002 from the origin to intersect

with the curve. The stress value at the intersection between this line and the stress-strain curve is assumed to be the yield stress for stainless-steel or sometimes is called 0.2% proof stress denoted by $\sigma_{0.2}$ [24].

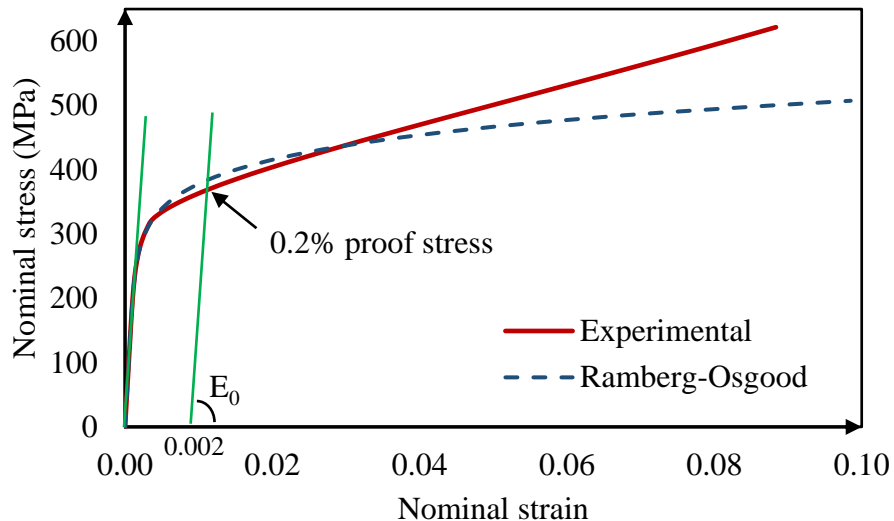


Figure 3.3 Typical nominal stress-strain curve of stainless-steel versus the basic Ramberg-Osgood equation

The effect of corner region for stainless-steel is even more obvious than that for low-carbon steel and must be accounted for. This region extends a distance of twice the steel thickness to each flat region from the corner radius (Figure 3.13). The stress-strain relationship of the flat regions is also applied to the corner regions since there was no specific stress-strain model in the literature proposed for the latter [25].

$$\sigma_{0.2,c} = \frac{1.673\sigma_{0.2,v}}{(r_i/t)^{0.126}} \quad (3.1)$$

$$\varepsilon = \frac{\sigma}{E_0} + p \left(\frac{\sigma}{\sigma_p} \right)^n \quad (3.2)$$

Several methods have been proposed to represent the full range stress-strain curve of stainless steel mainly based on the modification of the Ramberg-Osgood equation (Eq. (3.2)). The use of Ramberg-Osgood expression provides accurate stress-strain relationship up to $\sigma_{0.2}$ as shown in Figure 3.3. Beyond this limit, it cannot be accurately used to represent the relationship anymore. Hence, several methods have

been proposed to represent the stress-strain curve beyond this limit by using two-stage or three-stage Ramberg-Osgood modifications. Fernando et al. 2020 [1] discussed the use of both three-stage and two-stage expression and concluded that the three-stage expression gives better representation but seems to be out of favor due to its complexity while the two-stage expression, on the other hand, are still acceptable and is adopted due to its simplicity. We should be aware of different types of stainless-steel which are austenitic, duplex, and ferritic alloy. Only the austenitic and duplex steel alloy are considered in this study since they are more ductile compared to the ferritic steel alloy, and they also share the same formulas in terms of stress-strain property. The expressions for the full range of compressive stress-strain diagram of stainless-steel from Fernando et al. [1] are based on Eqs. (3.3) and (3.4).

for the initial range, $\sigma^{\text{com}} \leq \sigma_{0.2}^{\text{com}}$,

$$\varepsilon^{\text{com}} = \frac{\sigma^{\text{com}}}{E_0^{\text{com}}} + 0.002 \left(\frac{\sigma^{\text{com}}}{\sigma_{0.2}^{\text{com}}} \right)^{n^{\text{com}}} \quad (3.3)$$

for $\sigma^{\text{com}} > \sigma_{0.2}^{\text{com}}$,

$$\varepsilon^{\text{com}} = \frac{\sigma^{\text{com}} - \sigma_{0.2}^{\text{com}}}{E_{0.2}^{\text{com}}} + \left(\varepsilon_u^{\text{com}} - \frac{\sigma_u^{\text{com}} - \sigma_{0.2}^{\text{com}}}{E_{0.2}^{\text{com}}} - \varepsilon_{0.2}^{\text{com}} \right) \times \left(\frac{\sigma^{\text{com}} - \sigma_{0.2}^{\text{com}}}{\sigma_u^{\text{com}} - \sigma_{0.2}^{\text{com}}} \right) + \varepsilon_{0.2}^{\text{com}} \quad (3.4)$$

Note that the superscripts “com” and “ten” indicate compression and tension, respectively, and the strain hardening exponent of the second stage, strain hardening exponent of the first stage and tangent modulus at 0.2% proof stress are calculated from Eqs. (3.5)-(3.7), respectively.

$$l = \beta \left(\frac{\sigma_u^{\text{com}}}{\sigma^{\text{com}}} \right) + 0.15 \quad (3.5)$$

$$n^{\text{com}} = \frac{\ln(20)}{\ln(\sigma_{0.2}^{\text{com}} / \sigma_{0.01}^{\text{com}})} \quad (3.6)$$

$$E_{0.2}^{\text{com}} = \frac{E_0^{\text{com}}}{1 + 0.002n^{\text{com}} / e^{\text{com}}} \quad (3.7)$$

where $\beta = 0.985 \frac{\sigma_{0.2}^{\text{com}}}{\sigma_u^{\text{com}} - \sigma_{0.2}^{\text{com}}} - 0.0085$ and $e^{\text{com}} = \frac{\sigma_{0.2}^{\text{com}}}{E_0^{\text{com}}}$

The nominal compressive stress, strain and the nominal tensile strain are calculated from Eqs. (3.8)-(3.10), respectively, while the relationship between the 0.2% proof stress and the ultimate tensile stress is expressed in Eq. (3.11).

$$\sigma_u^{\text{com}} \cong \sigma_u^{\text{ten}} \left(1 + \varepsilon_u^{\text{ten}}\right)^2 \quad (3.8)$$

$$\varepsilon_u^{\text{com}} \cong 1 - \frac{1}{1 + \varepsilon_u^{\text{ten}}} \quad (3.9)$$

$$\varepsilon_u^{\text{ten}} = 1 - \left(\sigma_{0.2}^{\text{ten}} / \sigma_u^{\text{ten}}\right) \quad (3.10)$$

$$\frac{\sigma_{0.2}^{\text{ten}}}{\sigma_u^{\text{ten}}} = 0.2 + 185e^{\text{ten}} \quad (3.11)$$

Although the column is expected to be subjected mainly to compressive stress, however, at some load (or time) step, a portion of it will be subjected to tensile stress even though it is of small magnitude. Therefore, the stress-strain relationship in tension should be considered along with compression as well. The term nominal (stress or strain) is used here because the initial (original) cross-sectional area or gage length is used to calculate the stress-strain values during material testing instead of the actual one. Since the tensile stress-strain relationship of stainless-steel in the initial stage is almost the same to that in compression, the relationship proposed above can be used both in tension and compression and the properties should have the same value (0.2% proof stress, initial elastic modulus, strain hardening exponent, etc.).

To implement this stress-strain scheme, basic Ramberg-Osgood parameters must be obtained from experimental tests including the 0.2% proof stress ($\sigma_{0.2}$), the 0.01% proof stress ($\sigma_{0.01}$), and the initial elastic modulus (E_0). Test reports from [10] showed that the initial elastic modulus did vary though not so significant, from 195,000MPa to 207,900MPa. Nevertheless, the author assumed that it remains constant for all steel types with the value of 200,000MPa for simplicity. The 0.2% proof stress is treated as the yield stress as in the case of low-carbon steel which can be assumed and vary as we want regardless of steel type. However, there are no reports regarding the values of the 0.01% proof stress which also plays a role in the numerical derivation of the stress-strain curve though not as serious as the 0.2% proof stress. Reports from Arrayago et al. 2015 [26] showed that the values of the 0.2% and the 0.1% proof stress were very close although the strain was twice larger. Hence, as

an approximation, the 0.01% proof stress is assumed to be 70% of the steel yield stress.

$$\sigma_{0.01} \approx 0.70\sigma_{0.2} \quad (3.12)$$

All the prescribed expressions above are required to be converted into true stress-strain before being inputted into ABAQUS. Liu et al. 2022 [27] used Eqs. (3.13) and (3.14) to convert the nominal stress-strain into true stress-strain. As a comparison to show how much the true stress-strain values differ from the nominal ones, a plot of the true and nominal stress-strain curve of austenitic stainless-steel alloy with 0.2% proof stress of 291MPa is depicted in Figure 3.4.

$$\sigma_{\text{true}} = \sigma_{\text{nom}} (1 + \varepsilon_{\text{nom}}) \quad (3.13)$$

$$\varepsilon_{\text{true}} = \ln(1 + \varepsilon_{\text{nom}}) \quad (3.14)$$

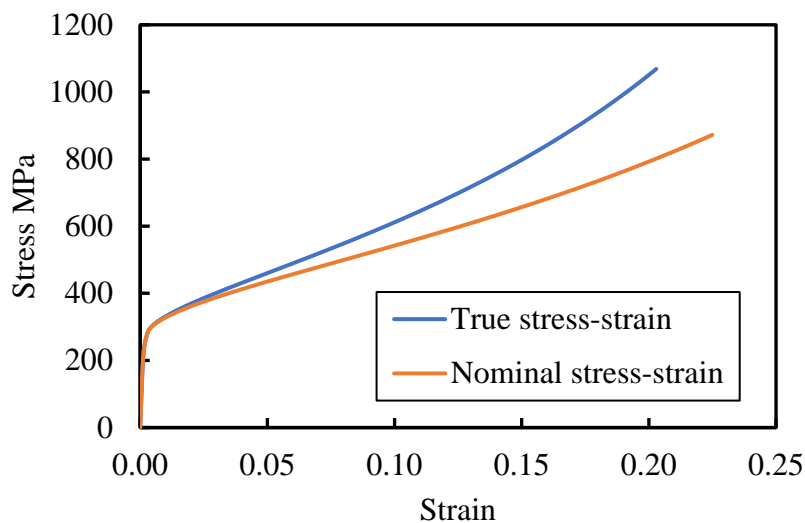


Figure 3.4 Nominal versus true stress-strain curve (austenitic or duplex alloy)

Even though the 0.2% proof stress is treated as yield stress, the stress-strain curve clearly does not show a linear relationship up to this value. To support this point, suppose we need to calculate the stress corresponding to the $\varepsilon_{0.2}$ of which value

we already know. For $\sigma_{0.2} = 291\text{MPa}$, we obtain $\varepsilon_{0.2} = 0.002 + \frac{291}{2 \times 10^5} = 0.003455$

and $\sigma = 0.003455 \times 2 \times 10^5 = 691\text{MPa}$.

We see that this stress is completely larger than the expected value of just 291MPa. So, only a portion of the initial stage exhibits a linear relationship. This limit is generally defined as the stress at 0.01% plastic strain as stated in Cruise & Gardner 2008 [28]. Another step to be considered is inputting the yield stress and plastic strain into ABAQUS software. The plastic strain can be calculated from Eq. (3.15).

$$\varepsilon_{pl} = \varepsilon_t - \varepsilon_{el} = \varepsilon_t - \frac{\sigma}{E_0} \quad (3.15)$$

In the case of low-carbon steel, the first plastic strain corresponding to the yield stress will be zero since its behavior is almost perfectly linear with well-defined yield point which almost coincides with the limit of proportionality. However, this does not exactly apply to stainless steel. Even though the 0.2% proof stress is assumed to be the yield stress, there is no specific point between the elastic and plastic region. Since the limit of proportionality is assumed to be up to 0.01% proof stress, we might underestimate a portion of the elastic region and instead treat that portion as a part of plastic region. Since the relationship in the initial elastic range is not perfectly linear, the first plastic strain will not be exactly zero. Hence, modification of the first plastic strain value needs to be made to ensure that the stress-strain values can be inputted into ABAQUS.

3.2.3 CONFINED CONCRETE

3.2.3.1 CONCRETE DAMAGED PLASTICITY

The Concrete Damaged Plasticity model available in ABAQUS is used to model the nonlinear behavior of concrete. Liu et al. 2022 [27] suggested using constant values of all parameters involved in the modeling including the dilation angle (ψ), flow potential eccentricity (e), the ratio of the second stress invariant on the tensile meridian to that on the compressive meridian (K_c), and the ratio of the compressive strength under biaxial loading to uniaxial compressive strength (f_{b0} / f'_c) of 30°, 0.1, 1.16 and 2/3, respectively. Tao et al. 2013 [2], on the other hand, suggested that constant values of these parameters should not be used due to complexity of confinement between steel tube and concrete. Tao et al. [2] further

stated that default values of 0.1 and 0 can be used for flow potential eccentricity and viscosity parameter, respectively, since they have no significant influence on the prediction accuracy. The ratio of the compressive strength under biaxial loading to uniaxial compressive strength can be predicted by Eqs. (3.16) and (3.17).

$$f_{b0} / f'_c = 1.5 (f'_c)^{-0.075} \quad (3.16)$$

$$K_c = 5.5 / (5 + 2(f'_c)^{0.075}) \quad (3.17)$$

Reports from Tao et al. 2013 [2] also indicated that dilation of concrete decreases with increasing of confinement, therefore, it is assumed that the dilation angle is a function of confinement factor, ξ_c , where:

$$\xi_c = \frac{A_s f_y}{A_c f'_c} \quad (3.18)$$

for $\xi_c \leq 0.5$

$$\psi = 56.3(1 - \xi_c) \quad (3.19)$$

for $\xi_c > 0.5$

$$\psi = 6.672 e^{\frac{7.4}{4.64 + \xi_c}} \quad (3.20)$$

3.2.3.2 STRESS-STRAIN RELATIONSHIP IN COMPRESSION

Tao et al. 2013 [2] investigated the finite element models of CFST (concrete-filled steel tubular) columns under axial compression while a three-stage stress-strain model proposed by Samani & Attard 2012 [23] was used to represent the full range stress-strain curve of confined concrete in compression. Since the current work structural behavior is the same to that of his except low-carbon steel tube is replaced by the stainless one, the three-stage stress-strain model is adopted herein. The second stage is where the strain lies between ε_{c0} and ε_{cc} with stress equals to the maximum compressive strength of concrete. In the above expressions, ε_{c0} , f_r , f'_c are the strain at peak stress, residual stress, and concrete compressive strength, respectively. The concrete stress in the first stage varies almost linearly with concrete elastic modulus calculated from Eq. (3.21) for normal-weight concrete provided by the ACI 318-19 [29].

$$E_c = 4700\sqrt{f'_c} \quad (3.21)$$

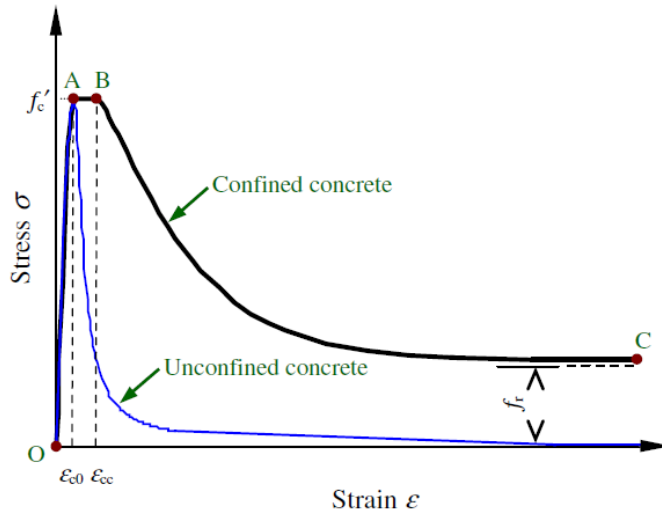


Figure 3.5 Stress-strain curve of confined and unconfined-concrete (Tao et al. 2013 [2])

for $0 < \varepsilon \leq \varepsilon_{c0}$

$$\frac{\sigma}{f'_c} = \frac{A \cdot X + B \cdot X^2}{1 + (A - 2)X + (B + 1)X^2} \quad (3.22)$$

for $\varepsilon \geq \varepsilon_{cc}$

$$\sigma = f_r + (f'_c - f_r) \exp \left[- \left(\frac{\varepsilon - \varepsilon_{cc}}{\alpha} \right)^\beta \right] \quad (3.23)$$

Table 3.1 Parameters for concrete stress-strain curve

Parameter	Section type	
	Rectangular	Circular
f_B	$\frac{0.25(1 + 0.027\sigma_{0.2})e^{\frac{-0.02\sqrt{B^2+D^2}}{t}}}{1 + 1.6e^{-10}(f'_c)^{4.8}}$	$\frac{(1 + 0.027\sigma_{0.2})e^{\frac{-0.02D}{t}}}{1 + 1.6e^{-10}(f'_c)^{4.8}}$
f_r	$0.1f'_c$	$0.7(1 - e^{-1.38\xi_c})f'_c \leq 0.25f'_c$
α	$0.005 + 0.0075\xi_c$	$0.04 - \frac{0.036}{1 + e^{6.08\xi_c - 3.49}}$
β	0.92	1.20

where $\varepsilon_{c0} = 76 \times 10^{-5} + \sqrt{(0.626f'_c - 4.33) \times 10^{-7}}$, $A = \frac{E_c \varepsilon_{c0}}{f'_c}$, $B = \frac{(A-1)^2}{0.55} - 1$

$$k = \left(2.9224 - 0.00367 f'_c \right) \left(\frac{f_B}{f'_c} \right)^{0.3124+0.002f'_c}, \quad \frac{\varepsilon_{cc}}{\varepsilon_{c0}} = e^k, \quad X = \frac{\varepsilon}{\varepsilon_{c0}}$$

3.2.3.3 STRESS-STRAIN RELATIONSHIP IN TENSION

The tensile stress-strain relationship of concrete is not as complex as that of the compressive one. Hafezolghorani et al. 2017 [30] suggested a maximum tensile stress (σ_{t0}) of 10% of the maximum compressive strength, increases linearly with slope E_c . Beyond this limit, the tensile stress then decreases linearly to the lower bound of 1% of σ_{t0} with corresponding strain of 10 times the cracking strain.

$$\text{cracking strain} \quad \varepsilon_{cr} = \frac{\sigma_{t0}}{E_c} \quad (3.24)$$

$$\text{modulus of rupture} \quad f_r = 0.62\lambda\sqrt{f'_c} \quad (3.25)$$

Hassanein et al. 2017 [31] employed similar scheme beyond the maximum tensile stress limit except that the maximum tensile stress of concrete was defined as $0.6\sqrt{\gamma_c f'_c}$ where γ_c was the strength reduction factor. In this work, however, the author prefers the maximum tensile stress assumed to be the modulus of rupture, f_r , provided by ACI standard [29] while the relationship beyond this limit remains the same to the procedure described above. Since both the modulus of rupture and the initial modulus of elasticity are a portion of square root of concrete compressive strength, the cracking strain and the ultimate tensile strain will always have fixed values regardless of the concrete compressive strength.

$$\text{cracking strain} \quad \varepsilon_{cr} = \frac{f_r}{E_c} = \frac{0.62\lambda\sqrt{f'_c}}{4700\sqrt{f'_c}} = 131.91 \times 10^{-6}$$

$$\text{ultimate strain} \quad \varepsilon_u = 10\varepsilon_{cr} = 1319.1 \times 10^{-6}$$

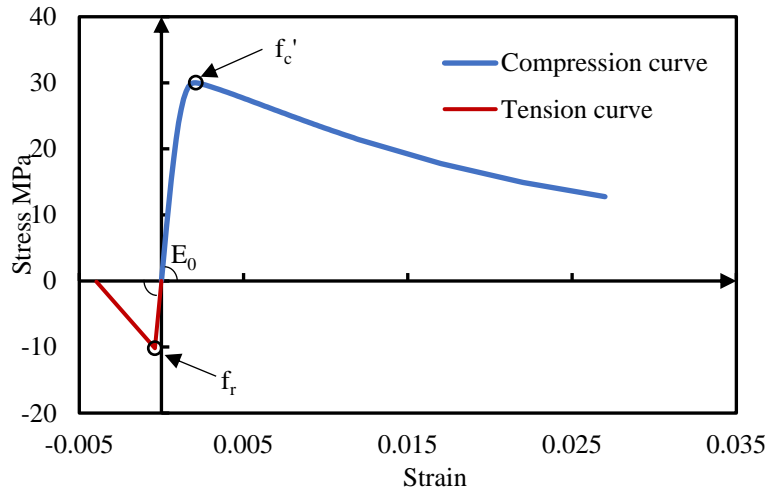


Figure 3.6 Typical confined-concrete stress-strain curve

3.3 FINITE ELEMENT MODELING

Since there is a limited amount of experimental test data regarding CFSST columns especially slender column and the collected data from the literatures are not enough to develop a competent predictive model, numerical simulation is a must to generate more data to be used in machine learning process. The Finite Element Method software comes in handy in this situation to simulate the behavior of CFSST columns, take ANSYS or ABAQUS as the examples. In this work, ABAQUS is preferred by the author.

3.3.1 INITIAL LOCAL GEOMETRIC IMPERFECTION

For square section, Tao et al. 2011 [25] performed nonlinear analysis assuming the initial imperfection shape of the steel tube to be as shown in Figure 3.7 which was described by Eq. (3.26), where σ_{cr} is the elastic critical buckling stress, calculated in accordance with AISC standards [32], while the imperfection value for circular section could be calculated as shown in Table 3.2 as proposed by Azad & Uy 2020 [33].

$$\omega = \frac{\omega_0}{4} \left(1 - \cos \frac{2\pi x}{B} \right) \left(1 - \cos \frac{2\pi y}{B} \right) \quad (3.26)$$

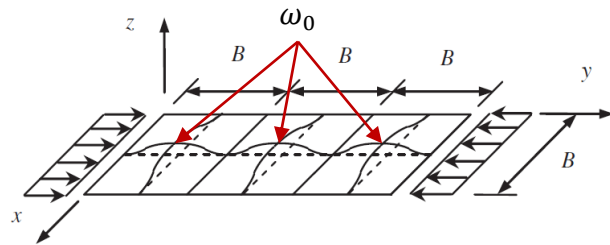


Figure 3.7 Assumed local imperfection for square section (Tao et al. 2011 [25])

Table 3.2 Initial local imperfection

Rectangular section	Circular section
$\omega_0 = 0.023(\sigma_{0.2} / \sigma_{cr})t$ $\sigma_{cr} = \frac{\pi^2 E_s}{3(1-\nu^2)} \left(\frac{t}{B}\right)^2$	$\omega_0 = t / 100$

Many researchers that have conducted the simulations on stub column confined by steel tube came to a conclusion that initial local imperfection has low to no effect on the CFST stub column compressive strength and get further minimized by concrete filling, therefore, could be omitted from the simulations ([25], [27], [33], [12]). It is most likely due to relatively small imperfection magnitude which is usually less than the maximum displacement from the linear buckling analysis in ABAQUS (Figure 3.8). For instance, the imperfection value of square section with 150mm width, 2mm steel tube thickness and steel yield strength of 300MPa is just 0.107mm, not to mention that this is even smaller for its circular section counterpart of just 0.02mm. Therefore, the author has opted to omit the local imperfection effect in the simulations.

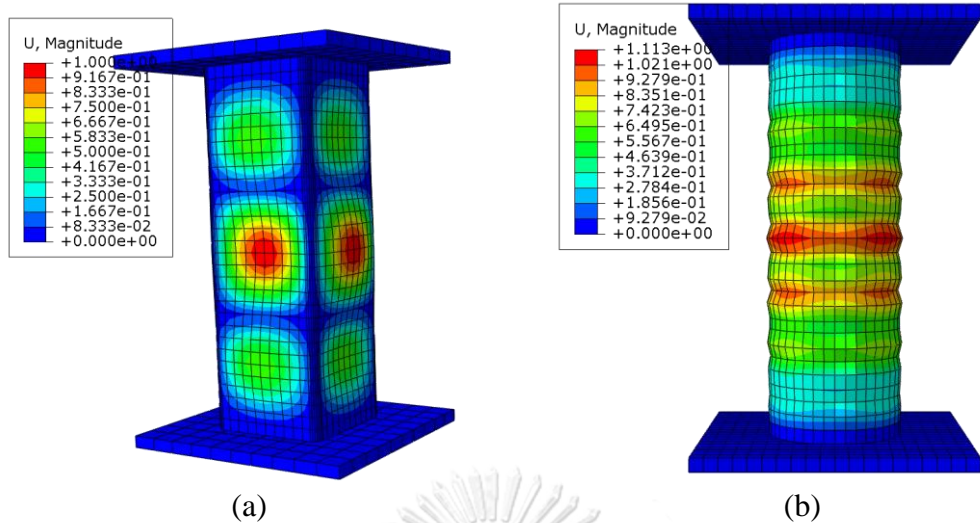


Figure 3.8 First eigen buckling mode of CFSST stub columns: (a) rectangular section
(b) circular section

3.3.2 INITIAL GLOBAL GEOMETRIC IMPERFECTION

As previously discussed, we already collected 184 columns data from the literature while 160 of them were of short columns. Hence, the goal of the simulation is to generate more data for long or slender columns. Since slender columns are prone to global buckling, the analysis must consist of two steps to account for this effect. The first step is the linear buckling analysis using the perturbation buckle analysis available in ABAQUS. Note that only the first buckling mode of the column is of interest. The column buckling shape and eigen buckling load are then inputted into the second step analysis using Static, Riks step in which the column buckling mode shape from the first analysis is scaled to match the desired initial global geometric imperfection value by model keyword modification.

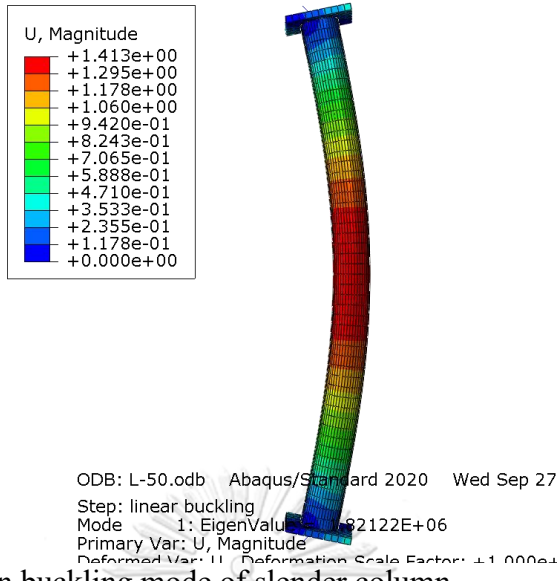


Figure 3.9 First eigen buckling mode of slender column

He et al. 2021 [11] performed compressive experimental tests on slender CFSST columns where global geometric imperfection was measured precisely. The tests were accompanied by numerical simulations in ABAQUS with different global imperfection values. The results from the finite-element models demonstrated accurate prediction compared to their experimental failure mode and the axial strength when the global imperfection value was chosen as $L_e/1000$. This value was also adopted by Hassanein et al. 2017 [31] to model the overall buckling behavior of the columns. Likewise, it is selected by the author herein to perform the simulation of slender CFSST columns.

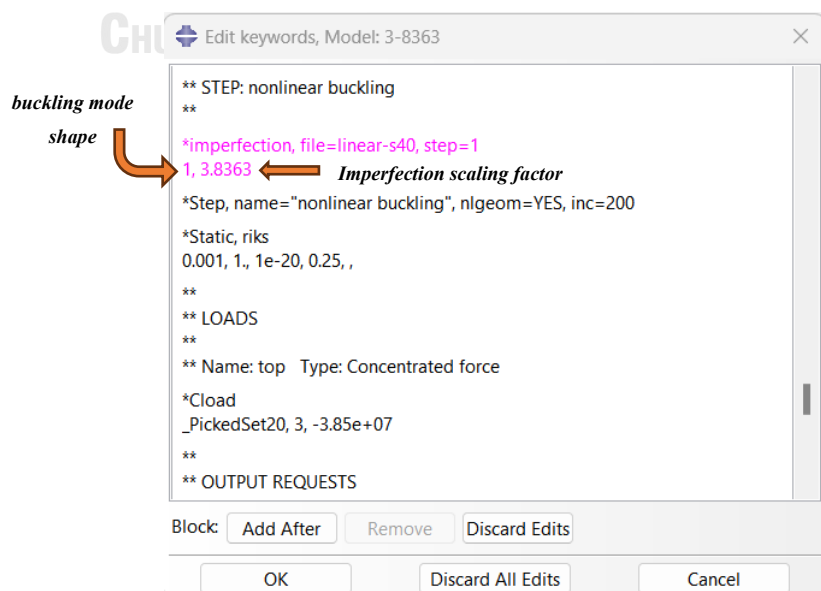


Figure 3.10 Keywords modification for initial imperfection

3.3.3 MODELING PROPERTIES

The core concrete and steel tube were both modeled with the 8-node brick elements with reduced integration (C3D8R). The 8-node element was applied to the steel tube to avoid numerical instabilities and convergence difficulty arising from using the 4-node shell element, even though some researchers suggested so. The surface contact between the core concrete and the steel tube were modeled using the “Surface-to-Surface-Contact” while the “Hard Contact” and the “Penalty” method were used to model the normal and tangential behavior of the interaction, respectively. He et al. used the friction coefficient of 0.25 which was stated that this value was used by Tao et al. 2011 [25]. Actually, Tao et al. [25] stated that this value was for low-carbon steel and not the stainless steel. For the latter, a friction coefficient of 0.6 was used [25]. The verification of the simulations with the literatures (Table 3.4) using this value showed good agreement; hence, this value was adopted in the subsequent work leading to the adoption of these parameters in the subsequent work, with average sectional mesh size of B/10.

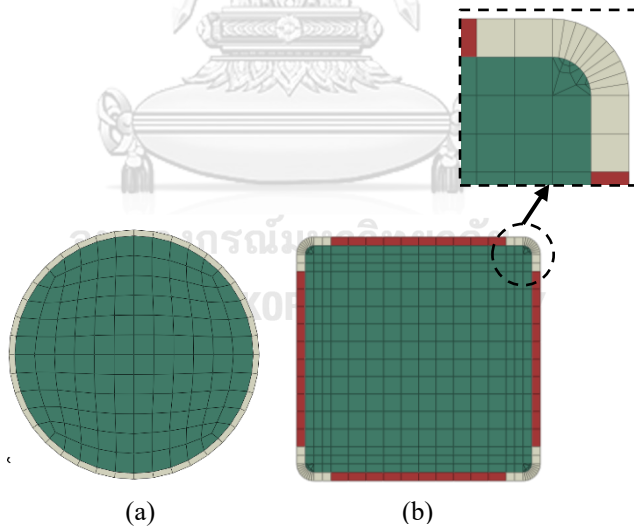


Figure 3.11 Typical sectional-mesh view: (a) circular section (b) rectangular section

Both core concrete and outer steel tube are assumed to be loaded simultaneously in such a manner that no longitudinal slip occurs between the two components contact surfaces and, thus, no consideration is required over slippage effect as done by Liu et al. 2022 [27]. Tao et al. 2016 [17] also studied the bond behavior of CFST columns with both carbon and stainless steel and concluded that stainless-steel bond strength was lower than carbon steel due to its smoother surfaces.

Additionally, concrete age also posed significant effect on the member's bond strength and should be taken into consideration in long-term design of the structures, especially when the load is applied to merely steel or concrete. If this effect is to be accounted for, the empirical formula proposed by Han et al. 2022 [12] could be used to determine the interfacial bond strength of recycled aggregate concrete-filled stainless-steel tubular columns (RACFSST) while also noting that concrete strength and recycled aggregate had no significant impact and, therefore, the calculation formula could be unified for RACFSST and CFSST columns.

$$\tau_u = \begin{cases} 0.150 & (t/D^2 \leq 0.00007) \\ 0.150 + 3300(t/D^2 - 0.00007) & (t/D^2 > 0.00007) \end{cases} \quad (3.27)$$

$$\tau_u = \begin{cases} 0.050 & (t/B^2 \leq 0.00011) \\ 0.050 + 3100(t/B^2 - 0.00011) & (t/B^2 > 0.00011) \end{cases} \quad (3.28)$$

The surfaces of each end of the column are tied to the reference points in the middle using "Tie Constraint" where the boundary conditions and load are applied to (in case of not including loading plate in the models). To simulate the pin-ended boundary conditions, each end is constrained against the translation in all directions and rotations about column's major axis except the translation along the major axis at the top.

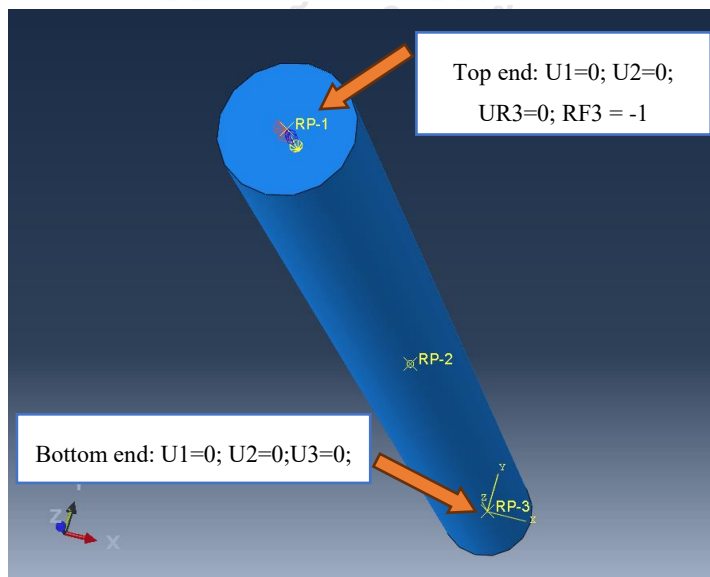


Figure 3.12 Column ends conditions (pin-ended)

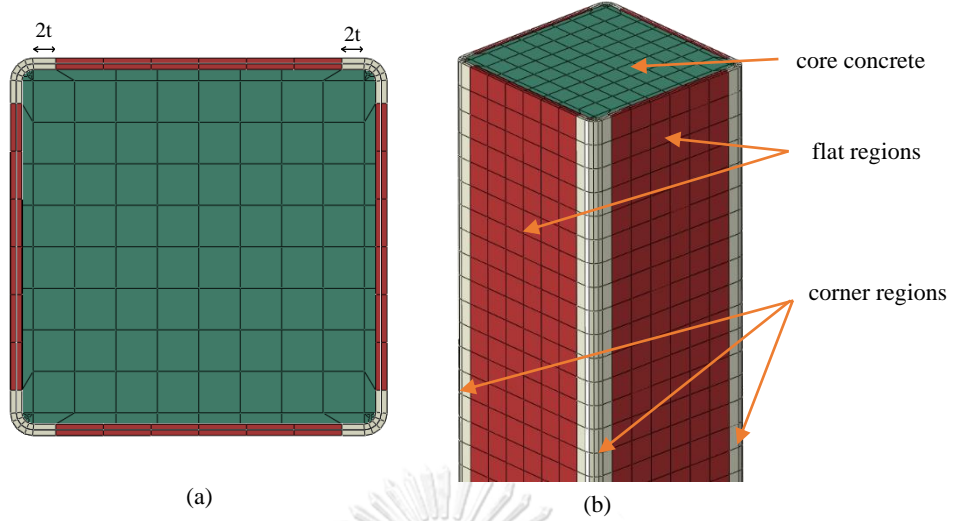


Figure 3.13 Corner regions of rectangular steel tube

3.3.4 LOADING TYPE

The loading plate was modeled as rigid-body element and tied to the surfaces of column using “Tie” constraint with the rigid plate acting as the master surface and column’s surface as the slave surface. Loadings were applied concentrically and statically to the reference point tied to the top surface of the column or the reference point on the loading plate. For stub column, displacement control was applied to load the column axially to 2% column’s length. Axially loading the stub column to any state beyond reaching 1% axial strain is already enough to terminate the analysis process. The author intentionally loads the column to 2% axial strain to gain a wide perspective of the loading curve trend. As mentioned by Uy et al. 2011 [10], the loading curve of stub column was classified into 3 types. The simulations result properly agreed with this statement as shown in Figure 3.14 in which columns corresponding to “Type A” and “Type B” curves were from the experimental programs of Uy et al. 2011 [10] while the one corresponding to “Type C” curve was a data from the current simulations. It can be presumed that loading the stub column to 2% axial strain was sufficient to depict its ascending and descending branch of the curve while the maximum load already occurred even with the axial strain less than 1% except for “Type A” curve column.

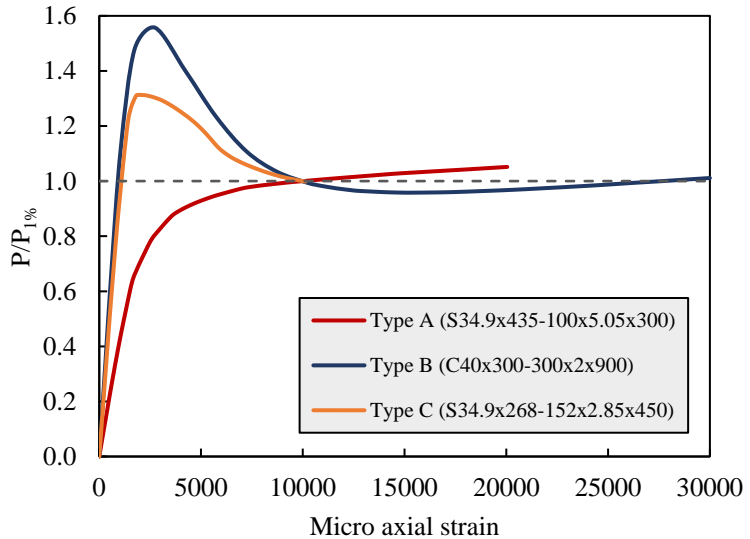


Figure 3.14 CFSST stub column loading curve

Due to complexity of the analysis involving nonlinearities including material (plasticity), boundary condition (contact problem) and geometric deformation (local and global buckling), the analysis is divided into multiple small increments in which loading magnitude is also divided according to each increment size. Material stiffness changes in each increment is accounted for by the reformulation of the stiffness matrix and the maximum increment size is set to 2% of the whole analysis size for circular stub column or 0.5% for rectangular stub column to avoid convergence difficulties from sudden stress or displacement jump.

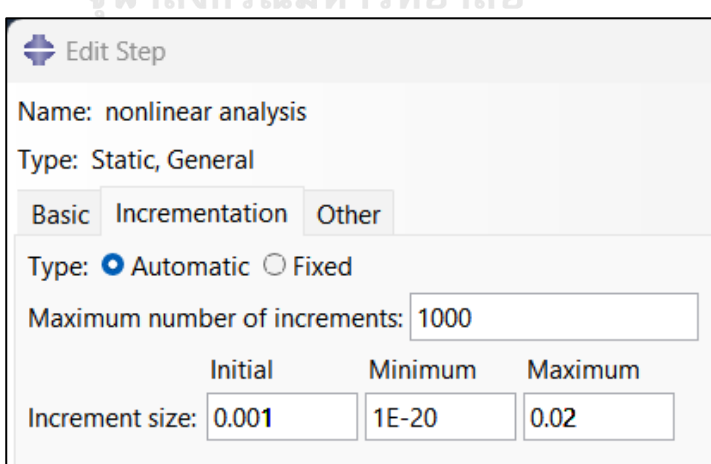


Figure 3.15 Increment size of stub columns nonlinear analysis

Smaller value for rectangular section is due to additional complexities of the corner region (both the material and mesh properties). These values are not fixed and

subjected to adjustment in some cases if the analysis has difficulties in converging. Based on these maximum increment sizes, each analysis needs approximately more than 50 and 200 increments for circular and rectangular stub column, respectively, where direct method is utilized to solve the global stiffness matrix as in the case of linear analysis. It is obvious that nonlinear analysis requires tremendous amount of computational resource comparing to linear one, not to mention possible multiple attempts in some increments if the solution fails to converge with the first attempt where its size will be then reduced to 25% its previous step and ABAQUS/STANDARD will attempt to repeat the analysis procedure using the new reduced-increment size. Had the analysis failed to converge, the solver will reduce the step size to another 25% of its previous size. This is called “cut-back” process, and the solver will terminate the analysis if the solution fails to converge within 5 cut-back iterations by default.

ABAQUS/STANDARD only grants access to adjusting the initial, minimum, and maximum increment size, and the subsequent increment size will be adjusted automatically by the solver which might lead to uneven step size. Therefore, it is hard to obtain the strength corresponding to the increment with exactly 1% axial strain, and linear interpolation between adjacent increment is used to calculate the 1% axial strain column strength. For slender columns, Static RIKS step with arc-length method was used to capture the post-buckling behavior of the member. Similar time-increment size was applied but the limit on the maximum increment size was larger than that of stub columns model since the algorithm can adjust the size automatically without strictly reducing the size to 25% its previous size if the solution of each increment fails to converge. Therefore, setting the maximum size to a very small value as in the case of stub columns would lead to long computational time and resources. The analysis process will be terminated as soon as the load-displacement curve start to descend, and maximum load is treated as the strength of the slender column (Figure 3.16).

3.3.5 CFSST COLUMN AXIAL STRENGTH DETERMINATION

The reaction force at the bottom and the displacement at mid-height are plotted in the axial force-displacement curve with the axial strength of the column

defined as the force at the peak point of the curve (Figure 3.16) for slender columns. For stub column, the axial strength is chosen to be the maximum load within 1% axial strain.

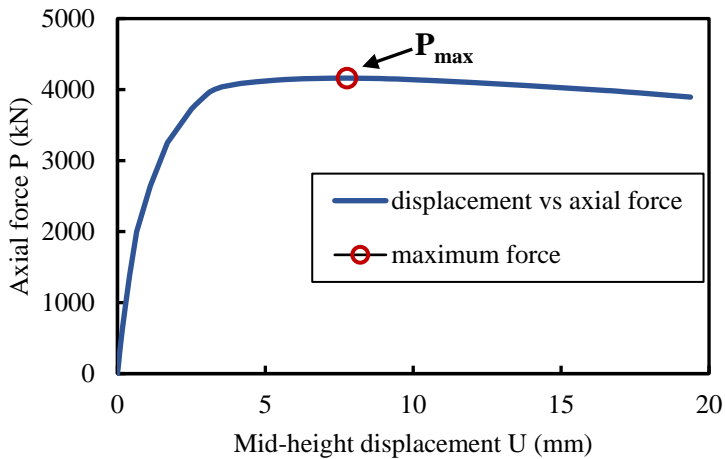


Figure 3.16 Typical mid-height displacement versus axial force curve

Alternatively, Tao et al. 2011 [25] used the Eq. (3.29) (derived from regression using type B and type C curve ultimate axial strain) to calculate the ultimate axial strain of the stainless-steel tubular columns for any curve type. Similarly, Han et al. 2022 [12] proposed Eqs. (3.30) & (3.31) to calculate the corresponding strain of the limit state for circular and square CFSST stub columns under axial compression.

$$\varepsilon_{cu} = 1850 + 13f_c' + (500 + 4.7f_c')\xi_c^{1.35} \quad (3.29)$$

$$\varepsilon_{scy} = 1300 + 12.5f_c' + (1950 + 6.27f_c')\xi_c^{0.4} \quad (3.30)$$

$$\varepsilon_{scy} = 1300 + 12.5f_c' + 1655\xi_c^{0.4} \quad (3.31)$$

In addition, the curve type could also be inferred to base on the confinement factor as shown in Table 3.3. However, these equations only came to our acknowledgement as the author has no intention of utilizing them to determine the ultimate limit state of CFSST stub columns since the determination from load-displacement curve is preferred to be more specific and to avoid possible error from regression equations.

Table 3.3 CFSST stub column curve type using confinement factor

Confinement factor	Load curve type
$\xi_c \geq 3.0$	Type A
$1.0 \leq \xi_c < 3.0$	Type B
$\xi_c < 1.0$	Type C

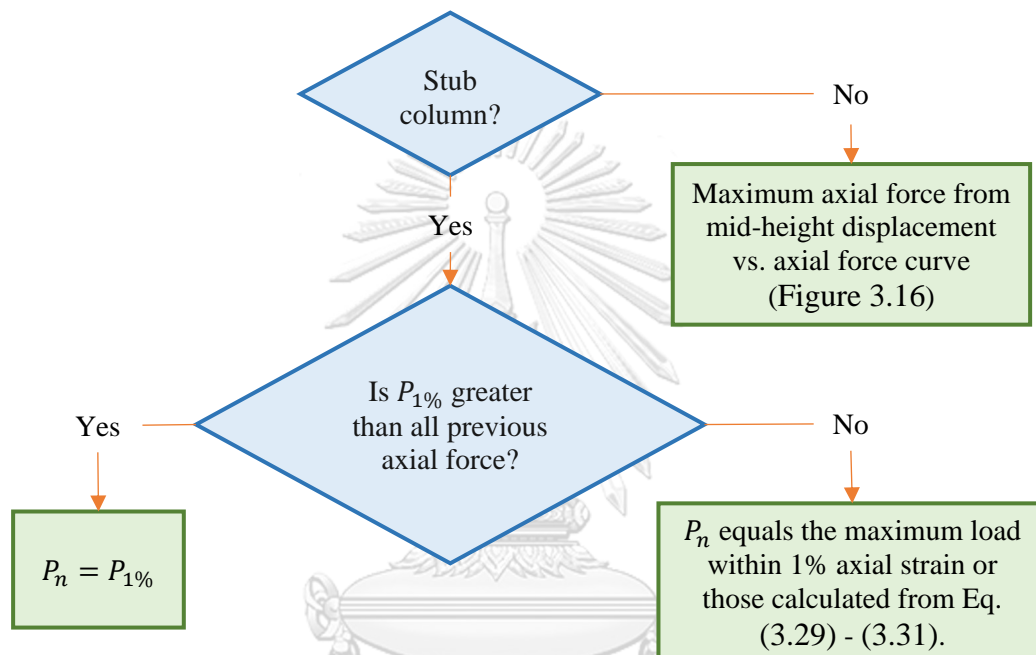


Figure 3.17 Flowchart of column axial strength determination from simulations and experimental tests

จุฬาลงกรณ์มหาวิทยาลัย

CHULALONGKORN UNIVERSITY

3.3.6 VERIFICATION OF THE FINITE-ELEMENT MODEL

A total of 40 CFSST column samples were modeled to compare with 24 stub column samples from Group I and 16 slender column samples from Group IV of the experimental program of Uy et al. 2011 [10].

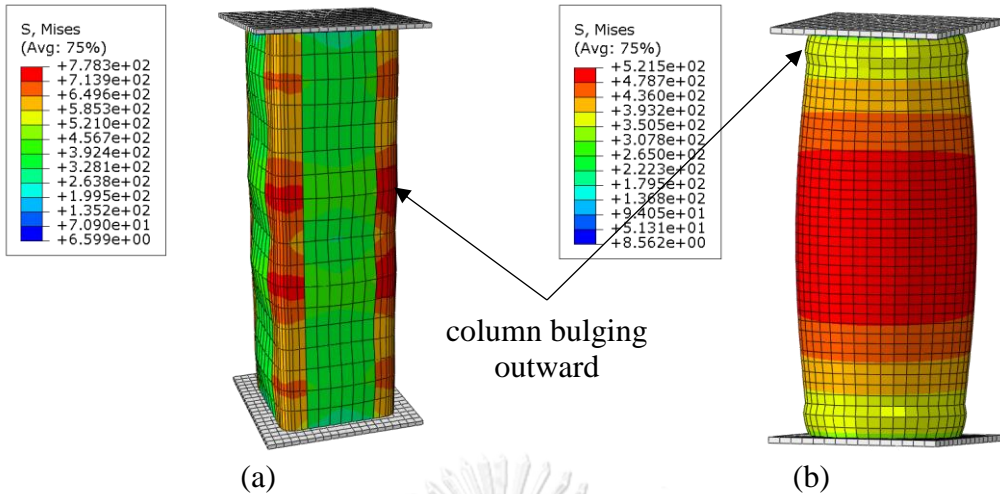


Figure 3.18 CFSST stub columns failure mode: (a) rectangular section (b) circular section

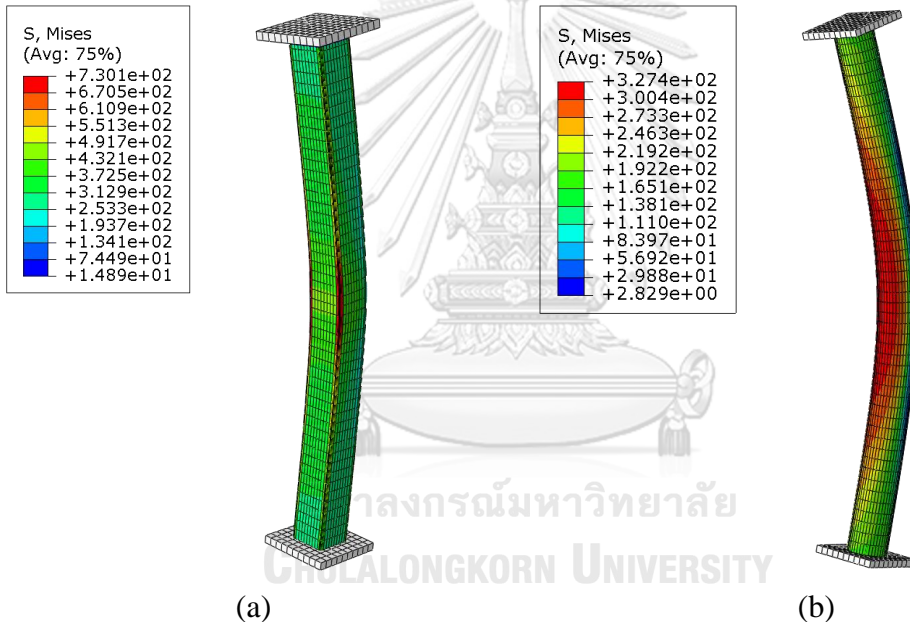


Figure 3.19 CFSST slender column failure mode: (a) rectangular section (b) circular column

There was no exact measurement of the initial global imperfection for the slender column group, and they were constructed in a manner that no initial imperfection occurred. However, it was not likely that they were perfectly straight columns and, thus, the imperfection value of $L_e / 20000$ was assumed by the current author to model the slender columns for validations purpose to those of Uy et al. 2011 [10]. The finite-element models demonstrated good agreement with the experimental values and, therefore, could be used to generate more CFSST columns data. Keep in mind that lower R-square value of the slender model not only came from the assumed

imperfection value, but also any unaware of imperfection in the experimental test (i.e., material strength, column dimensions) as the strength of sample C2-3a and C2-3b differed only by a small margin with concrete compressive strength of 36.3MPa and 75.4MPa, respectively. It is worth mentioning that this is also the reason these slender column data were only used to validate the finite-element models and not as the testing or training set in the machine learning process.

Table 3.4 Comparison of FEM models against the experimental programs

Nº	Type	Experimental name	P _{exp}	P _{FEM}	P _{FEM} / P _{exp}
1	Stub columns (Group I)	C20-50x1.2	109	114	1.049
2		C30-50x1.2	132	133	1.005
3		C20-50x1.6	136	137	1.007
4		C30-50x1.6	165	156	0.950
5		C20-100x1.6	424	368	0.868
6		C30-100x1.6	477	431	0.904
7		C20-127x1.6	675	483	0.716
8		C30-127x1.6	746	573	0.769
9		C20-150x1.6	809	627	0.776
10		C30-150x1.6	897	779	0.869
11		C20-200x2.0	1384	1034	0.747
12		C30-200x2.0	1536	1303	0.848
13		S20-50x2	239	203	0.851
14		S30-50x2	271	219	0.808
15		S20-50x3	361	384	1.062
16		S30-50x3	394	404	1.028
17		S20-100x3	711	653	0.918
18		S30-100x3	754	747	0.991
19		S20-100x5	1350	1319	0.977
20		S30-100x5	1448	1396	0.964
21		S20-150x3	1049	909	0.867
22		S30-150x3	1142	1232	1.080
23		S20-150x5	1801	1564	0.869
24		S30-150x5	1962	1714	0.874
25	Slender columns (Group IV)	C1-2a	579	544	0.939
26		C1-2b	851	843	0.991
27		C1-3a	358	416	1.163
28		C1-3b	732	543	0.741
29		C2-2a	446	374	0.838
30		C2-2b	693	625	0.902
31		C2-3a	383	283	0.738
32		C2-3b	390	395	1.013
33		S1-2a	697	693	0.994

Table 3.4 Comparison of FEM models against the experimental programs

Nº	Type	Experimental name	P_{exp}	P_{FEM}	$P_{\text{FEM}} / P_{\text{exp}}$
34		S1-2b	1023	1040	1.017
35		S1-3a	623	565	0.907
36		S1-3b	684	751	1.098
37		R1-2a	361	268	0.744
38		R1-2b	518	326	0.631
39		R1-3a	263	261	0.993
40		R1-3b	333	354	1.064

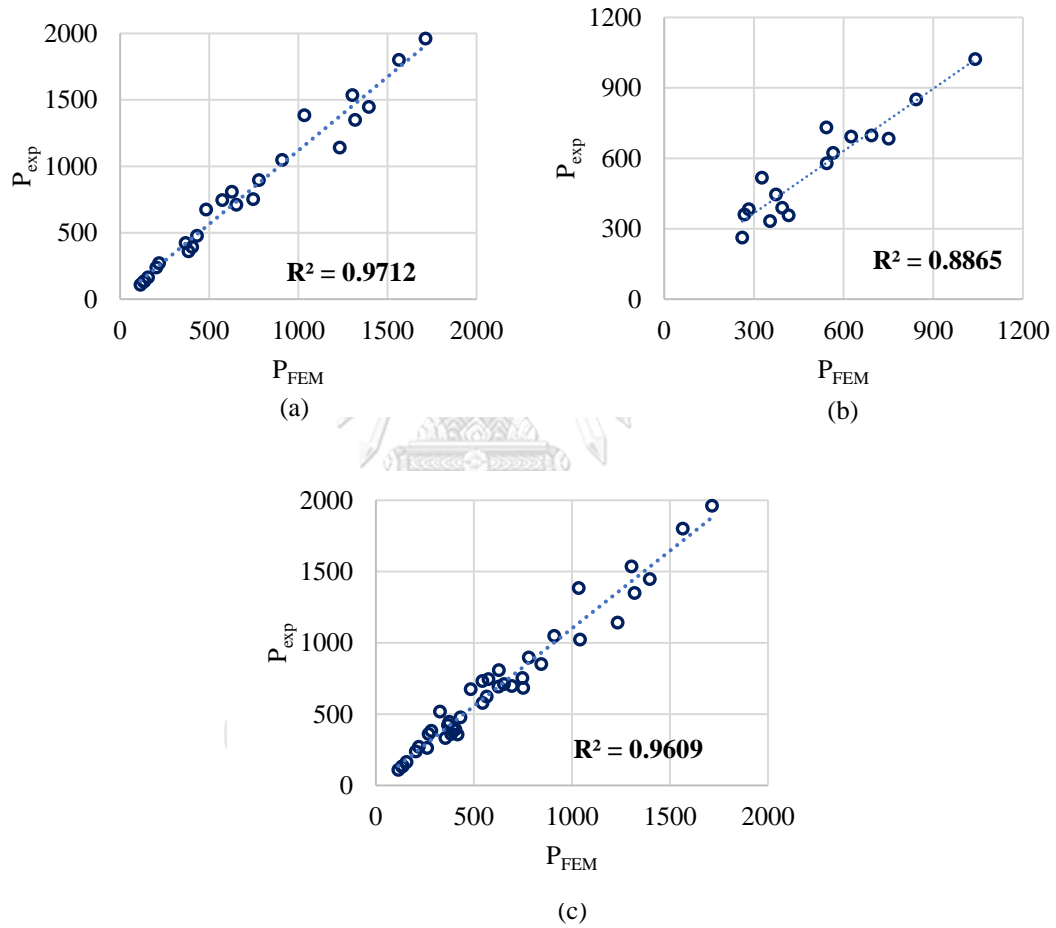


Figure 3.20 Verification of the FEM models: (a) stub columns, (b) slender columns (c) combined stub and slender columns

Additional comparison with the numerical program of Tao et al. 2011 [25] on stub rectangular columns were also made in which the confined concrete constitutive law was quite simpler than the current one and the effect of initial local imperfection was considered. The strengths of the current and their model had almost the same

values despite the initial imperfection neglected in the current model, thereby supporting the idea that this effect can be ignored.

Table 3.5 Comparison of the FEM models against the numerical programs

Nº	Type	Numerical name	P _{num}	P _{FEM}	P _{FEM} / P _{exp}
1	Stub columns	S20-50x2	201	203	1.010
2		S30-50x2	223	219	0.981
3		S20-50x3	362	384	1.060
4		S30-50x3	388	404	1.042
5		S20-100x3	736	653	0.887
6		S30-100x3	770	747	0.970
7		S20-100x5	1268	1319	1.040
8		S30-100x5	1323	1396	1.055
9		S20-150x3	966	909	0.941
10		S30-150x3	1212	1232	1.017
11		S20-150x5	1575	1564	0.993
12		S30-150x5	1709	1714	1.003

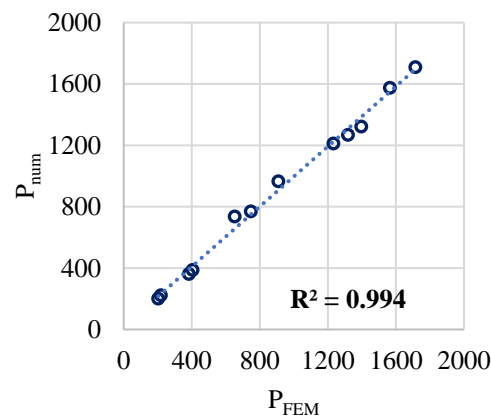


Figure 3.21 Verification of the FEM models against the numerical program

3.3.7 SIMULATED CFSST COLUMN DATA

Although we have already gathered substantial data of stub columns, an additional 1044 data consisting of both stub and slender CFSST columns have been simulated so far. For one specific column sample, either the strength of the concrete or stainless steel is changed to swiftly obtain new column data without having to repeat the modeling procedure for the same column sample over and over again. Usually, one sample is used to generate around 10 to 20 unique column data with different material strengths.

Note that the numbering of the simulated column data continues from those gathered from the experimental tests. This numbering will remain consistent throughout the whole work. The name of each column data starts with the letter “C”, “S”, and “R” to refer to circular, square, and rectangular section, respectively. It is then followed by the material and sectional properties. For instance, “C25x200-120x3x3000” refers to circular column with concrete and steel strength of 25MPa and 200MPa, respectively. The “-” sign was used to distinguish between material and dimensional properties. Therefore, this column has the section diameter, steel tube thickness and effective length of 120mm, 3mm, 3000mm, respectively. For rectangular columns, the dimensional properties are followed by section width, depth, steel tube thickness and column effective length.

Table 3.6 CFSST columns data from combined experimental and simulations

	Stub column		Slender column		Total
	Circular	Rectangular	Circular	Rectangular	
Literatures	47	25	12	0	84
Simulations	174	178	432	260	1044
Total	221	203	444	260	1128
Training	176	162	355	208	901
Testing	45	41	89	52	227



3.4 MACHINE LEARNING ALGORITHMS

3.4.1 GENERAL

Out of all the machine learning available, the Gaussian Process Regression (GPR) and the Extreme-Gradient Boost (XGBoost) are preferred by the current author. The algorithms are trained and tested using 80/20 rules in which 80% of the data is training set while the rest 20% is testing set. Table 3.7 briefly explains the pros and cons of both models. In addition to making predictions, the GPR also models the uncertainty (confident level) for each prediction as well, making it suitable for small data sets, while XGBoost focuses on making predictions from multiple weak learners (decision trees). Unlike linear regression where a general empirical formula is

proposed and then used to predict the value of new data, each algorithm here predicted the value of the new data (testing set) explicitly without developing any general formula.

Table 3.7 Pros and Cons of Gaussian Process Regression (GPR) and Extreme-Gradient Boost (XGBoost)

	Gaussian Process Regression	Extreme-Gradient Boost
Pros	<ol style="list-style-type: none"> 1. Probabilistic Predictions (prediction uncertainty) 2. Flexibility (Continuous or categorial data) 3. Incorporation of prior knowledge via kernel function 4. Small data set 5. Adaptive hyperparameter (can be learnt through maximum likelihood, eliminating manual tuning) 6. Interpolation and Extrapolation 7. Non-parametric (allows the model to capture and adapt to complex data pattern) 8. Scalability (SGPR and Parallelized GPR for large data set) 	<ol style="list-style-type: none"> 1. High predictive accuracy (combination of multiple weak learners) 2. Regularization (improve performance to unseen data) 3. Handling non-linear relationships 4. Efficient and suitable for large datasets 5. Flexibility (numerical and categorial features) 6. Easy to tune (Grid search or random search to find optimal hyperparameters)
Cons	<ol style="list-style-type: none"> 1. Not suitable for large data set 2. Computationally intensive due to its matrix operation 3. High memory usage with large data set or high-dimensional feature spaces. 4. Well-performed for interpolation while the opposite arises for extrapolation 	<ol style="list-style-type: none"> 1. Not suitable for very small datasets 2. Overfitting (if not properly tuned or the data set is small) 3. Complexity (for large number of trees) 4. Time-consuming and high memory usage during training

Gaussian Process Regression (GPR) is based on the concept of Gaussian processes, which are distributions over functions. It is developed based on multivariate normal distribution, kernels, non-parametric models, and joint and

conditional probability. Probability density function (PDF) is defined as shown in Eq. (3.32) for univariate variable (Figure 3.25) while the multivariate variable is in Eq. (3.33) where D is the number of the dimension, x represents the variable, μ is the mean vector of each independent variable and Σ is the $D \times D$ covariance matrix.

$$P_x(x) = \frac{1}{\sqrt{2\pi}\sigma} e^{-\frac{(x-\mu)^2}{2\sigma^2}} \quad (3.32)$$

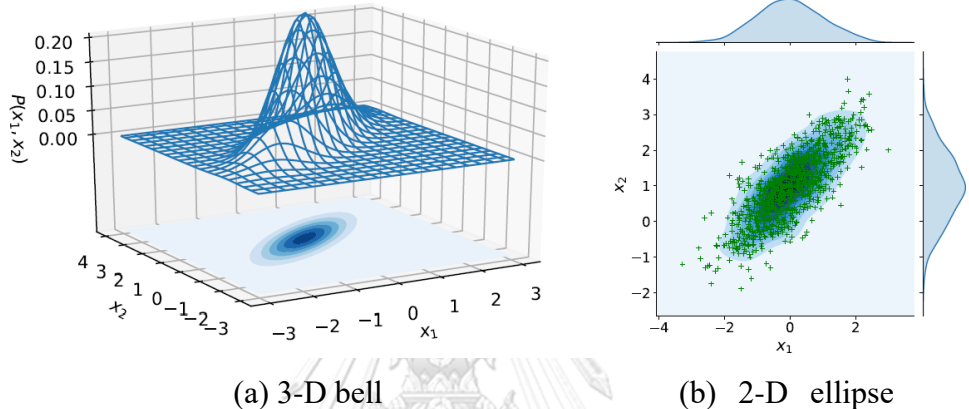


Figure 3.22 Multivariate normal distribution (Wang 2020 [34])

$$N(x|\mu, \Sigma) = \frac{1}{(2\pi)^{D/2} |\Sigma|^{1/2}} \exp\left[-\frac{1}{2}(x-\mu)^T \Sigma^{-1} (x-\mu)\right] \quad (3.33)$$

In GPR, we aim to model the underlying function that generates the observed data points. Instead of assuming a specific parametric form for the function, GPR treats the function as a random variable and places a prior distribution over it, typically assuming a Gaussian process prior. The prior distribution captures our beliefs about the smoothness and behavior of the underlying function. The key idea behind GPR is that the posterior distribution of the function, given the observed data, is also a Gaussian process. This means that we can compute the posterior distribution analytically, given the prior distribution and the observed data points. The posterior distribution provides a measure of uncertainty in the predictions and allows us to make predictions at any input point in the input space. For a set of data point, $D = \{(X_1, f_1), (X_2, f_2), (X_3, f_3)\}$, the joint gaussian multivariate distribution function with an assumed mean value of zero is written as

$$\begin{bmatrix} f_1 \\ f_2 \\ f_3 \end{bmatrix} \sim N \left(\begin{bmatrix} 0 \\ 0 \\ 0 \end{bmatrix}, \begin{bmatrix} k_{11} & k_{12} & k_{13} \\ k_{21} & k_{22} & k_{23} \\ k_{31} & k_{32} & k_{33} \end{bmatrix} \right)$$

Suppose that we want to predict the new function value, f_* , of the new data point which also follows normal distribution. The joint gaussian between the observed data points and the new point can be expressed as follows. Then the expected value and variance of the new function can be calculated from Eq. (3.34) and (3.35), respectively.

$$\begin{bmatrix} f \\ f_* \end{bmatrix} \sim N \left(\begin{bmatrix} 0 \\ 0 \end{bmatrix}, \begin{bmatrix} k_{11} & k_{12} & k_{13} & k_{1*} \\ k_{21} & k_{22} & k_{23} & k_{2*} \\ k_{31} & k_{32} & k_{33} & k_{3*} \\ k_{*1} & k_{*2} & k_{*3} & k_{**} \end{bmatrix} \right)$$

$$\mu_* = E(f_*) = K^T K^{-1} f \quad (3.34)$$

$$\sigma_* = K_* K^{-1} K_* + K_{**} \quad (3.35)$$

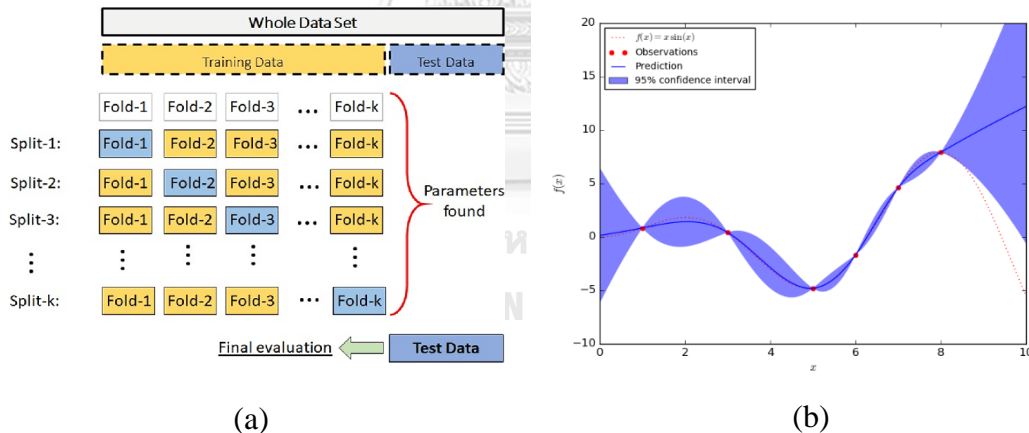
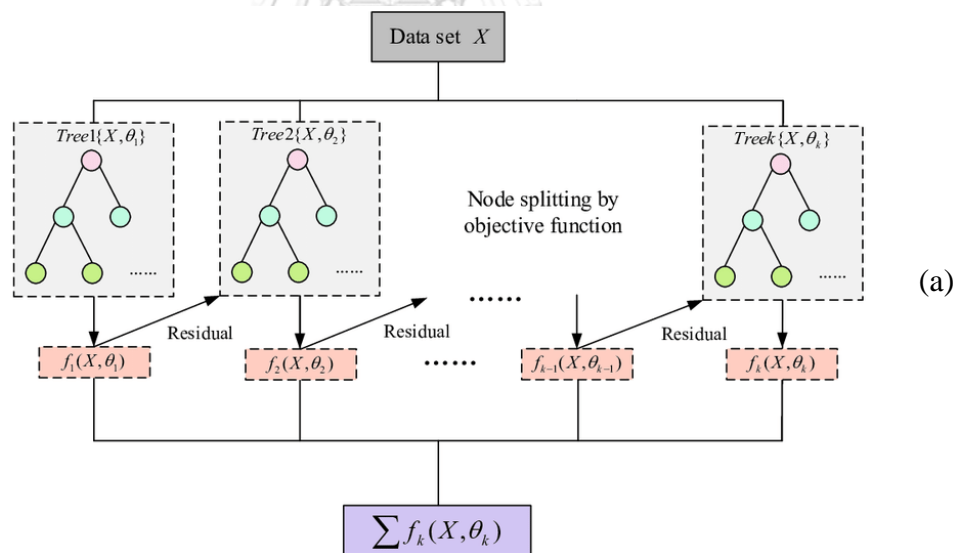


Figure 3.23 Gaussian Process Regression: (a) K-fold cross validation, (b) comparison between prediction and confident intervals of a function

In the GPR codes, the K-fold cross validation was performed to tune for optimal parameters. The whole data was first split into training and testing set, then the former one will be separated into, in our case, 10 folds where the first iteration treat the first fold and the rest as testing and training set, respectively. The process keeps repeating itself, treating the next fold as the testing set in the next iteration and the rest as training set and so on. For each iteration, the statistical accuracy

measurement parameters (R^2 , RMSE, MAE) were calculated and the average of those will be obtained at the end of the process. Be aware of the domain of testing data while making predictions using GPR since the predicted value tends to diverge significantly if one had to perform extrapolation as shown in Figure 3.23 (b) which is one of the disadvantages as described in Table 3.7.

The Extreme Gradient Boost (XGBoost) operates by sequentially adding weak predictive models, typically decision trees, to an ensemble, with each subsequent model correcting the errors of its predecessors (Figure 3.24 (a)). XGBoost employs a novel approach to gradient boosting, emphasizing both model performance and computational efficiency. It optimizes a loss function by iteratively fitting new trees to the negative gradient of the loss with respect to the predictions. Similar to GPR, grid search technique could be utilized to tune for optimal parameters. However, the code packages of XGBoost the author currently used didn't come with this function and the default values of all hyperparameters were left in their pristine condition.



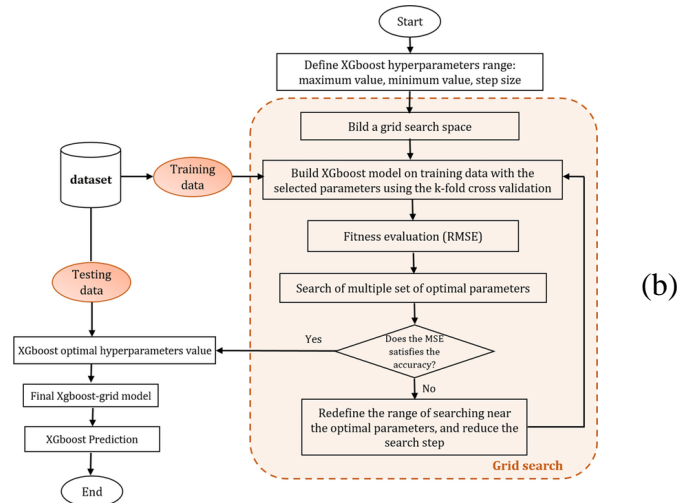


Figure 3.24 XGBoost (a) decision tree (b) grid search for optimal hyperparameters

Overall, the Gaussian Process Regression focuses on modeling functions and their uncertainty, making it suitable for cases with limited data and a need for probabilistic predictions. On the other hand, Extreme Gradient Boosting focuses on predictive accuracy by combining decision trees, making it more versatile for a wide range of tasks and larger datasets.

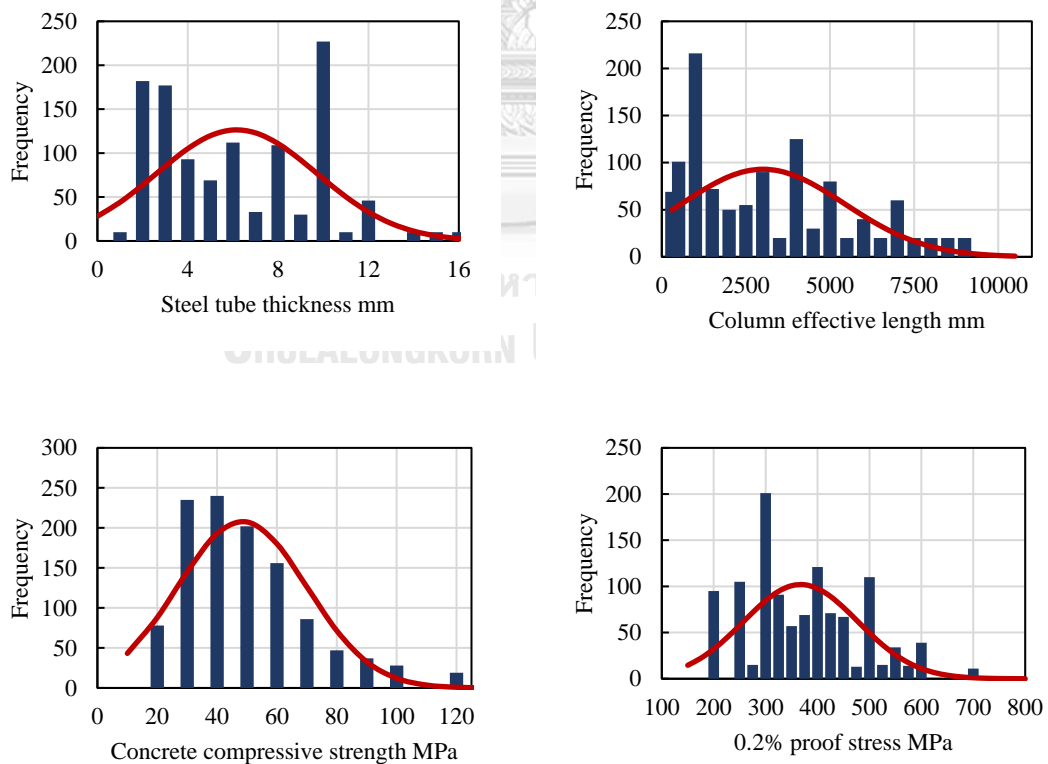
3.4.2 MACHINE LEARNING TRAINING PROCESS

Basic training input parameters are as shown in Table 3.8 to be used as training input parameters for the machine learning for both rectangular and circular sections as well as stub and slender columns. To develop and validate prediction accuracy of a model, a few things are required to be done first. To begin with, a large amount of data must be well prepared, which in this case is the data collected from the literature (Table 2.1) combined with those from the simulations (0). A subset of the data called the training set is then used to train the models while the rest, which is the testing set, is used to test the prediction accuracy of the models. In this work, the author split the data into two sets comprising 80% and 20% of the total data for training and testing, respectively, in a manner that as many as possible experimental column data used as the testing sets. Both stub and slender columns data were allocated accordingly to the aforementioned percentages.

Table 3.8 Training input parameters of each machine learning model

		Machine learning model			
		Stub-column		Slender-column	
		Circular	Rectangular	Circular	Rectangular
Training input parameters	f'_c	✓	✓	✓	✓
	$\sigma_{0.2}$	✓	✓	✓	✓
	D	✓	✓	✓	✓
	B	✗	✓	✗	✓
	t	✓	✓	✓	✓
	L_e	✗	✗	✓	✓

Each property of the column training input parameter is assumed to follow the normal distribution (Figure 3.25). The distribution of section width (B) is quite sparse since the majority of the columns' data are of circular section.



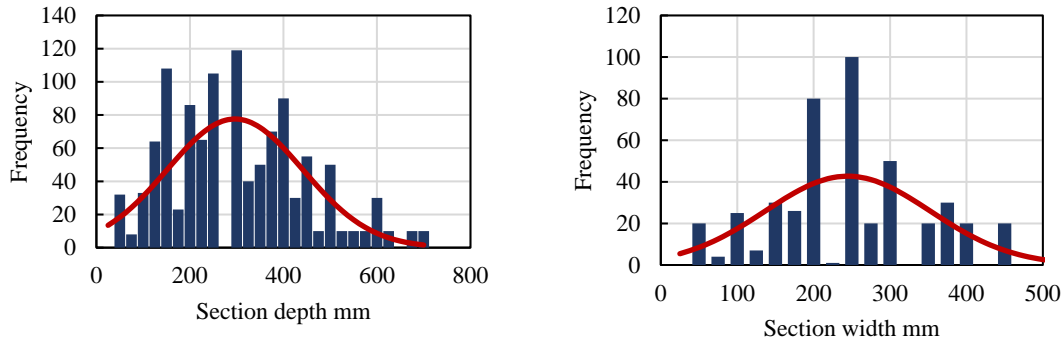


Figure 3.25 Normal distribution of column properties

Table 3.9 Machine learning model input parameters statistical properties

Notation	Minimum	Maximum	Mean	Variance	Standard deviation
B	50	580	244.6	11684	108
D	50	680	296.4	21026	145
t	1	16	6.2	13	4
L _e	150	8800	3010.4	5855706	2420
f _{c'}	20	120	48.4	468	22
σ _{0.2}	200	700	367.6	12159	110

3.4.3 STATISTICAL ACCURACY MEASUREMENT PARAMETERS

The statistical accuracy measurement parameters considered include R-square value or the coefficient of determination (R^2), mean actual error (MAE), and root mean square error (RMSE) calculated from Eqs. (3.36)-(3.38), respectively.

$$R^2 = 1 - \frac{\sum_{i=1}^n (P_i - \bar{P}_i)^2}{\sum_{i=1}^n (P_i - \mu_p)^2} \quad (3.36)$$

$$MAE = (1/n) \sum_{i=1}^n |P_i - \bar{P}_i| \quad (3.37)$$

$$RMSE = \sqrt{\frac{\sum_{i=1}^n (P_i - \bar{P}_i)^2}{n-1}} \quad (3.38)$$

where n , P_i , \bar{P}_i , and μ_p are the number of testing data, actual column strength, predicted column strength of regression line obtained from the relationship between actual columns data and predicted columns strength from machine learning algorithms, and mean predicted column compressive strength, respectively. The mean square error and root mean square error, statistically speaking, are just variance and standard deviation with all columns data treated as a sample while the population consists of infinite columns data.

3.5 CFSST COLUMN AXIAL STRENGTH DETERMINATION FROM STANDARD SPECIFICATIONS

3.5.1 EUROCODE 4

3.5.1.1 GENERAL

The “EN 1994-1-1 (2004) Eurocode 4: Design of composite steel and concrete structures – Part 1-1: General rules and rules for buildings” [35] (referred to as EC4, Eurocode 4 or Eurocode in the rest of this document) provided both general and simplified approaches for the design of composite structures with the latter adopted in this work. Since the standard only provided the specifications regarding the low-carbon and not the stainless steel, this leaves the author with no choice but to analyze the columns as if they were made of low-carbon steel. Further modification shall be made when stainless-steel formulations are available. All formulations and notations so far are based on the American standards such as the modulus of elasticity of concrete, modulus of rupture of concrete, etc. Thus, it is worth mentioning the essential notation and formulas needed in the case of EC4.

Nomenclature	
A	cross sectional area
A_c	cross sectional area of concrete
A_s	cross-sectional area of reinforcement
E_c	tangent modulus of elasticity of normal weight concrete at a stress of $\sigma_c = 0$
$E_{c(28)}$	tangent modulus of elasticity and at 28 days
$E_{c,eff}$	effective modulus of elasticity of concrete
E_{cd}	design value of modulus of elasticity of concrete
E_{cm}	secant modulus of elasticity of concrete
$E_c(t)$	tangent modulus of elasticity of normal weight concrete at a stress of

	$\sigma_c = 0$ and at time t
EI	bending stiffness
I	second moment of area of concrete section
L	length
M	bending moment
M_{Ed}	design value of the applied internal bending moment
N	axial force
N_{Ed}	design value of the applied axial force (tension or compression)
I_a	moment of inertia of structural steel
I_c	moment of inertia of concrete
N_{cr}	elastic critical buckling load
ULS	Ultimate Limit State
e	eccentricity
f_c	compressive strength of concrete
f_{cd}	design value of concrete compressive strength
f_{ck}	characteristic compressive cylinder strength of concrete at 28 days
f_{cm}	mean value of concrete cylinder compressive strength
f_y	yield strength of reinforcement
f_{yd}	design yield strength of reinforcement
f_{yk}	characteristic yield strength of reinforcement
i	radius of gyration
t	thickness, time being considered
t_0	the age of concrete at the time of loading
u	perimeter of concrete cross-section, having area A_c
x	neutral axis depth
α	angle, ratio
β	angle, ratio, coefficient
γ	partial factor
γ_c	partial factor for concrete
γ_s	partial factor for reinforcing or prestressing steel
γ_m	partial factor for a material property, taking account only of uncertainties in the material property itself, in geometric deviation and in the design model used
λ	slenderness ratio
v	poisson's ratio
$\varphi(t, t_0)$	creep coefficient, defining creep between times t and t_0 , related to elastic deformation at 28 days
$\varphi(\infty, t_0)$	final value of creep coefficient

3.5.1.2 MATERIAL PROPERTY

The design value of each material is reduced by corresponding partial factor depending on the Service Limit State (SLS) or the Ultimate Limit State (ULS). For

the latter, the partial factor for concrete and steel are 1.15 and 1, respectively. However, we are employing the standard to estimate the maximum capacity of the member without considering reduction factor regarding the safety design, thus, the partial factors of the material of the EC4 standard are omitted. The secant modulus of elasticity of concrete (E_{cm}) is given by Eq. (3.41). where f_{cm} is in MPa calculated from Eq. (3.42).

$$\text{for concrete} \quad f_{cd} = f_{ck} \quad (3.39)$$

$$\text{for steel} \quad f_{yd} = f_{yk} \quad (3.40)$$

$$E_{cm} = 22 \left(\frac{f_{cm}}{10} \right)^{0.3} \text{ (GPa)} \quad (3.41)$$

$$f_{cm} = f_{ck} + 8 \text{ MPa} \quad (3.42)$$

3.5.1.3 LIMITATIONS AND ASSUMPTIONS

The local buckling effect can be neglected in the design process provided the maximum slenderness limits in Table 6.3 of EC4 standard are not exceeded which can be summarized as follows.

$$\text{for circular steel section} \quad \max\left(\frac{d}{t}\right) = 90 \left(\frac{235}{f_y} \right) \quad (3.43)$$

$$\text{for rectangular steel section} \quad \max\left(\frac{h}{t}\right) = 52 \sqrt{\frac{235}{f_y}} \quad (3.44)$$

The specifications also provided the formulations to modify the concrete compressive strength in case of confined concrete, $f_{ck,c}$, depending on the effective lateral compressive stress, σ_2 , at the ULS due to confinement as calculated by Eqs. (3.45) & (3.46). Since there are no reports on the value of σ_2 , this modification is ignored, and the compressive strength of unconfined concrete is used instead. If this enhancement could be accounted for, the author expected significant improvement in its accuracy, especially for slender rectangular column (Figure 4.3).

$$\text{for } \sigma_2 \leq 0.05f_{ck}, \quad f_{ck,c} = f_{ck} \left(1 + 5\sigma_2 / f_{ck} \right) \quad (3.45)$$

$$\text{for } \sigma_2 > 0.05f_{ck}, \quad f_{ck,c} = f_{ck} \left(1.125 + 2.5\sigma_2 / f_{ck} \right) \quad (3.46)$$

The effect of creep in concrete should also be accounted for by reducing the value of E_{cm} to $E_{c,eff}$, where $N_{G,Ed}$ is the permanent part of normal force. Suppose the columns are loaded at the age of 28 days (as in the experimental tests from the literatures), the effect of creep can be omitted from the calculation procedure. This assumption leads to creep coefficient equal to zero and E_{cm} as $E_{c,eff}$. If this effect is to be accounted for, detailed formulas can be found in Annex B of the EN 1992-1-1:2004 [36]. Another limitation for the use of the “Simplified Method of Design” of EC4 was that it was limited to members of doubly symmetrical with uniform cross-section over the member length with rolled, cold formed or welded steel sections, and the relative slenderness, $\bar{\lambda}$, defined in the subsequent section, not exceeding two.

$$E_{c,eff} = E_{cm} \frac{1}{1 + (N_{G,Ed} / N_{Ed})\varphi_t} \quad (3.47)$$

3.5.1.4 LOCAL BUCKLING EFFECT

Unless the section slenderness limits are not exceeded, the local buckling effect must be accounted for as provided by section 4.4 of EN 1993-1-5:2006 standard [37], where the effective steel sectional-area ($A_{s,eff}$) is obtained by multiplying the reduction factor (ρ) by the initial area (A_s). The steel elements in our study case are assumed to behave as internal compression elements with equal compression stress on each outer side of the plate ($\sigma_1 = \sigma_2$) where the reduction factor can be calculated as follows.

$$A_{s,eff} = \rho A_s \quad (3.48)$$

for $\bar{\lambda}_p \leq 0.5 + \sqrt{0.085 - 0.055\psi}$,

$$\rho = 1 \quad (3.49)$$

for $\bar{\lambda}_p > 0.5 + \sqrt{0.085 - 0.055\psi}$,

$$\rho = \frac{\bar{\lambda}_p - 0.055(3 + \psi)}{\bar{\lambda}_p^2} \leq 1 \quad (3.50)$$

where ψ , \bar{b} , k_σ and σ_{cr} are the stress ratio, appropriate width, buckling factor corresponding to the stress ratio ψ and boundary conditions, and the elastic critical plate buckling stress, respectively.

$$\psi = \sigma_2 / \sigma_1 = 1 \quad (3.51)$$

$$\varepsilon = \sqrt{235 / f_y} \quad (3.52)$$

$$\bar{\lambda}_p = \sqrt{\frac{f_y}{\sigma_{cr}}} = \frac{\bar{b} / t}{28.4 \varepsilon \sqrt{k_\sigma}} \quad (3.53)$$

The appropriate width \bar{b} is to be taken as $b - 3t$ and D for rectangular hollow section and circular section, respectively. Furthermore, the buckling factor (k_σ) equals to four for the case of internal compression elements with equal stresses. If section slenderness limit is reached, the equivalent effective steel thickness corresponding to the effective area can be analytically calculated through the scheme of which the perimeter of the concrete core remains the same.

for circular section,

$$A_{s,eff} = \frac{\pi}{4} [(D - 2t + 2t_e)^2 - (D - 2t)^2] \quad (3.54)$$

for rectangular section,

$$A_{s,eff} = (B - 2t + 2t_e)(D - 2t + 2t_e) \quad (3.55)$$

Eqs. (3.54) and (3.55) can be manipulated and arranged into the form of quadratic equations of which the roots are the effective steel thicknesses to be solved for from Eq. (3.56) where:

$$a_1 = 1, a_2 = D, a_3 = -(1/\pi)A_{s,eff} \quad \text{for circular section}$$

$$a_1 = 4, a_2 = 2(B + D - 4t), a_3 = -A_{s,eff} \quad \text{for rectangular section}$$

$$t_e = \frac{-a_2 + \sqrt{a_2^2 - 4a_1a_3}}{2a_1} \quad (3.56)$$

3.5.1.5 NOMINAL AXIAL COMPRESSIVE STRENGTH

The plastic resistance to compression of a composite cross-section ($N_{pl,Rd}$) can be calculated by adding the plastic resistances of its components (Eq. (3.57)). For circular concrete-filled section, the increase in strength resulted from the confinement effect of the steel tube can be accounted for using Eq. (3.58), provided that the relative slenderness ($\bar{\lambda}$), calculated from Eq. (3.59), does not exceed 0.5.

$$N_{pl,Rd} = A_s f_{yd} + A_c f_{cd} \quad (3.57)$$

$$N_{pl,Rd} = \eta_{ao} A_s f_{yd} + A_c f_{cd} \left(1 + \eta_{co} \frac{t}{D} \frac{f_y}{f_{ck}} \right) \quad (3.58)$$

$$\bar{\lambda} = \sqrt{N_{pl,Rk} / N_{cr}} \quad (3.59)$$

where $\eta_{ao} = 0.25(3 + 2\bar{\lambda}) \leq 1.0$; $\eta_{co} = 4.9 - 18.5\bar{\lambda} + 17\bar{\lambda}^2 \geq 0$

$N_{pl,Rk}$ the characteristic value of the plastic resistance to compression

$$= A_s f_{yk} + A_c f_{ck}$$

N_{cr} the elastic critical normal force for the relevant buckling mode

$$= \frac{\pi^2 (EI)_{eff}}{L^2}$$

$(EI)_{eff}$ effective flexural stiffness

$$= E_s I_s + K_c E_{cm} I_c$$

As already mentioned that although the standard suggested the effect of creep to be included in the design which can be done by replacing E_{cm} with $E_{c,eff}$, it is neglected here and K_c was a correction factor taken as 0.6. For slender columns, the design value should satisfy (3.60) where χ is the reduction factor for the relevant buckling mode given in EN 1993-1-1, 6.3.1.2 in terms of the relative slenderness, and α is the imperfection factor for buckling curve taken as 0.21.

$$\frac{N_{Ed}}{\chi N_{pl,Rd}} \leq 1.0 \quad (3.60)$$

$$\chi = \frac{1}{\Phi + \sqrt{\Phi^2 - \bar{\lambda}^2}} \leq 1.0 \quad (3.61)$$

$$\Phi = 0.5 \left[1 + \alpha (\bar{\lambda} - 0.2) + \bar{\lambda}^2 \right] \quad (3.62)$$

Input:

steel tube diameter $D = 450\text{mm}$

steel tube thickness $t = 5\text{mm}$

characteristic concrete compressive strength $f_{ck} = 30\text{MPa}$

steel tube characteristic yield strength $f_{yk} = 300\text{MPa}$

column effective length $L = 4500\text{mm}$

design concrete compressive strength $f_{cd} = f_{ck} = 30\text{MPa}$

design steel yield strength $f_{yd} = f_{yk} = 300\text{MPa}$

Solution:

- check local buckling effect

assume nominal steel yield strength $f_y = f_{yk} = 300\text{MPa}$

for circular section $\max\left(\frac{d}{t}\right) = 90 \left(\frac{235}{f_y} \right) = 90 \left(\frac{235}{300} \right) = 70.5$

Since $\left(\frac{D}{t}\right) = \frac{450}{5} = 90 > 70.5$, local buckling effect must be considered.

We have $\psi = 1$, $k_\sigma = 4$, $\varepsilon = \sqrt{\frac{235}{f_y}} = 0.885$ and $\bar{b} = D = 450\text{mm}$

$$\text{then } \bar{\lambda}_p = \frac{(\bar{b}/t)}{28.4\epsilon\sqrt{k_\sigma}} = \frac{90}{28.4 \times 0.885 \times \sqrt{4}} = 1.79$$

$$\text{because } \bar{\lambda}_p > 0.5 + \sqrt{0.085 - 0.055\psi} = 0.673, \text{ then } \rho = \frac{1.79 - 0.055(3+1)}{1.79^2} = 0.49$$

$$\text{concrete area } A_c = \frac{\pi}{4}(450 - 2 \times 5)^2 = 152053 \text{ mm}^2$$

$$\text{steel tube area } A_s = \frac{\pi}{4} \times 450^2 - 152053 = 6990 \text{ mm}^2$$

$$\text{effective steel area } A_{s,\text{eff}} = 0.49 \times 6990 = 3425 \text{ mm}^2$$

$$\text{We then get } a_1 = 1, a_2 = 450 \text{ mm}, a_3 = -(1/\pi) \times 3425 = -1090 \text{ mm}^2$$

$$\Rightarrow \Delta = 450^2 - 4(1)(-1090) = 197960 \text{ mm}^2$$

$$\text{equivalent steel tube thickness } t_e = \frac{-450 + \sqrt{197960}}{2} = 2.464 \text{ mm} \approx 2.5 \text{ mm}$$

The sectional properties with $t_e = 2.5 \text{ mm}$ as the steel tube thickness are as follows:

$$D = 450 - 2 \times 5 + 2 \times 2.5 = 445 \text{ mm}$$

$$A_s = \frac{\pi}{4} \times 445^2 - 152053 = 3475 \text{ mm}^2$$

$$I_c = \frac{\pi}{64} (445 - 2 \times 2.5)^4 = 18.4 \times 10^8 \text{ mm}^4$$

$$I_s = \frac{\pi}{64} \times 445^2 - 18.4 \times 10^8 = 0.85 \times 10^8 \text{ mm}^4$$

- nominal axial compressive strength

$$\text{relative slenderness } \bar{\lambda} = \sqrt{\frac{N_{pl,Rk}}{N_{cr}}}$$

$$N_{pl,Rk} = (3475 \times 300 + 152053 \times 30) \times 10^{-3} = 5604.2 \text{ kN}$$

$$(EI)_{\text{eff}} = (2 \times 10^5 \times 0.85 \times 10^8 + 0.6 \times 32836.5 \times 18.4 \times 10^8) \times 10^{-9} = 53261.6 \text{kN}\cdot\text{m}^2$$

$$N_{\text{cr}} = \frac{\pi^2 \times 53261.6}{4.5^2} = 25959 \text{kN}$$

$$\Rightarrow \lambda = \sqrt{\frac{5604.2}{25959}} = 0.465$$

Since $\lambda < 0.5$, then $N_{\text{pl.Rd}} = \eta_{\text{ao}} A_s f_{\text{yd}} + A_c f_{\text{cd}} \left(1 + \eta_{\text{co}} \frac{t}{D} \frac{f_y}{f_{\text{ck}}} \right)$

$$\eta_{\text{ao}} = 0.25(3 + 2 \times 0.465) = 0.982 < 1$$

$$\eta_{\text{co}} = 4.9 - 18.5 \times 0.465 + 17 \times 0.465^2 = -0.026 < 0 \Rightarrow \eta_{\text{co}} = 0$$

$$\Rightarrow N_{\text{pl.Rd}} = (0.982 \times 3475 \times 300 + 152053 \times 30) \times 10^{-3} = 5585.8 \text{kN}$$

$$\Phi = 0.5 [1 + 0.21 \times (0.465 - 0.2) + 0.465^2] = 0.636$$

buckling mode reduction factor $\chi = \frac{1}{0.636 + \sqrt{0.636^2 - 0.465^2}} = 0.935 < 1.0$

We then obtain $N_{\text{Ed}} = 0.935 \times 5585.8 = 5222.2 \text{kN}$

Therefore, the axial force on this slender column must not exceed $N_{\text{Ed}} = 5222.2 \text{kN}$, which is the allowable axial compressive strength.

3.5.2 ANSI/AISC 360-22

3.5.2.1 GENERAL

This section provides general design specifications of concrete-filled steel tubular columns from the “ANSI/AISC 360-22 An American National Standard Specification for Structural Steel Buildings”. The standard proposed two methods for compressive strength analysis of filled concrete columns including Load Resistance Factor Design (LRFD) and Allowable Strength Design (ASD) with corresponding compressive strength called the Design Compressive Strength and Allowable Compressive Strength, respectively. Our main purpose is to compare the predictive

compressive strength obtained from the model with the nominal compressive strength from the design standard, not with the design nor allowable compressive strength.

$$\text{LRFD} \quad P_u \leq \phi_c P_n \quad (3.63)$$

$$\text{ASD} \quad P_s \leq P_n / \Omega_c \quad (3.64)$$

3.5.2.2 LIMITATIONS

The concrete compressive strength shall not be less than 21MPa nor more than 69MPa and not less than 21MPa nor more than 41MPa for normal and lightweight concrete, respectively. Also, the specified minimum yield stress of structural steel shall not exceed 525MPa. Any design attempt outside these limitations shall be in accordance with Appendix 2 of the standard, which expanded to the determination of only rectangular filled composite members with either the specified minimum yield stress of structural steel exceeding 525MPa but not exceeding 690MPa or the specified compressive strength exceeding 69MPa but not exceeding 100MPa and the maximum permitted width-to-thickness ratio for compression steel elements of $5\sqrt{E/F_y}$.

For filled composite members, the cross-sectional area of the structural steel shall comprise at least 1% of the total composite cross section. These limitations are not exhaustive since there are other rules regarding structural rebar (if any) in the composite section, but it is none of our concern because it is not used herein. Not all of our column's data are within the range of these limitations since the compressive strength of concrete and steel yield stress of structural steel are up to 120MPa and 700MPa, respectively. They are thus ignored, and the formulas provided in Appendix 2 will still be used for the columns exceeding the limitations in section I1.3 even though the Appendix 2 limitations themselves are not met.

3.5.2.3 SECTION CLASSIFICATION FOR LOCAL BUCKLING EFFECT

For filled concrete column, the section is classified into three categories for local buckling effect including compact, noncompact and slender-element composite

section according to slenderness ratio. Each section is classified as compact composite if the maximum width-to-thickness ratio, λ , of its compression steel elements does not exceed the limiting width-to-thickness ratio, λ_p . The section is classified as noncompact composite if its width-to-thickness ratio exceeds λ_p but is less than or equal to the width-to-thickness ratio limit for slender-element composite section, λ_r . In case λ exceeds λ_r , the section is then classified as slender-element composite section. The maximum permitted value of width-to-thickness ratio shall be as specified as shown in the table below.

Table 3.10 Limiting Width-to-Thickness Ratios for Compression Steel Elements in Composite Members Subjected to Axial Compression

Description of Element	Width-to-Thickness Ratio	Compact Composite /Noncompact composite	Noncompact Composite/Slender -Element Composite	Maximum Permitted
Walls of rectangular HSS and box sections of uniform thickness	b/t	$2.26\sqrt{E/F_y}$	$3.00\sqrt{E/F_y}$	$5.00\sqrt{E/F_y}$
Round HSS	D/t	$0.15E/F_y$	$0.19E/F_y$	$0.31E/F_y$

3.5.2.4 NOMINAL AXIAL COMPRESSIVE STRENGTH

The nominal axial compressive strength of filled composite members is calculated based on the ratio of P_{no} / P_e where P_{no} , P_e , $(EI)_{eff}$ and C_3 are the nominal axial compressive strength without length effects consideration, elastic critical buckling load, effective stiffness of composite section and coefficient for calculation of effective rigidity, respectively. The confinement effect between the steel tube and core concrete were accounted for via the modification of the effective stiffness, $(EI)_{eff}$, and the critical buckling stress (F_n).

$$\text{if } \frac{P_{no}}{P_e} \leq 2.25, \quad P_n = P_{no} \left(0.658^{P_{no}/P_e} \right) \quad (3.65)$$

$$\text{if } \frac{P_{no}}{P_e} > 2.25, \quad P_n = 0.877 P_e \quad (3.66)$$

$$P_e = \frac{\pi^2 (EI)_{eff}}{L_c^2} \quad (3.67)$$

$$(EI)_{eff} = E_s I_s + C_3 E_c I_c \quad (3.68)$$

$$C_3 = 0.45 + 3(A_s / A_g) \leq 0.9 \quad (3.69)$$

- for compact composite sections

$$P_{no} = P_p \quad (3.70)$$

where P_p is plastic axial compressive strength calculated from Eq. (3.71) and C_2 equals to 0.85 for rectangular sections and 0.95 for circular sections.

$$P_p = F_y A_s + C_2 f_c' A_c \quad (3.71)$$

- for noncompact composite sections

$$P_{no} = P_p - \frac{P_p - P_y}{(\lambda_r - \lambda_p)^2} (\lambda - \lambda_p)^2 \quad (3.72)$$

where $P_y = F_y A_s + 0.7 f_c' A_c$

- for slender-element composite sections

$$P_{no} = F_n A_s + 0.7 f_c' A_c \quad (3.73)$$

where the critical buckling stress for the structural steel section of filled composite members, F_n , is determined from Eq. (3.74) and (3.75) for rectangular filled sections and round filled sections, respectively.

$$F_n = \frac{9E_s}{\lambda^2} \quad (3.74)$$

$$F_n = \frac{0.72 F_y}{\left[\left(\frac{D}{t} \right) \frac{F_y}{E_s} \right]^{0.2}} \quad (3.75)$$

For columns exceeding the limitations in section I1.3 but not exceeding those in the Appendix 2 of the standard, the column compressive strength without consideration of length effect can be determined with some modifications as follows,

where λ is the maximum width-to-thickness ratio of compression steel elements multiplied by $\sqrt{F_y/E}$.

$$P_{no} = F_n A_s + 0.85 f_c' A_c \quad (3.76)$$

$$F_n = (1 - 0.075\lambda) F_y \quad (3.77)$$

To better understand the utilization of the standard, an example is provided to demonstrate how the maximum allowable axial compressive strength is calculated. Only one column data extracted from the list is illustrated here and the rest will be tabulated later with those calculated in accordance with other standards.

Input:

material strength $f_c' = 30 \text{ MPa}$ $F_y = 350 \text{ MPa}$

column dimension $B = 300 \text{ mm}$ $D = 300 \text{ mm}$ $t = 3 \text{ mm}$ $L_c = 3500 \text{ mm}$

modulus of elasticity of steel $E_s = 2 \times 10^5 \text{ MPa}$

modulus of elasticity of concrete $E_c = 4700 \sqrt{f_c'} = 25743 \text{ MPa}$

Solution:

- Section properties

$$A_g = 300^2 = 9 \times 10^4 \text{ mm}^2 \quad I_g = \frac{1}{12} \times 300^4 = 6.75 \times 10^8 \text{ mm}^4$$

$$A_c = (300 - 2 \times 3)^2 = 86436 \text{ mm}^2 \quad I_c = \frac{1}{12} (300 - 2 \times 3)^4 = 6.27 \times 10^8 \text{ mm}^4$$

$$A_s = 9 \times 10^4 - 86436 = 3564 \text{ mm}^2 \quad I_s = (6.75 - 6.27) \times 10^8 = 0.52 \times 10^8 \text{ mm}^4$$

- Section classification for local buckling

$$\lambda = \frac{300 - 4 \times 3}{3} = 96; \lambda_r = 3 \sqrt{(2 \times 10^5)/350} = 71.71$$

because $\lambda_r < \lambda$, the section is classified as slender-element composite section.

- Nominal axial compressive strength, P_n

axial compressive strength (without length effect) $P_{no} = F_n A_s + 0.7 f'_c A_c$

$$F_n = \frac{9 \times (2 \times 10^5)}{96^2} = 195.3 \text{ MPa}$$

$$\Rightarrow P_{no} = (195.3 \times 3564 + 0.7 \times 30 \times 86436) \times 10^{-3} = 2511.3 \text{ kN}$$

critical buckling load $P_e = \frac{\pi^2 (EI)_{eff}}{L_c^2}$

$$C_3 = 0.45 + 3 \left(\frac{3564}{9 \times 10^4} \right) = 0.569 < 0.9$$

$$\Rightarrow (EI)_{eff} = [(2 \times 10^5) \times 0.52 \times 10^8 + 0.569 \times 25743 \times 6.23 \times 10^8] \times 10^{-9} = 19596.8 \text{ kN} \cdot \text{m}^2$$

$$\Rightarrow P_e = \frac{\pi^2 \times 19596.8}{3.5^2} = 15788.8 \text{ kN}$$

since $\frac{P_{no}}{P_e} = \frac{2511.3}{15788.8} = 0.159 < 2.25$, then $P_n = 2511.3 \times 0.658^{0.159} = 2349.5 \text{ kN}$

จุฬาลงกรณ์มหาวิทยาลัย
CHULALONGKORN UNIVERSITY

CHAPTER 4

RESULTS AND DISCUSSIONS

4.1 PREDICTED STRENGTHS OF EACH PREDICTIVE METHOD

As mentioned previously, the testing data were selected to ensure its majority coming from experimental data in descending order. Table 4.1 listed the predictions of each predictive method for each testing set of all four column's groups, while Table 4.2 summarized the predictive reliability via statistical parameters. Out of these four models, the slender column models outperformed the stub column models due to larger amount of data, while the slender circular column model also outperformed the slender rectangular column model due to the same reason. In addition to those calculated from Eqs (3.36) - (3.38), the very basic statistical parameters including mean, variance and standard deviation of the ratio of the predicted over the actual strength were also included in assessing each method quality.

Table 4.1 Axial compressive strength predictions of CFSST columns

Column type	Nº	P _{act}	P _{GPR}	P _{XGBoost}	P _{EC4}	P _{AISC}
Rectangular stub columns	1	534	580	777	400	572
	2	687	779	657	498	720
	3	836	1114	1440	671	866
	4	1410	1306	1535	852	1080
	5	1488	1423	1333	957	1224
	6	1559	1580	1525	1071	1320
	35	1498	1554	2571	1006	1556
	36	1559	1680	2766	1106	1683
	37	1985	1856	2958	1371	1746
	38	2068	2190	3202	1576	2006
	40	1423	1573	2183	1620	1294
	42	923	1040	966	612	857
	59	239	207	219	131	167
	60	271	224	226	151	192
	61	361	346	372	219	279
	62	394	368	407	238	302
	63	711	614	817	439	559
	64	754	682	814	519	660
	65	1350	1233	1465	781	994
	66	1448	1296	1521	855	1088
	67	1049	1037	1050	597	847

Table 4.1 Axial compressive strength predictions of CFSST columns

Column type	N°	P _{act}	P _{GPR}	P _{XGBoost}	P _{EC4}	P _{AISC}
Circular stub columns	68	1142	1206	1194	789	1091
	69	1801	1556	1764	1027	1308
	70	1962	1727	1911	1204	1533
	84	3164	2913	4792	2193	2792
	825	2665	2833	3534	1626	2071
	826	2751	2918	3618	1735	2209
	827	2828	3024	3755	1843	2346
	828	3253	3443	4140	2167	2759
	829	3339	3598	4223	2275	2897
	830	3733	3605	3952	2223	2831
	831	3843	3704	4034	2331	2969
	832	3944	3808	4109	2440	3106
	833	4198	4146	4700	2764	3519
	834	4319	4270	4764	2872	3657
	835	4800	4687	5087	2820	3591
	836	5038	4977	5203	3037	3866
	837	5242	5190	5480	3253	4142
	838	5423	5398	5563	3469	4417
	839	5610	5585	6017	3685	4692
	840	5717	5517	5855	3417	4351
Circular full columns	7	699	739	566	587	495
	8	901	780	708	728	630
	9	1133	1373	1243	854	749
	10	1593	1246	820	1227	787
	11	1648	1540	1030	1375	927
	12	1674	2000	1137	1506	1052
	13	6134	4643	4131	5572	3866
	14	7076	4893	4207	6181	4194
	15	8088	5767	4207	6982	4636
	16	5601	4883	4405	5806	4089
	17	6848	5186	4977	6409	4410
	18	8230	6007	4977	7203	4846
	19	6171	5055	4405	5983	4257
	20	7193	5363	4977	6581	4574
	21	8432	6180	4977	7371	5005
	22	10190	8913	9018	8807	6942
	23	11032	9879	9760	12667	7904
	24	12926	9939	9760	14379	8870
	25	10304	9359	9314	9249	7362
	26	10260	10341	10378	13098	8314
	27	13499	10381	10378	14799	9269
	28	10533	9600	9423	9489	7590
	29	13240	10604	10488	13332	8536

Table 4.1 Axial compressive strength predictions of CFSST columns

Column type	Nº	P _{act}	P _{GPR}	P _{XGBoost}	P _{EC4}	P _{AISC}
Slender rectangular column	30	13265	10615	10488	15026	9485
	31	1293	1328	1179	1383	1198
	32	1332	1403	1306	1499	1308
	33	1625	1481	1147	2075	1382
	34	1672	1612	1146	2301	1504
	39	1708	1488	1031	1831	1325
	41	823	810	1021	936	734
	43	667	591	484	683	488
	44	1137	1049	979	823	689
	45	1680	1345	1015	1211	1013
	46	2181	1953	1910	1648	1377
	47	109	98	107	140	89
	48	132	120	127	158	107
	49	136	118	128	173	108
	50	165	142	151	190	124
	51	424	392	276	461	305
	52	477	465	318	537	378
	53	675	455	591	431	401
	54	746	539	742	552	516
	55	809	641	594	549	544
	56	897	803	767	724	710
	57	1384	1191	1324	925	920
	475	4736	4869	4726	3500	4528
	476	5042	5187	5364	3688	4796
	477	5335	5461	5393	3872	5060
	478	5629	5746	5814	4051	5322
	479	6126	6377	6499	4393	5838
	480	5883	5935	5951	4307	5649
	481	6196	6317	6242	4474	5905
	482	6445	6666	6685	4636	6157
	483	7074	7223	7216	4944	6655
	484	7646	7857	7788	5232	7142
	485	6937	7185	7013	5012	6699
	486	7247	7268	7434	5157	6944
	487	7698	7849	7966	5432	7425
	488	8242	8453	8520	5688	7897
	489	8975	8809	9029	5925	8005
	490	7862	8251	8246	5615	7215
	491	8514	8736	8797	5859	7691
	492	9119	9269	9365	6085	8158
	493	9665	9845	9953	6295	8616
	494	10792	11257	10706	6668	9506
	495	7610	9754	9233	5583	7102

Table 4.1 Axial compressive strength predictions of CFSST columns

Column type	Nº	P _{act}	P _{GPR}	P _{XGBoost}	P _{EC4}	P _{AISC}
Slender circular column	496	8956	10903	10851	6458	8236
	497	10233	11918	14370	7323	9363
	498	11520	12672	15382	8180	10482
	499	12770	13105	17152	9027	11358
	500	8597	11173	9249	6263	7973
	501	9979	12668	10870	7130	9100
	502	11267	13958	14373	7989	10220
	503	12546	14838	15386	8839	11334
	504	13752	15154	17154	9680	12112
	505	12389	16539	15653	8912	11410
	506	13793	17572	16682	9753	12515
	507	15075	17730	18634	10585	13143
	508	5493	5630	5246	5315	3388
	509	6384	6181	6112	6308	4021
	510	15385	17407	17185	11996	14327
	511	16482	18523	17957	12806	15414
	512	18838	19145	20719	13608	16495
	513	5560	5486	5338	5330	3388
	514	6439	6130	6188	6322	4021
	515	1780	1641	1639	1085	1248
	516	2041	1927	2011	1264	1444
	517	2337	2227	2795	1441	1638
	518	2612	2494	2786	1614	1831
	519	2877	2735	3141	1785	2023
	520	1860	1670	1811	1100	1248
	521	2709	2551	2958	1627	1831
	522	3263	3094	3221	1965	2213
	523	3707	3639	3491	2292	2590
	524	4832	4201	4315	2914	4002
	525	2594	2536	3248	1484	1638
	526	3177	3113	3552	1824	2023
Slender square column	71	525	701	611	556	537
	72	504	545	611	515	497
	73	481	518	540	487	470
	74	498	524	585	493	470
	75	429	394	609	468	446
	76	424	368	523	440	418
	77	737	910	748	691	659
	78	670	743	647	639	607
	79	639	690	571	601	570
	80	575	743	748	634	601
	81	555	588	645	585	555
	82	540	537	573	551	523

Table 4.1 Axial compressive strength predictions of CFSST columns

Column type	Nº	P _{act}	P _{GPR}	P _{XGBoost}	P _{EC4}	P _{AISC}
	85	791	862	938	924	898
	86	842	894	988	968	949
	87	889	931	1070	1009	999
	88	929	970	1107	1047	1047
	89	967	1006	1183	1081	1093
	90	897	1076	1183	1048	961
	91	1107	1266	1373	1273	1171
	92	1278	1498	1549	1465	1365
	93	1451	1738	1624	1629	1543
	94	1612	2018	1809	1768	1708
	95	1000	1127	849	1092	1019
	96	1036	1142	931	1127	1056
	97	1112	1174	986	1163	1094
	98	1212	1332	990	1304	1243
	99	1281	1450	1100	1376	1317
	100	1033	1043	1186	1108	1042
	101	1168	1208	1326	1211	1158
	102	1387	1342	1482	1299	1267
	103	1098	984	1240	917	1114
	104	1254	1089	1341	1000	1224
	105	875	932	1290	987	897
	106	1033	1113	1359	1137	1049
	107	1178	1266	1488	1263	1188
	108	983	1055	1371	830	970
	109	1150	1202	1530	950	1113
	110	1421	1633	1863	1127	1364
	111	1183	1193	1517	942	1108
	112	1398	1453	1854	1027	1191
	113	1547	1628	1997	1100	1292
	114	1685	1695	2108	1162	1387
	115	6136	6188	5863	5208	5884
	116	7496	7700	7143	6544	7113
	117	8841	9031	8716	7827	8315
	118	9884	10136	9795	9074	9493
	119	6812	6832	6091	5355	5932
	120	2372	2243	2292	2537	2395
	121	2620	2476	2846	2765	2641
	122	2864	2679	3139	2968	2875
	123	2585	2253	2298	2162	2583
	124	2827	3106	2965	3017	2929
	125	3082	2870	3396	3500	3301
	126	3471	3270	3747	3942	3723
	127	4228	4175	4367	4740	4520

Table 4.1 Axial compressive strength predictions of CFSST columns

Column type	Nº	P _{act}	P _{GPR}	P _{XGBoost}	P _{EC4}	P _{AISC}
	128	4575	4723	5086	5097	4898
	129	3355	3108	3340	3750	3540
	130	3732	3476	3697	4174	3951
	131	4531	4270	4408	4937	4730
	132	4879	4787	5009	5278	5099
	133	4388	4014	4523	4773	4558
	134	5152	4862	5189	5448	5293
	135	11366	11816	10058	11776	11379
	136	12735	13226	10830	13384	12795
	137	14104	14637	11223	14875	14189
	138	15425	15965	14751	16338	15563
	139	14715	15059	11740	15172	14511
	140	16030	16651	12194	16627	15878
	141	19644	20220	17781	20281	19355
	142	20748	21426	19514	21638	20656
	143	22303	22586	20764	22967	21940
	144	23464	23690	21296	24268	23208
	145	9417	9931	9082	10037	9555
	146	10757	11313	9918	11551	10957
	147	12057	12739	10358	13026	12332
	148	13418	14169	12852	14465	13680
	149	11033	11588	9658	11575	11015
	150	12416	13156	10794	13047	12385
	151	13775	14704	11143	14482	13728
	152	16082	16167	13769	15880	15045
	153	13931	14734	12456	14494	13762
	154	17827	19120	16031	18564	17631
	155	6434	6453	5910	7224	6767
	156	7344	7349	6938	8223	7717
	157	8297	8395	8270	9149	8626
	158	9028	9451	9396	10004	9498
	159	7428	7380	6416	8133	7634
	160	8414	8332	8024	9058	8541
	161	9324	9437	9012	9911	9410

Table 4.2 Machine learning predictive model statistical parameters

Type	Section	Model	Mean	Variance	SD	MAE	RMSE	R ²
Stub column	Rectangular	GPR	0.995	0.009	0.094	112.7	136.3	0.9935
		XGBoost	1.172	0.058	0.241	388.4	579.7	0.9423
		AISC	0.841	0.010	0.102	432.3	581.5	0.9863
		EC4	0.655	0.009	0.096	850.5	1078.2	0.9793

	Circular	GPR	0.873	0.014	0.120	778.2	1246.4	0.9802
		XGBoost	0.796	0.025	0.158	1010.6	1553.0	0.9586
		AISC	0.707	0.011	0.104	1394.1	2041.6	0.9857
		EC4	0.967	0.036	0.190	543.9	811.2	0.9722
Slender column	Rectangular	GPR	1.051	0.012	0.110	774.6	1325.0	0.9697
		XGBoost	1.083	0.014	0.119	953.0	1603.1	0.9653
		AISC	0.848	0.015	0.122	916.9	1099.3	0.9804
		EC4	0.706	0.009	0.094	2180.3	2523.0	0.9682
	Circular	GPR	1.040	0.007	0.085	229.3	335.7	0.9987
		XGBoost	1.049	0.027	0.165	570.4	963.0	0.9906
		AISC	1.005	0.004	0.060	150.1	230.2	0.9986
		EC4	1.027	0.012	0.111	391.4	514.1	0.9956

4.2 VISUALIZATION OF THE PREDICTIVE MODELS

To better perceive the capability of each predictive method, 7 figures are used to depict each model's results. The first 4 figures (left to right, top to bottom) illustrate the predicted strength (vertical axis) against the actual strength (horizontal axis) of GPR, XGBoost, AISC and EC4, respectively. The next two figures show the ratio of the predicted over the actual strength of ML method (GPR, XGBoost) and standard specifications (AISC, EC4). The last figure shows the comparison of the statistical accuracy measurement parameters as already summarized in Table 4.2. Note that both MAE and RMSE were scaled down by a factor of 1000 to ensure they won't dwarf out other parameters plotting on the same scale. Be aware that all models' results were not plotted on a consistent scale. For instance, the ratio of the predicted over the actual strength of rectangular stub column model were plotted from 0.4 to 1.8 on the vertical axis and from 0 to 7 on the horizontal axis while the same of circular stub column model were from 0.4 to 1.6 and 0 to 3, and vice versa. Among all parameters, the variance was the only one barely visible due to its small magnitude.

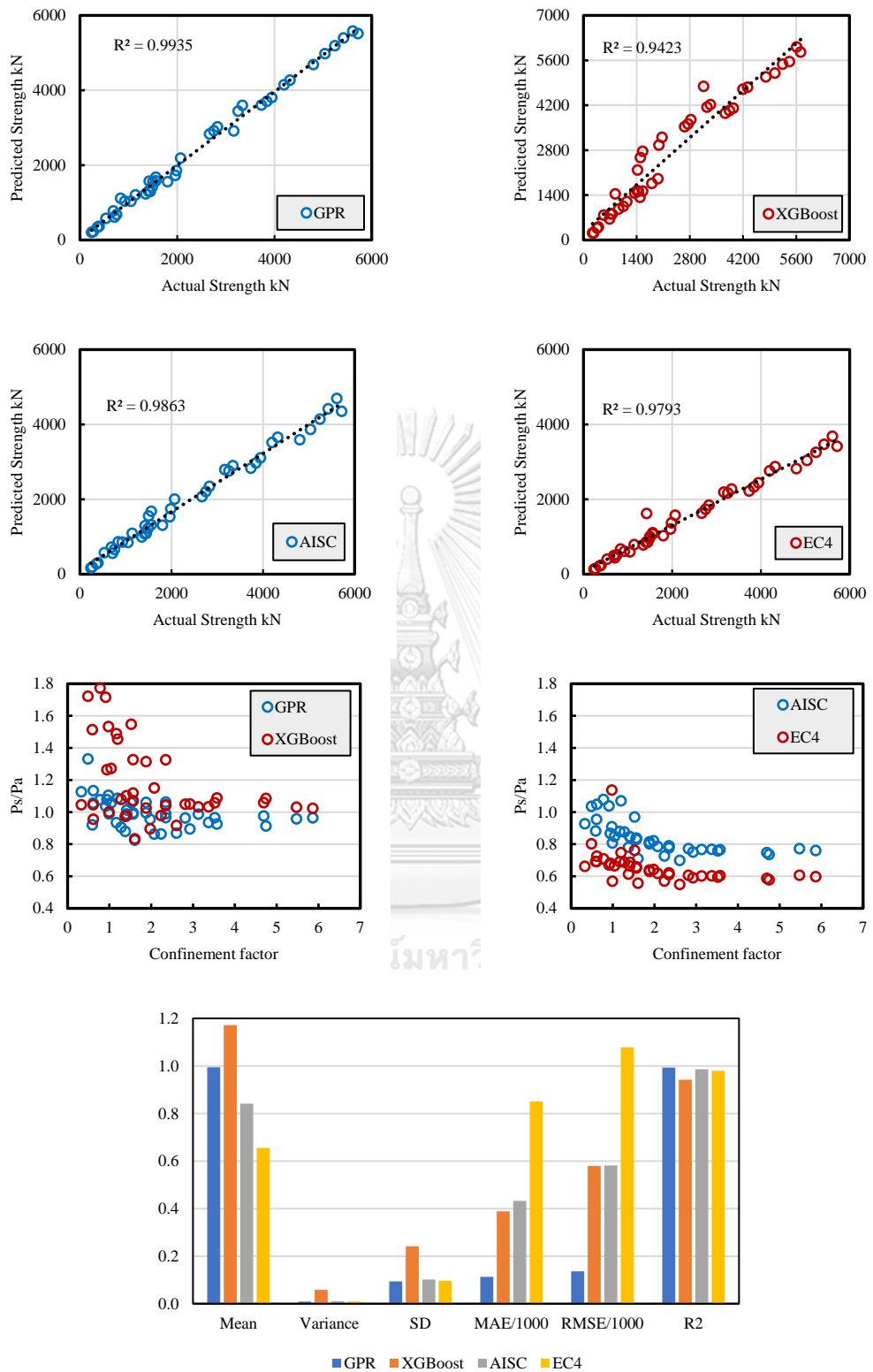


Figure 4.1 Rectangular stub column model charts results

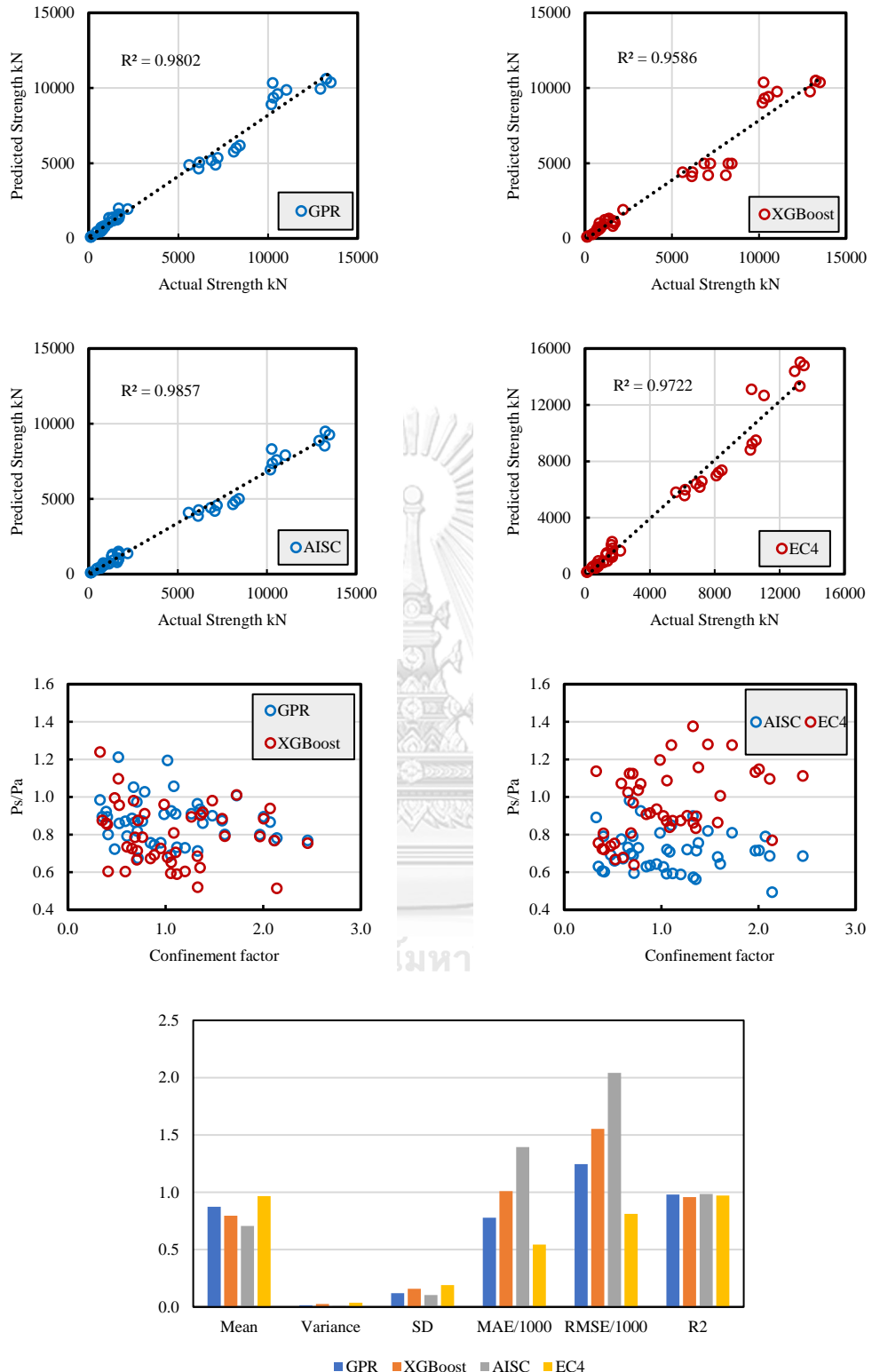


Figure 4.2 Circular stub column model charts results

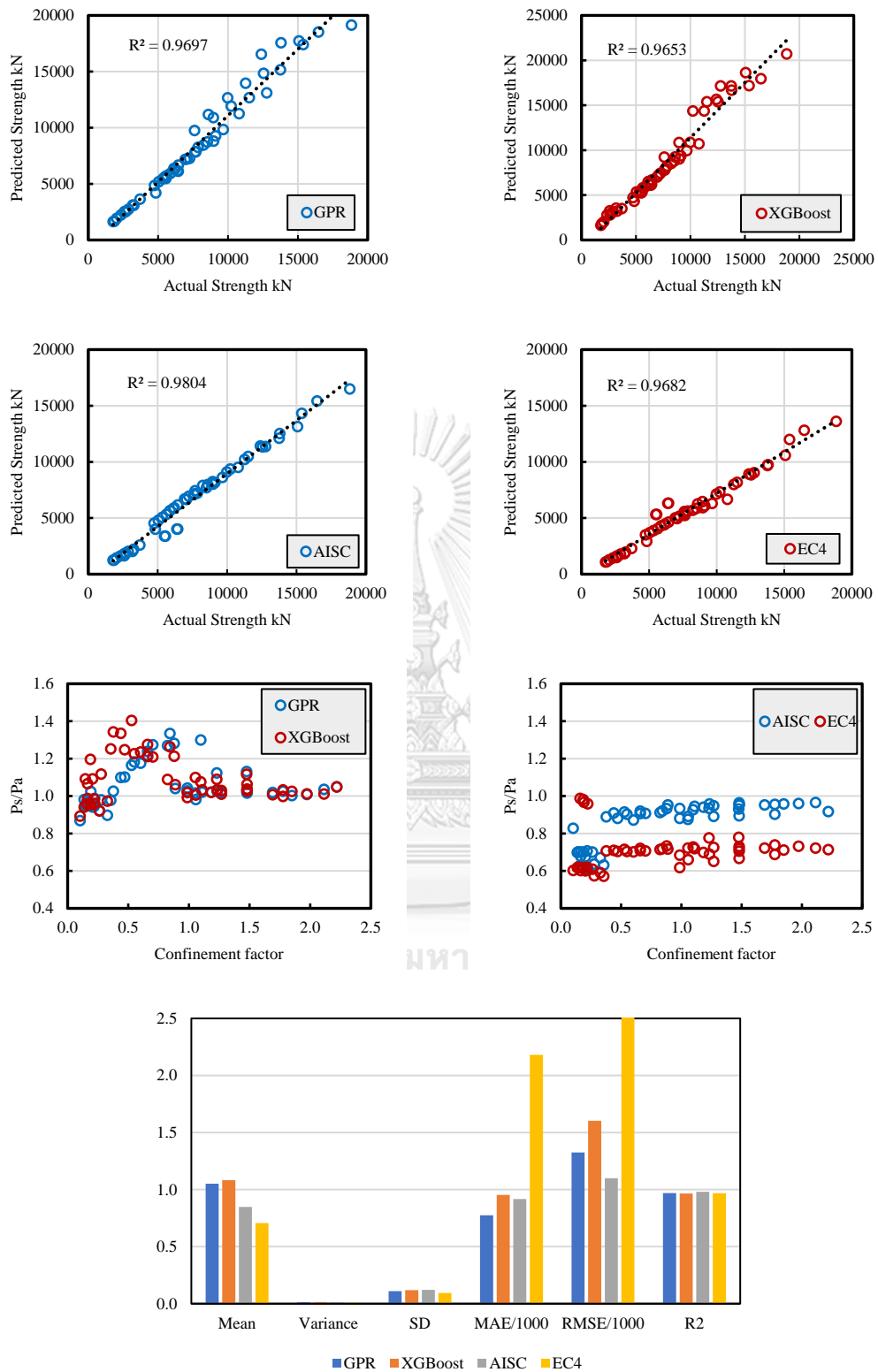


Figure 4.3 Slender rectangular column model charts results

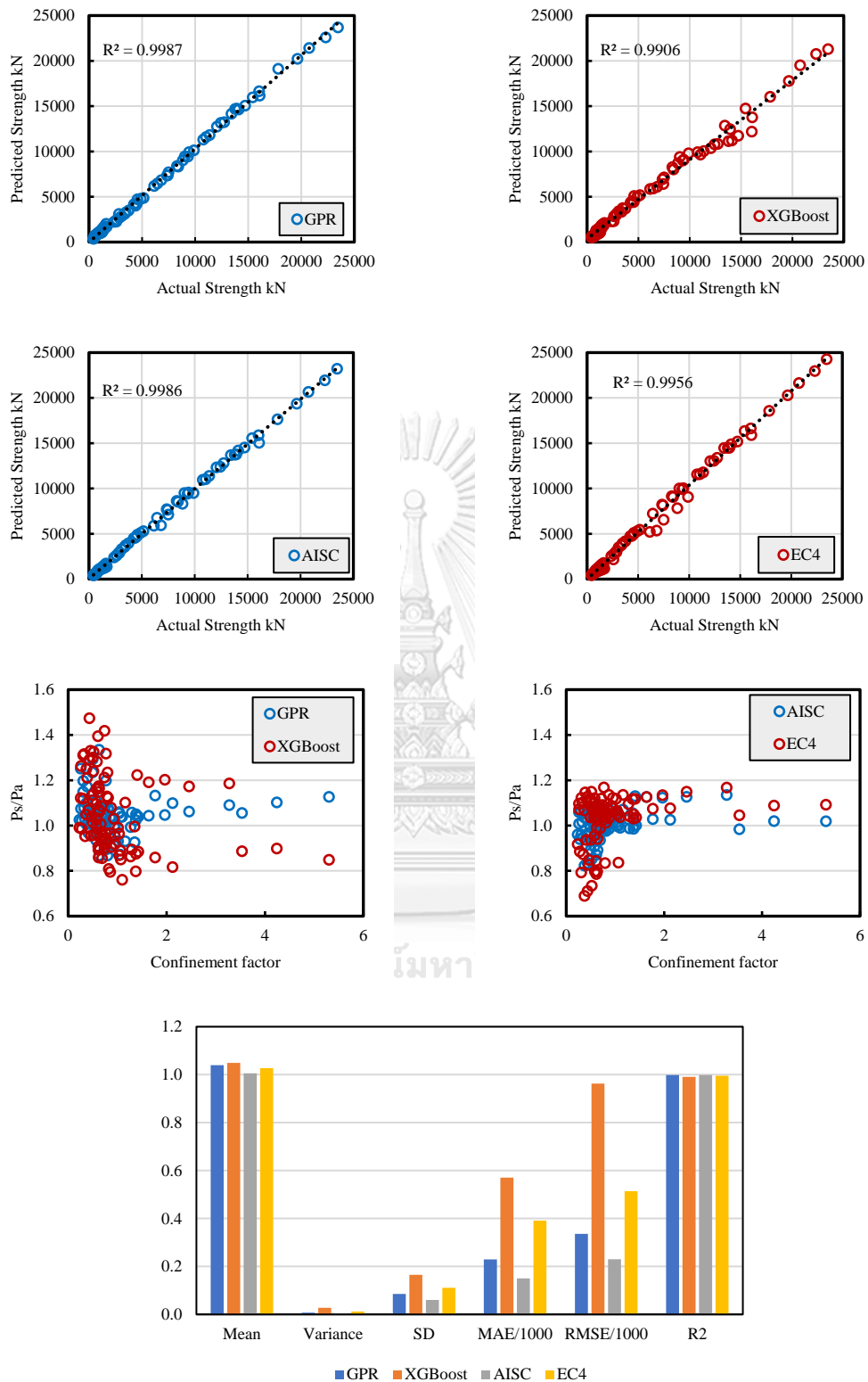


Figure 4.4 Slender circular column model charts results

4.3 ASSESSMENT AND THE PREFERRED PREDICTIVE METHODS

The GPR outperformed the XGBoost in every aspect of each model. For rectangular stub column model, the GPR had higher R-square value as well as closer mean value to 1 and smaller values for remaining parameters compared to the XGBoost which obviously made it clear about which model is suitable for this case. On the other hand, the XGBoost partially overestimated the actual column strengths, specifically in the confinement factor range of less than 2.5. The author firmly believes that high R-square value does not really imply the model performance since it only explains the correlation level between the predicted and the actual one. One's value could be very high, yet it might provide wrong predictions with large error gap leading to the investigation on other statistical parameters (mean, variance, standard deviation, etc.) to conclude one's predictive accuracy. The same thing can be said for the other three models resulting in GPR being preferred over XGBoost. Factors affecting the performance of XGBoost could be the lack of tuning for optimal hyperparameters in the current algorithm, and the amount of data was still not large enough for it to exploit its full potential as the algorithm that performs well with large data set.

The AISC specifications showed superiority in predicting the column's strength compared to the EC4 with smaller coefficient of variance and higher R-square value. It's obvious how the EC4 prediction tends to scatter all around, as indicated by larger coefficient of variance compared to the AISC. The EC4 was more conservative but less accurate than the AISC for rectangular stub column model with almost all predicted ratio less than 0.8 across the whole confinement factor range, while the opposite applied to the circular stub columns model due to strength increase from confinement effect. The same things can be concluded for the slender columns model of both sections.

CHAPTER 5

CONCLUSIONS

The complex behavior of the concrete-filled stainless-steel tubular columns were well modeled using the finite-element method to generate an enormous amount of columns data plus those from the experimental tests for machine learning algorithms using GPR and XGBoost to predict the axial compressive strength of the CFST columns. As a result, the GPR slightly outperformed the XGBoost model in every model while the comparisons with the standard specifications also showed the potential use of the machine learning algorithms instead in the future while the American specifications demonstrated better prediction accuracy than the Eurocode 4.

There are quite a few factors that could be the reason for the EC4 predictive inferiority. As specified by the EC4, the strength enhancement of confined-concrete can be calculated with the presence of the effective lateral compressive stress, σ_2 . The absence of this variable led to the ignorance of column strength enhancement resulting in strength underestimation especially for slender rectangular columns (Figure 4.3). Other possible factors could be the ignorance of the limitations of the specifications including local slenderness, material properties and the initial imperfection. The assumed imperfection for slender column of EC4 was taken as $L/200$ for reinforcement ratio (ρ_s) not exceeding 3% or $L/300$ for reinforcement ratio greater than 3% but not exceeding 6%. Since the current work considered the columns confined by steel tube without additional reinforcement, the specifications were supposed to predict the strength of columns with the imperfection value of $L/300$, while the current work assumed its magnitude of just $L/1000$ resulting in the underestimation of slender column strength especially for rectangular section. The increase in strength due to confinement effect for circular sections tend to overestimate the strength of the column (Figure 4.4) but still seem acceptable since those predictions lied within the $\pm 20\%$ boundary with a few lying outside this range. The AISC limitations, of course, were also exceeded in terms of material properties but only for a minor part of the columns data.

The possibility of using the trained models to predict the axial strength of CFSST columns can be ensured since they would provide higher accuracy, not to mention that, if possible, only the experimental data were used as the testing set. Even with a total column data of just 1128, these four ML models already exhibited the potential as surrogate-assisted models in predicting the CFSST columns axial strength with rectangular stub column model and slender rectangular column model even outperformed the two standard specifications used in this work, owing to the fact that substantial data were provided in the training process. However, the comparisons need to be modified once the provisions for stainless steel become available. One, nevertheless, should not blindly employ the method since awareness over predicted strength must be taken care of, especially regarding the nature of the distribution of each new testing set comparing to the distribution of training sets since these machine learning algorithms tend to provide low accuracy for making predictions outside training boundary. To mitigate this issue, more columns data should be added to the training set to expand the model prediction accuracy across larger domain.

Future study case could be expanded to develop a unified model which would be more versatile, capable of predicting the axial compressive strength of the CFSST columns of any section type (rectangular, circular, elliptical...) or column length (stub or slender) instead of one model for one section or column length. To achieve this, an enormous amount of data must be gathered to provide more general understanding to different column types to the machine algorithms, as well as to eliminate potential error since the behavior of rectangular and circular sections alone are quite different already, not to mention the case where more section types other than these two are considered.

APPENDIX A SIMULATED CFSST COLUMNS DATA

This section lists all the simulated slender columns data using ABAQUS and the procedure described above. Note that the numbering order continues from those collected from the literatures (Table 2.1).

Nº	Name	B	D	t	L _e	f _{c'}	σ _{0.2}	P _n
85	C30x370-126x7x2630	-	126	7	2630	30	370	791
86	C40x370-126x7x2630	-	126	7	2630	40	370	842
87	C50x370-126x7x2630	-	126	7	2630	50	370	889
88	C60x370-126x7x2630	-	126	7	2630	60	370	929
89	C70x370-126x7x2630	-	126	7	2630	70	370	967
90	C20x230-220x3.5x4400	-	220	3.5	4400	20	230	897
91	C30x230-220x3.5x4400	-	220	3.5	4400	30	230	1107
92	C40x230-220x3.5x4400	-	220	3.5	4400	40	230	1278
93	C50x230-220x3.5x4400	-	220	3.5	4400	50	230	1451
94	C60x230-220x3.5x4400	-	220	3.5	4400	60	230	1612
95	C20x320-120x8x960	-	120	8	960	20	320	1000
96	C25x320-120x8x960	-	120	8	960	25	320	1036
97	C30x320-120x8x960	-	120	8	960	30	320	1112
98	C50x320-120x8x960	-	120	8	960	50	320	1212
99	C60x320-120x8x960	-	120	8	960	60	320	1281
100	C40x350-180x3x3500	-	180	3	3500	40	350	1033
101	C50x350-180x3x3500	-	180	3	3500	50	350	1168
102	C60x350-180x3x3500	-	180	3	3500	60	350	1387
103	C40x450-180x3x3500	-	180	3	3500	40	450	1098
104	C50x450-180x3x3500	-	180	3	3500	50	450	1254
105	C30x250-200x2.5x4000	-	200	2.5	4000	30	250	875
106	C40x250-200x2.5x4000	-	200	2.5	4000	40	250	1033
107	C50x250-200x2.5x4000	-	200	2.5	4000	50	250	1178
108	C30x350-200x2.5x4000	-	200	2.5	4000	30	350	983
109	C40x350-200x2.5x4000	-	200	2.5	4000	40	350	1150
110	C60x350-200x2.5x4000	-	200	2.5	4000	60	350	1421
111	C40x450-200x2.5x4000	-	200	2.5	4000	40	450	1183
112	C50x500-200x2.5x4000	-	200	2.5	4000	50	500	1398
113	C60x500-200x2.5x4000	-	200	2.5	4000	60	500	1547
114	C70x500-200x2.5x4000	-	200	2.5	4000	70	500	1685

Nº	Name	B	D	t	L _e	f _{c'}	σ _{0.2}	P _n
115	C30x300-450x5x4500	-	450	5	4500	30	300	6136
116	C40x300-450x5x4500	-	450	5	4500	40	300	7496
117	C50x300-450x5x4500	-	450	5	4500	50	300	8841
118	C60x300-450x5x4500	-	450	5	4500	60	300	9884
119	C30x400-450x5x4500	-	450	5	4500	30	400	6812
120	C40x400-250x5x4500	-	250	5	4500	40	400	2372
121	C50x400-250x5x4500	-	250	5	4500	50	400	2620
122	C60x400-250x5x4500	-	250	5	4500	60	400	2864
123	C40x500-250x5x4500	-	250	5	4500	40	500	2585
124	C70x300-250x5x4500	-	250	5	4500	70	300	2827
125	C30x300-300x8x5000	-	300	8	5000	30	300	3082
126	C40x300-300x8x5000	-	300	8	5000	40	300	3471
127	C60x300-300x8x5000	-	300	8	5000	60	300	4228
128	C70x300-300x8x5000	-	300	8	5000	70	300	4575
129	C30x350-300x8x5000	-	300	8	5000	30	350	3355
130	C40x350-300x8x5000	-	300	8	5000	40	350	3732
131	C60x350-300x8x5000	-	300	8	5000	60	350	4531
132	C70x350-300x8x5000	-	300	8	5000	70	350	4879
133	C50x400-300x8x5000	-	300	8	5000	50	400	4388
134	C70x400-300x8x5000	-	300	8	5000	70	400	5152
135	C30x350-500x14x5500	-	500	14	5500	30	350	11366
136	C40x350-500x14x5500	-	500	14	5500	40	350	12735
137	C50x350-500x14x5500	-	500	14	5500	50	350	14104
138	C60x350-500x14x5500	-	500	14	5500	60	350	15425
139	C40x450-500x14x5500	-	500	14	5500	40	450	14715
140	C50x450-500x14x5500	-	500	14	5500	50	450	16030
141	C70x500-500x14x5500	-	500	14	5500	70	500	19644
142	C80x500-500x14x5500	-	500	14	5500	80	500	20748
143	C90x500-500x14x5500	-	500	14	5500	90	500	22303
144	C100x500-500x14x5500	-	500	14	5500	100	500	23464
145	C30x300-500x12x6000	-	500	12	6000	30	300	9417
146	C40x300-500x12x6000	-	500	12	6000	40	300	10757
147	C50x300-500x12x6000	-	500	12	6000	50	300	12057
148	C60x300-500x12x6000	-	500	12	6000	60	300	13418
149	C30x400-500x12x6000	-	500	12	6000	30	400	11033
150	C40x400-500x12x6000	-	500	12	6000	40	400	12416

Nº	Name	B	D	t	L _e	f _{c'}	σ _{0.2}	P _n
151	C50x400-500x12x6000	-	500	12	6000	50	400	13775
152	C60x400-500x12x6000	-	500	12	6000	60	400	16082
153	C40x500-500x12x6000	-	500	12	6000	40	500	13931
154	C70x500-500x12x6000	-	500	12	6000	70	500	17827
155	C30x300-450x10x7500	-	450	10	7500	30	300	6434
156	C40x300-450x10x7500	-	450	10	7500	40	300	7344
157	C50x300-450x10x7500	-	450	10	7500	50	300	8297
158	C60x300-450x10x7500	-	450	10	7500	60	300	9028
159	C30x400-450x10x7500	-	450	10	7500	30	400	7428
160	C40x400-450x10x7500	-	450	10	7500	40	400	8414
161	C50x400-450x10x7500	-	450	10	7500	50	400	9324
162	C60x400-450x10x7500	-	450	10	7500	60	400	10096
163	C40x500-450x10x7500	-	450	10	7500	40	500	9189
164	C80x500-450x10x7500	-	450	10	7500	80	500	12560
165	C30x400-680x16x8000	-	680	16	8000	30	400	20299
166	C40x400-680x16x8000	-	680	16	8000	40	400	22789
167	C50x400-680x16x8000	-	680	16	8000	50	400	25393
168	C60x400-680x16x8000	-	680	16	8000	60	400	27784
169	C40x450-680x16x8000	-	680	16	8000	40	450	24428
170	C60x450-680x16x8000	-	680	16	8000	60	450	29348
171	C80x450-680x16x8000	-	680	16	8000	80	450	33996
172	C60x500-680x16x8000	-	680	16	8000	60	500	33970
173	C80x500-680x16x8000	-	680	16	8000	80	500	35623
174	C120x500-680x16x8000	-	680	16	8000	120	500	44882
175	C25x250-450x3.6x4000	-	450	3.6	4000	25	250	4763
176	C30x250-450x3.6x4000	-	450	3.6	4000	30	250	5535
177	C40x250-450x3.6x4000	-	450	3.6	4000	40	250	6933
178	C25x350-450x3.6x4000	-	450	3.6	4000	25	350	5297
179	C30x350-450x3.6x4000	-	450	3.6	4000	30	350	6006
180	C60x350-450x3.6x4000	-	450	3.6	4000	60	350	10196
181	C30x450-450x3.6x4000	-	450	3.6	4000	30	450	6448
182	C25x500-450x3.6x4000	-	450	3.6	4000	25	500	6060
183	C40x500-450x3.6x4000	-	450	3.6	4000	40	500	8066
184	C60x500-450x3.6x4000	-	450	3.6	4000	60	500	10854
185	C70x500-600x12x8200	-	600	12	8200	70	500	22564
186	C80x500-600x12x8200	-	600	12	8200	80	500	24225

Nº	Name	B	D	t	L _e	f _{c'}	σ _{0.2}	P _n
187	C90x500-600x12x8200	-	600	12	8200	90	500	26401
188	C100x500-600x12x8200	-	600	12	8200	100	500	27999
189	C120x600-600x12x8200	-	600	12	8200	120	600	33366
190	C70x600-600x12x8200	-	600	12	8200	70	600	24427
191	C80x600-600x12x8200	-	600	12	8200	80	600	26430
192	C90x700-600x12x8200	-	600	12	8200	90	700	29212
193	C100x700-600x12x8200	-	600	12	8200	100	700	31302
194	C120x700-600x12x8200	-	600	12	8200	120	700	34698
195	C70x500-530x8x5300	-	530	8	5300	70	500	18738
196	C80x500-530x8x5300	-	530	8	5300	80	500	20499
197	C90x500-530x8x5300	-	530	8	5300	90	500	22277
198	C100x500-530x8x5300	-	530	8	5300	100	500	24017
199	C80x600-530x8x5300	-	530	8	5300	80	600	21569
200	C100x600-530x8x5300	-	530	8	5300	100	600	25113
201	C120x600-530x8x5300	-	530	8	5300	120	600	28510
202	C90x700-530x8x5300	-	530	8	5300	90	700	24309
203	C100x700-530x8x5300	-	530	8	5300	100	700	26090
204	C120x700-530x8x5300	-	530	8	5300	120	700	29594
205	C25x200-300x6x3800	-	300	6	3800	25	200	2333
206	C35x200-300x6x3800	-	300	6	3800	35	200	2822
207	C50x200-300x6x3800	-	300	6	3800	50	200	3579
208	C70x200-300x6x3800	-	300	6	3800	70	200	4530
209	C25x600-300x6x3800	-	300	6	3800	25	600	4219
210	C35x600-300x6x3800	-	300	6	3800	35	600	4706
211	C50x600-300x6x3800	-	300	6	3800	50	600	5388
212	C90x600-300x6x3800	-	300	6	3800	90	600	7342
213	C35x250-300x6x3800	-	300	6	3800	35	250	2982
214	C50x250-300x6x3800	-	300	6	3800	50	250	3782
215	C25x200-400x10x7800	-	400	10	7800	25	200	3683
216	C35x200-400x10x7800	-	400	10	7800	35	200	4362
217	C50x200-400x10x7800	-	400	10	7800	50	200	5147
218	C25x450-400x10x7800	-	400	10	7800	25	450	5648
219	C30x450-400x10x7800	-	400	10	7800	30	450	5982
220	C35x450-400x10x7800	-	400	10	7800	35	450	5985
221	C40x450-400x10x7800	-	400	10	7800	40	450	6489
222	C60x450-400x10x7800	-	400	10	7800	60	450	7802

Nº	Name	B	D	t	L _e	f' _c	σ _{0.2}	P _n
223	C70x450-400x10x7800	-	400	10	7800	70	450	8330
224	C90x450-400x10x7800	-	400	10	7800	90	450	9270
225	C25x600-500x9x6300	-	500	9	6300	25	600	11048
226	C35x600-500x9x6300	-	500	9	6300	35	600	12402
227	C80x600-500x9x6300	-	500	9	6300	80	600	18314
228	C100x600-500x9x6300	-	500	9	6300	100	600	21065
229	C35x700-500x9x6300	-	500	9	6300	35	700	13314
230	C80x700-500x9x6300	-	500	9	6300	80	700	19396
231	C90x700-500x9x6300	-	500	9	6300	90	700	20732
232	C100x700-500x9x6300	-	500	9	6300	100	700	21778
233	C120x700-500x9x6300	-	500	9	6300	120	700	24619
234	C50x200-500x9x6300	-	500	9	6300	50	200	9722
235	C25x280-220x3.6x3300	-	220	3.6	3300	25	280	1276
236	C30x280-220x3.6x3300	-	220	3.6	3300	30	280	1390
237	C35x280-220x3.6x3300	-	220	3.6	3300	35	280	1521
238	C45x280-220x3.6x3300	-	220	3.6	3300	45	280	1768
239	C50x280-220x3.6x3300	-	220	3.6	3300	50	280	1879
240	C30x320-220x3.6x3300	-	220	3.6	3300	30	320	1486
241	C35x320-220x3.6x3300	-	220	3.6	3300	35	320	1603
242	C40x320-220x3.6x3300	-	220	3.6	3300	40	320	1724
243	C50x320-220x3.6x3300	-	220	3.6	3300	50	320	1947
244	C60x320-220x3.6x3300	-	220	3.6	3300	60	320	2193
245	C25x280-320x5x3800	-	320	5	3800	25	280	2879
246	C30x280-320x5x3800	-	320	5	3800	30	280	3176
247	C35x280-320x5x3800	-	320	5	3800	35	280	3438
248	C40x280-320x5x3800	-	320	5	3800	40	280	3742
249	C45x280-320x5x3800	-	320	5	3800	45	280	4046
250	C30x320-320x5x3800	-	320	5	3800	30	320	3299
251	C35x320-320x5x3800	-	320	5	3800	35	320	3642
252	C40x320-320x5x3800	-	320	5	3800	40	320	3937
253	C45x320-320x5x3800	-	320	5	3800	45	320	4237
254	C70x320-320x5x3800	-	320	5	3800	70	320	5692
255	C25x280-420x6x4200	-	420	6	4200	25	280	4996
256	C35x280-420x6x4200	-	420	6	4200	35	280	6076
257	C40x280-420x6x4200	-	420	6	4200	40	280	6658
258	C45x280-420x6x4200	-	420	6	4200	45	280	7162

Nº	Name	B	D	t	L _e	f' _c	σ _{0.2}	P _n
259	C60x280-420x6x4200	-	420	6	4200	60	280	8776
260	C30x380-420x6x4200	-	420	6	4200	30	380	6324
261	C35x380-420x6x4200	-	420	6	4200	35	380	6862
262	C40x380-420x6x4200	-	420	6	4200	40	380	7409
263	C45x380-420x6x4200	-	420	6	4200	45	380	7825
264	C80x380-420x6x4200	-	420	6	4200	80	380	11796
265	C25x200-280x3x2800	-	280	3	2800	25	200	1861
266	C30x200-280x3x2800	-	280	3	2800	30	200	2126
267	C35x200-280x3x2800	-	280	3	2800	35	200	2387
268	C40x200-280x3x2800	-	280	3	2800	40	200	2644
269	C45x200-280x3x2800	-	280	3	2800	45	200	2902
270	C25x380-280x3x2800	-	280	3	2800	25	380	2298
271	C30x380-280x3x2800	-	280	3	2800	30	380	2543
272	C35x380-280x3x2800	-	280	3	2800	35	380	2660
273	C40x380-280x3x2800	-	280	3	2800	40	380	3052
274	C45x380-280x3x2800	-	280	3	2800	45	380	3289
275	C35x540-560x9.5x8500	-	560	9.5	8500	35	540	13076
276	C45x540-560x9.5x8500	-	560	9.5	8500	45	540	12044
277	C50x540-560x9.5x8500	-	560	9.5	8500	50	540	15541
278	C60x540-560x9.5x8500	-	560	9.5	8500	60	540	17011
279	C80x540-560x9.5x8500	-	560	9.5	8500	80	540	19994
280	C35x380-560x9.5x8500	-	560	9.5	8500	35	380	11325
281	C45x380-560x9.5x8500	-	560	9.5	8500	45	380	12840
282	C60x380-560x9.5x8500	-	560	9.5	8500	60	380	15148
283	C80x380-560x9.5x8500	-	560	9.5	8500	80	380	17970
284	C100x380-560x9.5x8500	-	560	9.5	8500	100	380	20629
285	C30x320-480x8x6800	-	480	8	6800	30	320	7247
286	C40x320-480x8x6800	-	480	8	6800	40	320	8162
287	C50x320-480x8x6800	-	480	8	6800	50	320	9627
288	C60x320-480x8x6800	-	480	8	6800	60	320	10632
289	C70x320-480x8x6800	-	480	8	6800	70	320	11883
290	C30x420-480x8x6800	-	480	8	6800	30	420	8234
291	C40x420-480x8x6800	-	480	8	6800	40	420	9418
292	C50x420-480x8x6800	-	480	8	6800	50	420	10319
293	C60x420-480x8x6800	-	480	8	6800	60	420	11523
294	C70x420-480x8x6800	-	480	8	6800	70	420	11703

Nº	Name	B	D	t	L _e	f _{c'}	σ _{0.2}	P _n
295	C30x450-460x6x6600	-	460	6	6600	30	450	6980
296	C40x450-460x6x6600	-	460	6	6600	40	450	8130
297	C45x450-460x6x6600	-	460	6	6600	45	450	8618
298	C60x450-460x6x6600	-	460	6	6600	60	450	10334
299	C70x400-460x6x6600	-	460	6	6600	70	400	10862
300	C30x400-460x6x6600	-	460	6	6600	30	400	6667
301	C40x400-460x6x6600	-	460	6	6600	40	400	7771
302	C45x400-460x6x6600	-	460	6	6600	45	400	8333
303	C60x350-460x6x6600	-	460	6	6600	60	350	9637
304	C70x350-460x6x6600	-	460	6	6600	70	350	10647
305	C25x280-170x2.5x2600	-	170	2.5	2600	25	280	720
306	C30x280-170x2.5x2600	-	170	2.5	2600	30	280	768
307	C35x280-170x2.5x2600	-	170	2.5	2600	35	280	871
308	C40x280-170x2.5x2600	-	170	2.5	2600	40	280	928
309	C45x280-170x2.5x2600	-	170	2.5	2600	45	280	991
310	C25x250-170x2.5x2600	-	170	2.5	2600	25	250	689
311	C30x250-170x2.5x2600	-	170	2.5	2600	30	250	765
312	C35x250-170x2.5x2600	-	170	2.5	2600	35	250	837
313	C40x250-170x2.5x2600	-	170	2.5	2600	40	250	912
314	C45x250-170x2.5x2600	-	170	2.5	2600	45	250	982
315	C25x320-580x9x5800	-	580	9	5800	25	320	10557
316	C35x320-580x9x5800	-	580	9	5800	35	320	12595
317	C45x320-580x9x5800	-	580	9	5800	45	320	14486
318	C70x320-580x9x5800	-	580	9	5800	70	320	20049
319	C90x320-580x9x5800	-	580	9	5800	90	320	23431
320	C25x420-580x9x5800	-	580	9	5800	25	420	12110
321	C35x420-580x9x5800	-	580	9	5800	35	420	14123
322	C45x420-580x9x5800	-	580	9	5800	45	420	16154
323	C70x420-580x9x5800	-	580	9	5800	70	420	21461
324	C90x420-580x9x5800	-	580	9	5800	90	420	25379
325	C45x600-620x10x7200	-	620	10	7200	45	600	20790
326	C60x600-620x10x7200	-	620	10	7200	60	600	24102
327	C80x600-620x10x7200	-	620	10	7200	80	600	28498
328	C100x600-620x10x7200	-	620	10	7200	100	600	32527
329	C120x600-620x10x7200	-	620	10	7200	120	600	37061
330	C45x540-620x10x7200	-	620	10	7200	45	540	19882

Nº	Name	B	D	t	L _e	f' _c	σ _{0.2}	P _n
331	C60x540-620x10x7200	-	620	10	7200	60	540	23195
332	C80x540-620x10x7200	-	620	10	7200	80	540	27256
333	C100x540-620x10x7200	-	620	10	7200	100	540	31717
334	C120x540-620x10x7200	-	620	10	7200	120	540	35972
335	C25x250-520x5x4800	-	520	5	4800	25	250	6632
336	C35x250-520x5x4800	-	520	5	4800	35	250	8511
337	C40x250-520x5x4800	-	520	5	4800	40	250	9413
338	C45x250-520x5x4800	-	520	5	4800	45	250	10333
339	C70x250-520x5x4800	-	520	5	4800	70	250	14534
340	C25x320-520x5x4800	-	520	5	4800	25	320	7198
341	C35x320-520x5x4800	-	520	5	4800	35	320	9055
342	C40x320-520x5x4800	-	520	5	4800	40	320	9978
343	C45x320-520x5x4800	-	520	5	4800	45	320	10898
344	C70x320-520x5x4800	-	520	5	4800	70	320	13847
345	C25x280-230x3x3600	-	230	3	3600	25	280	1261
346	C35x280-230x3x3600	-	230	3	3600	35	280	1528
347	C40x280-230x3x3600	-	230	3	3600	40	280	1644
348	C45x280-230x3x3600	-	230	3	3600	45	280	1791
349	C50x280-230x3x3600	-	230	3	3600	50	280	1913
350	C25x380-230x3x3600	-	230	3	3600	25	380	1432
351	C35x380-230x3x3600	-	230	3	3600	35	380	1688
352	C40x380-230x3x3600	-	230	3	3600	40	380	1840
353	C45x380-230x3x3600	-	230	3	3600	45	380	1972
354	C50x380-230x3x3600	-	230	3	3600	50	380	2080
355	C25x380-330x5x4900	-	330	5	4900	25	380	3202
356	C45x380-330x5x4900	-	330	5	4900	45	380	4345
357	C60x380-330x5x4900	-	330	5	4900	60	380	5116
358	C70x380-330x5x4900	-	330	5	4900	70	380	5672
359	C90x380-330x5x4900	-	330	5	4900	90	380	6539
360	C25x420-330x5x4900	-	330	5	4900	25	420	3350
361	C45x420-330x5x4900	-	330	5	4900	45	420	4507
362	C60x420-330x5x4900	-	330	5	4900	60	420	5277
363	C70x420-330x5x4900	-	330	5	4900	70	420	5848
364	C90x420-330x5x4900	-	330	5	4900	90	420	6629
365	C25x540-360x7.8x6900	-	360	7.8	6900	25	540	4604
366	C45x540-360x7.8x6900	-	360	7.8	6900	45	540	5675

Nº	Name	B	D	t	L _e	f _{c'}	σ _{0.2}	P _n
367	C50x540-360x7.8x6900	-	360	7.8	6900	50	540	5795
368	C80x540-360x7.8x6900	-	360	7.8	6900	80	540	7374
369	C90x540-360x7.8x6900	-	360	7.8	6900	90	540	7719
370	C25x420-360x7.8x6900	-	360	7.8	6900	25	420	4162
371	C45x420-360x7.8x6900	-	360	7.8	6900	45	420	5242
372	C50x420-360x7.8x6900	-	360	7.8	6900	50	420	5479
373	C80x420-360x7.8x6900	-	360	7.8	6900	80	420	6862
374	C90x420-360x7.8x6900	-	360	7.8	6900	90	420	7199
375	C30x540-660x15x8600	-	660	15	8600	30	540	21248
376	C45x540-660x15x8600	-	660	15	8600	45	540	24941
377	C60x540-660x15x8600	-	660	15	8600	60	540	28546
378	C80x540-660x15x8600	-	660	15	8600	80	540	32604
379	C100x540-660x15x8600	-	660	15	8600	100	540	36153
380	C70x420-660x15x8600	-	660	15	8600	70	420	27555
381	C80x420-660x15x8600	-	660	15	8600	80	420	29570
382	C90x420-660x15x8600	-	660	15	8600	90	420	30265
383	C100x420-660x15x8600	-	660	15	8600	100	420	34066
384	C120x420-660x15x8600	-	660	15	8600	120	420	37636
385	C20x230-350x10x4000	-	350	10	4000	20	230	3650
386	C30x230-350x10x4000	-	350	10	4000	30	230	4328
387	C40x230-350x10x4000	-	350	10	4000	40	230	5008
388	C50x230-350x10x4000	-	350	10	4000	50	230	5672
389	C60x230-350x10x4000	-	350	10	4000	60	230	6367
390	C20x280-350x10x4000	-	350	10	4000	20	280	4167
391	C30x280-350x10x4000	-	350	10	4000	30	280	4834
392	C40x280-350x10x4000	-	350	10	4000	40	280	5479
393	C50x280-350x10x4000	-	350	10	4000	50	280	6125
394	C80x280-350x10x4000	-	350	10	4000	80	280	8139
395	C20x250-150x7x1800	-	150	7	1800	20	250	911
396	C25x250-150x7x1800	-	150	7	1800	25	250	967
397	C50x250-150x7x1800	-	150	7	1800	50	250	1234
398	C60x250-150x7x1800	-	150	7	1800	60	250	1327
399	C70x250-150x7x1800	-	150	7	1800	70	250	1446
400	C20x400-150x7x1800	-	150	7	1800	20	400	1306
401	C25x400-150x7x1800	-	150	7	1800	25	400	1363
402	C50x400-150x7x1800	-	150	7	1800	50	400	1600

Nº	Name	B	D	t	L _e	f _{c'}	σ _{0.2}	P _n
403	C60x400-150x7x1800	-	150	7	1800	60	400	1736
404	C70x400-150x7x1800	-	150	7	1800	70	400	1835
405	C20x280-400x5.7x6400	-	400	5.7	6400	20	280	3487
406	C30x280-400x5.7x6400	-	400	5.7	6400	30	280	4264
407	C40x280-400x5.7x6400	-	400	5.7	6400	40	280	5081
408	C50x280-400x5.7x6400	-	400	5.7	6400	50	280	5831
409	C60x280-400x5.7x6400	-	400	5.7	6400	60	280	6499
410	C30x600-400x5.7x6400	-	400	5.7	6400	30	600	5755
411	C40x600-400x5.7x6400	-	400	5.7	6400	40	600	6562
412	C50x600-400x5.7x6400	-	400	5.7	6400	50	600	7166
413	C60x600-400x5.7x6400	-	400	5.7	6400	60	600	8103
414	C90x600-400x5.7x6400	-	400	5.7	6400	90	600	10264
415	C30x350-180x3x3000	-	180	3	3000	30	350	1009
416	C35x350-180x3x3000	-	180	3	3000	35	350	1069
417	C40x350-180x3x3000	-	180	3	3000	40	350	1144
418	C50x350-180x3x3000	-	180	3	3000	50	350	1284
419	C35x400-180x3x3000	-	180	3	3000	35	400	1122
420	C30x580-220x3.5x4400	-	220	3.5	4400	30	580	1482
421	C40x580-220x3.5x4400	-	220	3.5	4400	40	580	1708
422	C60x580-220x3.5x4400	-	220	3.5	4400	60	580	2053
423	C80x580-220x3.5x4400	-	220	3.5	4400	80	580	2359
424	C100x580-220x3.5x4400	-	220	3.5	4400	100	580	2641
425	C20x200-180x10x4000	-	180	10	4000	20	200	963
426	C25x200-180x10x4000	-	180	10	4000	25	200	1004
427	C40x200-180x10x4000	-	180	10	4000	40	200	1136
428	C50x200-180x10x4000	-	180	10	4000	50	200	1207
429	C90x200-180x10x4000	-	180	10	4000	90	200	1303
430	C20x480-180x10x4000	-	180	10	4000	20	480	1671
431	C25x480-180x10x4000	-	180	10	4000	25	480	1720
432	C40x480-180x10x4000	-	180	10	4000	40	480	1860
433	C60x480-180x10x4000	-	180	10	4000	60	480	2032
434	C90x480-180x10x4000	-	180	10	4000	90	480	2229
435	C30x250-150x3x3500	-	150	3	3500	30	250	519
436	C35x250-150x3x3500	-	150	3	3500	35	250	552
437	C40x250-150x3x3500	-	150	3	3500	40	250	586
438	C50x250-150x3x3500	-	150	3	3500	50	250	646

Nº	Name	B	D	t	L _e	f _{c'}	σ _{0.2}	P _n
439	C30x350-150x3x3500	-	150	3	3500	30	350	585
440	C20x250-120x8x960	-	120	8	960	20	250	816
441	C25x250-120x8x960	-	120	8	960	25	250	854
442	C30x250-120x8x960	-	120	8	960	30	250	889
443	C40x250-120x8x960	-	120	8	960	40	250	952
444	C60x250-120x8x960	-	120	8	960	60	250	1102
445	C20x360-310x11x6820	-	310	11	6820	20	360	3176
446	C30x360-310x11x6820	-	310	11	6820	30	360	3572
447	C40x360-310x11x6820	-	310	11	6820	40	360	3824
448	C50x360-310x11x6820	-	310	11	6820	50	360	4162
449	C60x360-310x11x6820	-	310	11	6820	60	360	4394
450	C70x360-310x11x6820	-	310	11	6820	70	360	4632
451	C80x360-310x11x6820	-	310	11	6820	80	360	4839
452	C90x360-310x11x6820	-	310	11	6820	90	360	5030
453	C100x360-310x11x6820	-	310	11	6820	100	360	5216
454	C120x360-310x11x6820	-	310	11	6820	120	360	5547
455	C20x360-130x2.4x2400	-	130	2.4	2400	20	360	437
456	C40x360-130x2.4x2400	-	130	2.4	2400	40	360	585
457	C60x360-130x2.4x2400	-	130	2.4	2400	60	360	718
458	C80x360-130x2.4x2400	-	130	2.4	2400	80	360	827
459	C100x360-130x2.4x2400	-	130	2.4	2400	100	360	937
460	C20x470-130x2.4x2400	-	130	2.4	2400	20	470	494
461	C40x470-130x2.4x2400	-	130	2.4	2400	40	470	646
462	C60x470-130x2.4x2400	-	130	2.4	2400	60	470	765
463	C80x470-130x2.4x2400	-	130	2.4	2400	80	470	894
464	C100x470-130x2.4x2400	-	130	2.4	2400	100	470	1011
465	C25x200-120x3x3000	-	120	3	3000	25	200	286
466	C30x200-120x3x3000	-	120	3	3000	30	200	305
467	C35x200-120x3x3000	-	120	3	3000	35	200	323
468	C25x300-120x3x3000	-	120	3	3000	25	300	347
469	C30x300-120x3x3000	-	120	3	3000	30	300	366
470	C30x470-126x7x2630	-	126	7	2630	30	470	904
471	C40x470-126x7x2630	-	126	7	2630	40	470	954
472	C50x470-126x7x2630	-	126	7	2630	50	470	1003
473	C60x470-126x7x2630	-	126	7	2630	60	470	1048
474	C70x470-126x7x2630	-	126	7	2630	70	470	1088

Nº	Name	B	D	t	L _e	f _{c'}	σ _{0.2}	P _n
475	S25x300-300x10x5000	300	300	10	5000	25	300	4736
476	S30x300-300x10x5000	300	300	10	5000	30	300	5042
477	S35x300-300x10x5000	300	300	10	5000	35	300	5335
478	S40x300-300x10x5000	300	300	10	5000	40	300	5629
479	S50x300-300x10x5000	300	300	10	5000	50	300	6126
480	S30x400-300x10x5000	300	300	10	5000	30	400	5883
481	S35x400-300x10x5000	300	300	10	5000	35	400	6196
482	S40x400-300x10x5000	300	300	10	5000	40	400	6445
483	S50x400-300x10x5000	300	300	10	5000	50	400	7074
484	S60x400-300x10x5000	300	300	10	5000	60	400	7646
485	S35x500-300x10x5000	300	300	10	5000	35	500	6937
486	S40x500-300x10x5000	300	300	10	5000	40	500	7247
487	S50x500-300x10x5000	300	300	10	5000	50	500	7698
488	S60x500-300x10x5000	300	300	10	5000	60	500	8242
489	S70x500-300x10x5000	300	300	10	5000	70	500	8975
490	S40x600-300x10x5000	300	300	10	5000	40	600	7862
491	S50x600-300x10x5000	300	300	10	5000	50	600	8514
492	S60x600-300x10x5000	300	300	10	5000	60	600	9119
493	S70x600-300x10x5000	300	300	10	5000	70	600	9665
494	S90x600-300x10x5000	300	300	10	5000	90	600	10792
495	S30x200-400x12x3600	400	400	12	3600	30	200	7610
496	S40x200-400x12x3600	400	400	12	3600	40	200	8956
497	S50x200-400x12x3600	400	400	12	3600	50	200	10233
498	S60x200-400x12x3600	400	400	12	3600	60	200	11520
499	S70x200-400x12x3600	400	400	12	3600	70	200	12770
500	S30x250-400x12x3600	400	400	12	3600	30	250	8597
501	S40x250-400x12x3600	400	400	12	3600	40	250	9979
502	S50x250-400x12x3600	400	400	12	3600	50	250	11267
503	S60x250-400x12x3600	400	400	12	3600	60	250	12546
504	S70x250-400x12x3600	400	400	12	3600	70	250	13752
505	S50x320-400x12x3600	400	400	12	3600	50	320	12389
506	S60x320-400x12x3600	400	400	12	3600	60	320	13793
507	S70x320-400x12x3600	400	400	12	3600	70	320	15075
508	R50x360-250x400x2x2000	250	400	2	2000	50	360	5493
509	R60x360-250x400x2x2000	250	400	2	2000	60	360	6384
510	S50x560-400x12x3600	400	400	12	3600	50	560	15385

Nº	Name	B	D	t	L _e	f _{c'}	σ _{0.2}	P _n
511	S60x560-400x12x3600	400	400	12	3600	60	560	16482
512	S70x560-400x12x3600	400	400	12	3600	70	560	18838
513	R50x420-250x400x2x2000	250	400	2	2000	50	420	5560
514	R60x420-250x400x2x2000	250	400	2	2000	60	420	6439
515	S25x200-250x2x2500	250	250	2	2500	25	200	1780
516	S30x200-250x2x2500	250	250	2	2500	30	200	2041
517	S35x200-250x2x2500	250	250	2	2500	35	200	2337
518	S40x200-250x2x2500	250	250	2	2500	40	200	2612
519	S45x200-250x2x2500	250	250	2	2500	45	200	2877
520	S25x250-250x2x2500	250	250	2	2500	25	250	1860
521	S40x250-250x2x2500	250	250	2	2500	40	250	2709
522	S50x250-250x2x2500	250	250	2	2500	50	250	3263
523	S60x250-250x2x2500	250	250	2	2500	60	250	3707
524	S80x250-250x2x2500	250	250	2	2500	80	250	4832
525	S35x380-250x2x2500	250	250	2	2500	35	380	2594
526	S45x380-250x2x2500	250	250	2	2500	45	380	3177
527	S50x380-250x2x2500	250	250	2	2500	50	380	3424
528	S60x380-250x2x2500	250	250	2	2500	60	380	3992
529	S70x380-250x2x2500	250	250	2	2500	70	380	4528
530	S60x520-250x2x2500	250	250	2	2500	60	520	4242
531	S80x520-250x2x2500	250	250	2	2500	80	520	5286
532	S90x520-250x2x2500	250	250	2	2500	90	520	5874
533	S100x520-250x2x2500	250	250	2	2500	100	520	6393
534	S120x520-250x2x2500	250	250	2	2500	120	520	7473
535	S20x280-440x10x6000	440	440	10	6000	20	280	7601
536	S35x280-440x10x6000	440	440	10	6000	35	280	9764
537	S45x280-440x10x6000	440	440	10	6000	45	280	11153
538	S60x280-440x10x6000	440	440	10	6000	60	280	13259
539	S70x280-440x10x6000	440	440	10	6000	70	280	14587
540	S25x360-440x10x6000	440	440	10	6000	25	360	9601
541	S35x360-440x10x6000	440	440	10	6000	35	360	11108
542	S45x360-440x10x6000	440	440	10	6000	45	360	12563
543	S60x360-440x10x6000	440	440	10	6000	60	360	14728
544	S70x360-440x10x6000	440	440	10	6000	70	360	16112
545	S40x450-440x10x6000	440	440	10	6000	40	450	13006
546	S50x450-440x10x6000	440	440	10	6000	50	450	14565

Nº	Name	B	D	t	L _e	f _{c'}	σ _{0.2}	P _n
547	S60x450-440x10x6000	440	440	10	6000	60	450	15990
548	S80x450-440x10x6000	440	440	10	6000	80	450	18803
549	S100x450-440x10x6000	440	440	10	6000	100	450	21364
550	S50x560-440x10x6000	440	440	10	6000	50	560	15954
551	S60x560-440x10x6000	440	440	10	6000	60	560	17359
552	S80x560-440x10x6000	440	440	10	6000	80	560	19973
553	S100x560-440x10x6000	440	440	10	6000	100	560	23008
554	S120x560-440x10x6000	440	440	10	6000	120	560	25698
555	S25x200-330x6x6600	330	330	6	6600	25	200	3204
556	S35x200-330x6x6600	330	330	6	6600	35	200	3855
557	S40x200-330x6x6600	330	330	6	6600	40	200	4186
558	S60x200-330x6x6600	330	330	6	6600	60	200	5130
559	S80x200-330x6x6600	330	330	6	6600	80	200	6245
560	S25x280-330x6x6600	330	330	6	6600	25	280	3690
561	S35x280-330x6x6600	330	330	6	6600	35	280	4445
562	S40x280-330x6x6600	330	330	6	6600	40	280	4694
563	S70x280-330x6x6600	330	330	6	6600	70	280	6399
564	S100x280-330x6x6600	330	330	6	6600	100	280	7863
565	S25x380-330x6x6600	330	330	6	6600	25	380	4229
566	S50x380-330x6x6600	330	330	6	6600	50	380	5870
567	S70x380-330x6x6600	330	330	6	6600	70	380	7047
568	S90x380-330x6x6600	330	330	6	6600	90	380	8072
569	S100x380-330x6x6600	330	330	6	6600	100	380	8543
570	S30x500-330x6x6600	330	330	6	6600	30	500	5045
571	S50x500-330x6x6600	330	330	6	6600	50	500	6398
572	S70x500-330x6x6600	330	330	6	6600	70	500	7599
573	S90x500-330x6x6600	330	330	6	6600	90	500	8579
574	S120x500-330x6x6600	330	330	6	6600	120	500	10095
575	S20x200-250x2x2000	250	250	2	2000	20	200	1524
576	S30x200-250x2x2000	250	250	2	2000	30	200	2066
577	S40x200-250x2x2000	250	250	2	2000	40	200	2667
578	S50x200-250x2x2000	250	250	2	2000	50	200	3173
579	S60x200-250x2x2000	250	250	2	2000	60	200	3804
580	S20x300-250x2x2000	250	250	2	2000	20	300	1689
581	S30x300-250x2x2000	250	250	2	2000	30	300	2263
582	S40x300-250x2x2000	250	250	2	2000	40	300	2850

Nº	Name	B	D	t	L _e	f _{c'}	σ _{0.2}	P _n
583	S50x300-250x2x2000	250	250	2	2000	50	300	3415
584	S60x300-250x2x2000	250	250	2	2000	60	300	3984
585	S20x360-250x2x2000	250	250	2	2000	20	360	1783
586	S30x360-250x2x2000	250	250	2	2000	30	360	2360
587	S40x360-250x2x2000	250	250	2	2000	40	360	2904
588	S50x360-250x2x2000	250	250	2	2000	50	360	3509
589	S60x360-250x2x2000	250	250	2	2000	60	360	4085
590	S20x420-250x2x2000	250	250	2	2000	20	420	1865
591	S30x420-250x2x2000	250	250	2	2000	30	420	2443
592	S40x420-250x2x2000	250	250	2	2000	40	420	3039
593	S50x420-250x2x2000	250	250	2	2000	50	420	3525
594	S60x420-250x2x2000	250	250	2	2000	60	420	4191
595	R20x200-250x400x2x2000	250	400	2	2000	20	200	2820
596	R30x200-250x400x2x2000	250	400	2	2000	30	200	3276
597	R40x200-250x400x2x2000	250	400	2	2000	40	200	4180
598	R50x200-250x400x2x2000	250	400	2	2000	50	200	5044
599	R60x200-250x400x2x2000	250	400	2	2000	60	200	6037
600	R20x300-250x400x2x2000	250	400	2	2000	20	300	2562
601	R30x300-250x400x2x2000	250	400	2	2000	30	300	3482
602	R40x300-250x400x2x2000	250	400	2	2000	40	300	2820
603	R50x300-250x400x2x2000	250	400	2	2000	50	300	5328
604	R60x300-250x400x2x2000	250	400	2	2000	60	300	6208
605	R20x360-250x400x2x2000	250	400	2	2000	20	360	2670
606	R30x360-250x400x2x2000	250	400	2	2000	30	360	3614
607	R40x360-250x400x2x2000	250	400	2	2000	40	360	4557
608	S100x320-400x12x3600	400	400	12	3600	100	320	18882
609	S120x320-400x12x3600	400	400	12	3600	120	320	21406
610	R20x420-250x400x2x2000	250	400	2	2000	20	420	2772
611	R30x420-250x400x2x2000	250	400	2	2000	30	420	3724
612	R40x420-250x400x2x2000	250	400	2	2000	40	420	4650
613	S100x560-400x12x3600	400	400	12	3600	100	560	22855
614	S120x560-400x12x3600	400	400	12	3600	120	560	23303
615	R20x200-250x400x2x3000	250	400	2	3000	20	200	2239
616	R30x200-250x400x2x3000	250	400	2	3000	30	200	3061
617	R40x200-250x400x2x3000	250	400	2	3000	40	200	3920
618	R50x200-250x400x2x3000	250	400	2	3000	50	200	4755

Nº	Name	B	D	t	L _e	f _{c'}	σ _{0.2}	P _n
619	R60x200-250x400x2x3000	250	400	2	3000	60	200	5618
620	R20x300-250x400x2x3000	250	400	2	3000	20	300	2466
621	R30x300-250x400x2x3000	250	400	2	3000	30	300	3329
622	R40x300-250x400x2x3000	250	400	2	3000	40	300	4191
623	R50x300-250x400x2x3000	250	400	2	3000	50	300	5034
624	R60x300-250x400x2x3000	250	400	2	3000	60	300	5831
625	R20x360-250x400x2x3000	250	400	2	3000	20	360	2601
626	R30x360-250x400x2x3000	250	400	2	3000	30	360	3484
627	R40x360-250x400x2x3000	250	400	2	3000	40	360	4344
628	R50x360-250x400x2x3000	250	400	2	3000	50	360	5128
629	R60x360-250x400x2x3000	250	400	2	3000	60	360	6014
630	R20x420-250x400x2x3000	250	400	2	3000	20	420	2706
631	R30x420-250x400x2x3000	250	400	2	3000	30	420	3611
632	R40x420-250x400x2x3000	250	400	2	3000	40	420	4471
633	R50x420-250x400x2x3000	250	400	2	3000	50	420	5307
634	R60x420-250x400x2x3000	250	400	2	3000	60	420	6175
635	R30x200-180x220x3x2200	180	220	3	2200	30	200	1423
636	R40x200-180x220x3x2200	180	220	3	2200	40	200	1740
637	R50x200-180x220x3x2200	180	220	3	2200	50	200	2047
638	R60x200-180x220x3x2200	180	220	3	2200	60	200	2361
639	R70x200-180x220x3x2200	180	220	3	2200	70	200	2669
640	R30x280-180x220x3x2200	180	220	3	2200	30	280	1615
641	R40x280-180x220x3x2200	180	220	3	2200	40	280	1928
642	R50x280-180x220x3x2200	180	220	3	2200	50	280	2231
643	R60x280-180x220x3x2200	180	220	3	2200	60	280	2547
644	R70x280-180x220x3x2200	180	220	3	2200	70	280	2847
645	R30x350-180x220x3x2200	180	220	3	2200	30	350	1756
646	R40x350-180x220x3x2200	180	220	3	2200	40	350	2073
647	R50x350-180x220x3x2200	180	220	3	2200	50	350	2385
648	R60x350-180x220x3x2200	180	220	3	2200	60	350	2708
649	R70x350-180x220x3x2200	180	220	3	2200	70	350	3018
650	R30x420-180x220x3x2200	180	220	3	2200	30	420	1878
651	R40x420-180x220x3x2200	180	220	3	2200	40	420	2197
652	R50x420-180x220x3x2200	180	220	3	2200	50	420	2541
653	R60x420-180x220x3x2200	180	220	3	2200	60	420	2824
654	R70x420-180x220x3x2200	180	220	3	2200	70	420	3173

Nº	Name	B	D	t	L _e	f _{c'}	σ _{0.2}	P _n
655	R30x200-180x220x3x4000	180	220	3	4000	30	200	1179
656	R40x200-180x220x3x4000	180	220	3	4000	40	200	1374
657	R50x200-180x220x3x4000	180	220	3	4000	50	200	1550
658	R70x200-180x220x3x4000	180	220	3	4000	70	200	1890
659	R90x200-180x220x3x4000	180	220	3	4000	90	200	2197
660	R30x280-180x220x3x4000	180	220	3	4000	30	280	1353
661	R40x280-180x220x3x4000	180	220	3	4000	40	280	1563
662	R50x280-180x220x3x4000	180	220	3	4000	50	280	1751
663	R70x280-180x220x3x4000	180	220	3	4000	70	280	2086
664	R90x280-180x220x3x4000	180	220	3	4000	90	280	2393
665	R30x350-180x220x3x4000	180	220	3	4000	30	350	1415
666	R40x350-180x220x3x4000	180	220	3	4000	40	350	1682
667	R50x350-180x220x3x4000	180	220	3	4000	50	350	1884
668	R70x350-180x220x3x4000	180	220	3	4000	70	350	2241
669	R90x350-180x220x3x4000	180	220	3	4000	90	350	2552
670	R30x420-180x220x3x4000	180	220	3	4000	30	420	1535
671	R40x420-180x220x3x4000	180	220	3	4000	40	420	1755
672	R50x420-180x220x3x4000	180	220	3	4000	50	420	1973
673	R70x420-180x220x3x4000	180	220	3	4000	70	420	2340
674	R90x420-180x220x3x4000	180	220	3	4000	90	420	2249
675	C30x300-300x2x900	-	300	2	900	30	300	2690
676	C40x300-300x2x900	-	300	2	900	40	300	3347
677	C60x300-300x2x900	-	300	2	900	60	300	4702
678	C70x300-300x2x900	-	300	2	900	70	300	5409
679	C90x300-300x2x900	-	300	2	900	90	300	6737
680	C30x450-300x2x900	-	300	2	900	30	450	3041
681	C40x450-300x2x900	-	300	2	900	40	450	3693
682	C60x450-300x2x900	-	300	2	900	60	450	5017
683	C70x450-300x2x900	-	300	2	900	70	450	5696
684	C90x450-300x2x900	-	300	2	900	90	450	7077
685	C20x250-250x2x750	-	250	2	750	20	250	1413
686	C30x250-250x2x750	-	250	2	750	30	250	1852
687	C50x250-250x2x750	-	250	2	750	50	250	2765
688	C70x250-250x2x750	-	250	2	750	70	250	3730
689	C90x250-250x2x750	-	250	2	750	90	250	4650
690	C20x320-250x2x750	-	250	2	750	20	320	1565

Nº	Name	B	D	t	L _e	f _{c'}	σ _{0.2}	P _n
691	C30x320-250x2x750	-	250	2	750	30	320	1991
692	C50x320-250x2x750	-	250	2	750	50	320	2922
693	C70x320-250x2x750	-	250	2	750	70	320	3874
694	C90x320-250x2x750	-	250	2	750	90	320	4820
695	C20x280-400x10x1200	-	400	10	1200	20	280	7112
696	C40x280-400x10x1200	-	400	10	1200	40	280	9265
697	C60x280-400x10x1200	-	400	10	1200	60	280	10877
698	C80x280-400x10x1200	-	400	10	1200	80	280	13018
699	C100x280-400x10x1200	-	400	10	1200	100	280	15244
700	C20x520-400x10x1200	-	400	10	1200	20	520	10786
701	C40x520-400x10x1200	-	400	10	1200	40	520	13271
702	C60x520-400x10x1200	-	400	10	1200	60	520	15488
703	C80x520-400x10x1200	-	400	10	1200	80	520	17432
704	C100x520-400x10x1200	-	400	10	1200	100	520	19019
705	C20x250-360x10x1080	-	360	10	1080	20	250	8200
706	C40x250-360x10x1080	-	360	10	1080	40	250	10072
707	C60x250-360x10x1080	-	360	10	1080	60	250	11354
708	C80x250-360x10x1080	-	360	10	1080	80	250	12889
709	C100x250-360x10x1080	-	360	10	1080	100	250	14526
710	C20x500-360x10x1080	-	360	10	1080	20	500	9083
711	C40x500-360x10x1080	-	360	10	1080	40	500	11101
712	C60x500-360x10x1080	-	360	10	1080	60	500	12929
713	C80x500-360x10x1080	-	360	10	1080	80	500	14560
714	C100x500-360x10x1080	-	360	10	1080	100	500	15917
715	C30x360-500x10x1500	-	500	10	1500	30	360	13273
716	C50x360-500x10x1500	-	500	10	1500	50	360	16163
717	C70x360-500x10x1500	-	500	10	1500	70	360	19076
718	C90x360-500x10x1500	-	500	10	1500	90	360	22430
719	C120x360-500x10x1500	-	500	10	1500	120	360	27703
720	C30x420-500x10x1500	-	500	10	1500	30	420	14512
721	C50x420-500x10x1500	-	500	10	1500	50	420	17746
722	C70x420-500x10x1500	-	500	10	1500	70	420	20195
723	C90x420-500x10x1500	-	500	10	1500	90	420	23607
724	C120x420-500x10x1500	-	500	10	1500	120	420	28814
725	C20x200-150x1x450	-	150	1	450	20	200	450
726	C30x200-150x1x450	-	150	1	450	30	200	611

Nº	Name	B	D	t	L _e	f _{c'}	σ _{0.2}	P _n
727	C40x200-150x1x450	-	150	1	450	40	200	763
728	C50x200-150x1x450	-	150	1	450	50	200	927
729	C60x200-150x1x450	-	150	1	450	60	200	1133
730	C20x300-150x1x450	-	150	1	450	20	300	516
731	C30x300-150x1x450	-	150	1	450	30	300	673
732	C40x300-150x1x450	-	150	1	450	40	300	837
733	C50x300-150x1x450	-	150	1	450	50	300	1004
734	C60x300-150x1x450	-	150	1	450	60	300	1176
735	C20x250-280x3x840	-	280	3	840	20	250	2023
736	C30x250-280x3x840	-	280	3	840	30	250	2538
737	C40x250-280x3x840	-	280	3	840	40	250	3063
738	C50x250-280x3x840	-	280	3	840	50	250	3640
739	C60x250-280x3x840	-	280	3	840	60	250	4223
740	C20x360-280x3x840	-	280	3	840	20	360	2508
741	C30x360-280x3x840	-	280	3	840	30	360	2920
742	C40x360-280x3x840	-	280	3	840	40	360	3429
743	C50x360-280x3x840	-	280	3	840	50	360	4002
744	C60x360-280x3x840	-	280	3	840	60	360	4570
745	C20x200-120x4x360	-	120	4	360	20	200	615
746	C25x200-120x4x360	-	120	4	360	25	200	667
747	C30x200-120x4x360	-	120	4	360	30	200	716
748	C35x200-120x4x360	-	120	4	360	35	200	760
749	C40x200-120x4x360	-	120	4	360	40	200	801
750	C20x300-120x4x360	-	120	4	360	20	300	791
751	C25x300-120x4x360	-	120	4	360	25	300	846
752	C30x300-120x4x360	-	120	4	360	30	300	900
753	C35x300-120x4x360	-	120	4	360	35	300	951
754	C40x300-120x4x360	-	120	4	360	40	300	1002
755	C20x200-100x2x300	-	100	2	300	20	200	324
756	C25x200-100x2x300	-	100	2	300	25	200	352
757	C30x200-100x2x300	-	100	2	300	30	200	376
758	C35x200-100x2x300	-	100	2	300	35	200	401
759	C40x200-100x2x300	-	100	2	300	40	200	433
760	C20x300-100x2x300	-	100	2	300	20	300	409
761	C25x300-100x2x300	-	100	2	300	25	300	445
762	C30x300-100x2x300	-	100	2	300	30	300	478

Nº	Name	B	D	t	L _e	f _{c'}	σ _{0.2}	P _n
763	C35x300-100x2x300	-	100	2	300	35	300	507
764	C40x300-100x2x300	-	100	2	300	40	300	533
765	C30x320-200x6.6x600	-	200	6.6	600	30	320	2342
766	C40x320-200x6.6x600	-	200	6.6	600	40	320	2618
767	C50x320-200x6.6x600	-	200	6.6	600	50	320	2889
768	C60x320-200x6.6x600	-	200	6.6	600	60	320	3153
769	C70x320-200x6.6x600	-	200	6.6	600	70	320	3407
770	C30x450-200x6.6x600	-	200	6.6	600	30	450	2903
771	C40x450-200x6.6x600	-	200	6.6	600	40	450	3186
772	C50x450-200x6.6x600	-	200	6.6	600	50	450	3460
773	C60x450-200x6.6x600	-	200	6.6	600	60	450	3728
774	C70x450-200x6.6x600	-	200	6.6	600	70	450	4001
775	C30x280-200x8x600	-	200	8	600	30	280	2640
776	C40x280-200x8x600	-	200	8	600	40	280	2920
777	C50x280-200x8x600	-	200	8	600	50	280	3186
778	C60x280-200x8x600	-	200	8	600	60	280	3431
779	C70x280-200x8x600	-	200	8	600	70	280	3658
780	C30x450-200x8x600	-	200	8	600	30	450	3632
781	C40x450-200x8x600	-	200	8	600	40	450	3929
782	C50x450-200x8x600	-	200	8	600	50	450	4215
783	C60x450-200x8x600	-	200	8	600	60	450	4493
784	C70x450-200x8x600	-	200	8	600	70	450	4763
785	C30x320-288x3.6x860	-	288	3.6	860	30	320	3144
786	C40x320-288x3.6x860	-	288	3.6	860	40	320	3674
787	C50x320-288x3.6x860	-	288	3.6	860	50	320	4283
788	C60x320-288x3.6x860	-	288	3.6	860	60	320	4893
789	C70x320-288x3.6x860	-	288	3.6	860	70	320	5469
790	C30x500-288x3.6x860	-	288	3.6	860	30	500	4114
791	C40x500-288x3.6x860	-	288	3.6	860	40	500	4586
792	C50x500-288x3.6x860	-	288	3.6	860	50	500	5004
793	C60x500-288x3.6x860	-	288	3.6	860	60	500	5548
794	C70x500-288x3.6x860	-	288	3.6	860	70	500	6131
795	C20x250-150x2.4x450	-	150	2.4	450	20	250	732
796	C30x250-150x2.4x450	-	150	2.4	450	30	250	852
797	C40x250-150x2.4x450	-	150	2.4	450	40	250	989
798	C45x250-150x2.4x450	-	150	2.4	450	45	250	1073

Nº	Name	B	D	t	L _e	f _{c'}	σ _{0.2}	P _n
799	C50x250-150x2.4x450	-	150	2.4	450	50	250	1148
800	C20x360-150x2.4x450	-	150	2.4	450	20	360	905
801	C30x360-150x2.4x450	-	150	2.4	450	30	360	1058
802	C40x360-150x2.4x450	-	150	2.4	450	40	360	1177
803	C45x360-150x2.4x450	-	150	2.4	450	45	360	1237
804	C50x360-150x2.4x450	-	150	2.4	450	50	360	1298
805	C20x280-330x3.3x1000	-	330	3.3	1000	20	280	2869
806	C40x280-330x3.3x1000	-	330	3.3	1000	40	280	4350
807	C60x280-330x3.3x1000	-	330	3.3	1000	60	280	5936
808	C70x280-330x3.3x1000	-	330	3.3	1000	70	280	6805
809	C90x280-330x3.3x1000	-	330	3.3	1000	90	280	8310
810	C20x500-330x3.3x1000	-	330	3.3	1000	20	500	4066
811	C40x500-330x3.3x1000	-	330	3.3	1000	40	500	5304
812	C60x500-330x3.3x1000	-	330	3.3	1000	60	500	6800
813	C70x500-330x3.3x1000	-	330	3.3	1000	70	500	7543
814	C90x500-330x3.3x1000	-	330	3.3	1000	90	500	9149
815	C30x360-450x6x1500	-	450	6	1500	30	360	8569
816	C50x360-450x6x1500	-	450	6	1500	50	360	11015
817	C70x360-450x6x1500	-	450	6	1500	70	360	13907
818	C90x360-450x6x1500	-	450	6	1500	90	360	16850
819	C120x360-450x6x1500	-	450	6	1500	120	360	21380
820	C30x520-450x6x1500	-	450	6	1500	30	520	10661
821	C50x520-450x6x1500	-	450	6	1500	50	520	12963
822	C70x520-450x6x1500	-	450	6	1500	70	520	15455
823	C90x520-450x6x1500	-	450	6	1500	90	520	18353
824	C120x520-450x6x1500	-	450	6	1500	120	520	22754
825	S20x200-200x10x600	200	200	10	600	20	200	2665
826	S25x200-200x10x600	200	200	10	600	25	200	2751
827	S30x200-200x10x600	200	200	10	600	30	200	2828
828	S45x200-200x10x600	200	200	10	600	45	200	3253
829	S50x200-200x10x600	200	200	10	600	50	200	3339
830	S20x300-200x10x600	200	200	10	600	20	300	3733
831	S25x300-200x10x600	200	200	10	600	25	300	3843
832	S30x300-200x10x600	200	200	10	600	30	300	3944
833	S45x300-200x10x600	200	200	10	600	45	300	4198
834	S50x300-200x10x600	200	200	10	600	50	300	4319

Nº	Name	B	D	t	L _e	f _{c'}	σ _{0.2}	P _n
835	S20x400-200x10x600	200	200	10	600	20	400	4800
836	S30x400-200x10x600	200	200	10	600	30	400	5038
837	S40x400-200x10x600	200	200	10	600	40	400	5242
838	S50x400-200x10x600	200	200	10	600	50	400	5423
839	S60x400-200x10x600	200	200	10	600	60	400	5610
840	S20x500-200x10x600	200	200	10	600	20	500	5717
841	S30x500-200x10x600	200	200	10	600	30	500	5969
842	S40x500-200x10x600	200	200	10	600	40	500	6189
843	S50x500-200x10x600	200	200	10	600	50	500	6385
844	S60x500-200x10x600	200	200	10	600	60	500	6584
845	R20x200-160x240x6x600	160	240	6	600	20	200	1801
846	R25x200-160x240x6x600	160	240	6	600	25	200	1819
847	R30x200-160x240x6x600	160	240	6	600	30	200	2104
848	R45x200-160x240x6x600	160	240	6	600	45	200	2451
849	R50x200-160x240x6x600	160	240	6	600	50	200	2610
850	R20x300-160x240x6x600	160	240	6	600	20	300	2315
851	R25x300-160x240x6x600	160	240	6	600	25	300	2395
852	R30x300-160x240x6x600	160	240	6	600	30	300	2503
853	R45x300-160x240x6x600	160	240	6	600	45	300	2938
854	R50x300-160x240x6x600	160	240	6	600	50	300	3107
855	R20x400-160x240x6x600	160	240	6	600	20	400	2943
856	R30x400-160x240x6x600	160	240	6	600	30	400	3121
857	R40x400-160x240x6x600	160	240	6	600	40	400	3327
858	R50x400-160x240x6x600	160	240	6	600	50	400	3593
859	R60x400-160x240x6x600	160	240	6	600	60	400	3883
860	R20x500-160x240x6x600	160	240	6	600	20	500	3513
861	R30x500-160x240x6x600	160	240	6	600	30	500	3709
862	R40x500-160x240x6x600	160	240	6	600	40	500	3898
863	R50x500-160x240x6x600	160	240	6	600	50	500	4119
864	R60x500-160x240x6x600	160	240	6	600	60	500	4370
865	S20x250-150x4.8x450	150	150	4.8	450	20	250	1200
866	S25x250-150x4.8x450	150	150	4.8	450	25	250	1262
867	S30x250-150x4.8x450	150	150	4.8	450	30	250	1336
868	S40x250-150x4.8x450	150	150	4.8	450	40	250	1504
869	S50x250-150x4.8x450	150	150	4.8	450	50	250	1689
870	S20x400-150x4.8x450	150	150	4.8	450	20	400	1772

Nº	Name	B	D	t	L _e	f' _c	σ _{0.2}	P _n
871	S25x400-150x4.8x450	150	150	4.8	450	25	400	1829
872	S30x400-150x4.8x450	150	150	4.8	450	30	400	1880
873	S40x400-150x4.8x450	150	150	4.8	450	40	400	1999
874	S50x400-150x4.8x450	150	150	4.8	450	50	400	2161
875	R20x250-250x360x10x800	250	360	10	800	20	250	5022
876	R30x250-250x360x10x800	250	360	10	800	30	250	5527
877	R40x250-250x360x10x800	250	360	10	800	40	250	6171
878	R50x250-250x360x10x800	250	360	10	800	50	250	6930
879	R60x250-250x360x10x800	250	360	10	800	60	250	7589
880	R20x320-250x360x10x800	250	360	10	800	20	320	6170
881	R30x320-250x360x10x800	250	360	10	800	30	320	6548
882	R40x320-250x360x10x800	250	360	10	800	40	320	7180
883	R50x320-250x360x10x800	250	360	10	800	50	320	7647
884	R60x320-250x360x10x800	250	360	10	800	60	320	8399
885	R20x360-250x360x10x800	250	360	10	800	20	360	6804
886	R30x360-250x360x10x800	250	360	10	800	30	360	7208
887	R40x360-250x360x10x800	250	360	10	800	40	360	7680
888	R50x360-250x360x10x800	250	360	10	800	50	360	8335
889	R60x360-250x360x10x800	250	360	10	800	60	360	9035
890	R20x450-250x360x10x800	250	360	10	800	20	450	8235
891	R30x450-250x360x10x800	250	360	10	800	30	450	8690
892	R40x450-250x360x10x800	250	360	10	800	40	450	9077
893	R50x450-250x360x10x800	250	360	10	800	50	450	9749
894	R60x450-250x360x10x800	250	360	10	800	60	450	10191
895	S25x300-300x9x900	300	300	9	900	25	300	5467
896	S35x300-300x9x900	300	300	9	900	35	300	6093
897	S45x300-300x9x900	300	300	9	900	45	300	6821
898	S60x300-300x9x900	300	300	9	900	60	300	7942
899	S70x300-300x9x900	300	300	9	900	70	300	8709
900	S25x450-300x9x900	300	300	9	900	25	450	7626
901	S35x450-300x9x900	300	300	9	900	35	450	8028
902	S45x450-300x9x900	300	300	9	900	45	450	8539
903	S60x450-300x9x900	300	300	9	900	60	450	9715
904	S70x450-300x9x900	300	300	9	900	70	450	10401
905	C25x200-100x2x2400	-	100	2	2400	25	200	199
906	C30x200-100x2x2400	-	100	2	2400	30	200	213

Nº	Name	B	D	t	L _e	f' _c	σ _{0.2}	P _n
907	C35x200-100x2x2400	-	100	2	2400	35	200	226
908	C25x300-100x2x2400	-	100	2	2400	25	300	230
909	C30x300-100x2x2400	-	100	2	2400	30	300	246
910	C25x200-200x8x3600	-	200	8	3600	25	200	1234
911	C30x200-200x8x3600	-	200	8	3600	30	200	1250
912	C35x200-200x8x3600	-	200	8	3600	35	200	1311
913	C25x300-200x8x3600	-	200	8	3600	25	300	1544
914	C30x300-200x8x3600	-	200	8	3600	30	300	1637
915	C20x250-200x2x3600	-	200	2	3600	20	250	696
916	C30x250-200x2x3600	-	200	2	3600	30	250	890
917	C40x250-200x2x3600	-	200	2	3600	40	250	1068
918	C50x250-200x2x3600	-	200	2	3600	50	250	1236
919	C60x250-200x2x3600	-	200	2	3600	60	250	1393
920	C20x400-200x2x3600	-	200	2	3600	20	400	829
921	C30x400-200x2x3600	-	200	2	3600	30	400	1028
922	C40x400-200x2x3600	-	200	2	3600	40	400	1217
923	C50x400-200x2x3600	-	200	2	3600	50	400	1391
924	C60x400-200x2x3600	-	200	2	3600	60	400	1556
925	C30x300-100x2.6x1000	-	100	2.6	1000	30	300	411
926	C40x300-100x2.6x1000	-	100	2.6	1000	40	300	467
927	C45x300-100x2.6x1000	-	100	2.6	1000	45	300	493
928	C50x300-100x2.6x1000	-	100	2.6	1000	50	300	522
929	C55x300-100x2.6x1000	-	100	2.6	1000	55	300	550
930	C60x300-100x2.6x1000	-	100	2.6	1000	60	300	573
931	C30x280-120x3x1100	-	120	3	1100	30	280	576
932	C40x280-120x3x1100	-	120	3	1100	40	280	657
933	C45x280-120x3x1100	-	120	3	1100	45	280	693
934	C50x280-120x3x1100	-	120	3	1100	50	280	734
935	C55x280-120x3x1100	-	120	3	1100	55	280	776
936	C60x280-120x3x1100	-	120	3	1100	60	280	815
937	S30x300-150x8x500	150	150	8	500	30	300	2310
938	S40x300-150x8x500	150	150	8	500	40	300	2411
939	S50x300-150x8x500	150	150	8	500	50	300	2520
940	S30x350-150x8x500	150	150	8	500	30	350	2626
941	S40x350-150x8x500	150	150	8	500	40	350	2738
942	S50x350-150x8x500	150	150	8	500	50	350	2825

Nº	Name	B	D	t	L _e	f _{c'}	σ _{0.2}	P _n
943	S60x350-150x8x500	150	150	8	500	60	350	2938
944	S80x350-150x8x500	150	150	8	500	80	350	3276
945	S30x400-150x8x500	150	150	8	500	30	400	2900
946	S40x400-150x8x500	150	150	8	500	40	400	3037
947	S50x400-150x8x500	150	150	8	500	50	400	3108
948	S60x400-150x8x500	150	150	8	500	60	400	3204
949	S80x400-150x8x500	150	150	8	500	80	400	3305
950	S30x500-150x8x500	150	150	8	500	30	500	3409
951	S40x500-150x8x500	150	150	8	500	40	500	3534
952	S50x500-150x8x500	150	150	8	500	50	500	3646
953	S60x500-150x8x500	150	150	8	500	60	500	3762
954	S80x500-150x8x500	150	150	8	500	80	500	4011
955	R30x400-100x150x4x450	100	150	4	450	30	400	1253
956	R40x400-100x150x4x450	100	150	4	450	40	400	1336
957	R50x400-100x150x4x450	100	150	4	450	50	400	1435
958	R60x400-100x150x4x450	100	150	4	450	60	400	1544
959	R80x400-100x150x4x450	100	150	4	450	80	400	1792
960	R30x500-100x150x4x450	100	150	4	450	30	500	1490
961	R40x500-100x150x4x450	100	150	4	450	40	500	1566
962	R50x500-100x150x4x450	100	150	4	450	50	500	1656
963	R60x500-100x150x4x450	100	150	4	450	60	500	1751
964	R80x500-100x150x4x450	100	150	4	450	80	500	1974
965	R30x400-100x150x2x450	100	150	2	450	30	400	774
966	R40x400-100x150x2x450	100	150	2	450	40	400	898
967	R50x400-100x150x2x450	100	150	2	450	50	400	1040
968	R60x400-100x150x2x450	100	150	2	450	60	400	1190
969	R80x400-100x150x2x450	100	150	2	450	80	400	1483
970	R30x500-100x150x2x450	100	150	2	450	30	500	845
971	R40x500-100x150x2x450	100	150	2	450	40	500	986
972	R50x500-100x150x2x450	100	150	2	450	50	500	1117
973	R60x500-100x150x2x450	100	150	2	450	60	500	1257
974	R80x500-100x150x2x450	100	150	2	450	80	500	1551
975	R25x280-180x240x4x720	180	240	4	720	25	280	1885
976	R35x280-180x240x4x720	180	240	4	720	35	280	2268
977	R45x280-180x240x4x720	180	240	4	720	45	280	2658
978	R60x280-180x240x4x720	180	240	4	720	60	280	3264

Nº	Name	B	D	t	L _e	f _{c'}	σ _{0.2}	P _n
979	R70x280-180x240x4x720	180	240	4	720	70	280	3668
980	R25x350-180x240x4x720	180	240	4	720	25	350	2124
981	R35x350-180x240x4x720	180	240	4	720	35	350	2472
982	R45x350-180x240x4x720	180	240	4	720	45	350	2851
983	R60x350-180x240x4x720	180	240	4	720	60	350	3440
984	R70x350-180x240x4x720	180	240	4	720	70	350	3847
985	R30x420-180x240x4x720	180	240	4	720	30	420	2513
986	R40x420-180x240x4x720	180	240	4	720	40	420	2865
987	R50x420-180x240x4x720	180	240	4	720	50	420	3240
988	R60x420-180x240x4x720	180	240	4	720	60	420	3626
989	R80x420-180x240x4x720	180	240	4	720	80	420	4427
990	R30x500-180x240x4x720	180	240	4	720	30	500	2755
991	R40x500-180x240x4x720	180	240	4	720	40	500	3103
992	R50x500-180x240x4x720	180	240	4	720	50	500	3455
993	R60x500-180x240x4x720	180	240	4	720	60	500	3826
994	R80x500-180x240x4x720	180	240	4	720	80	500	4608
995	S25x280-360x8x1080	360	360	8	1080	25	280	6067
996	S35x280-360x8x1080	360	360	8	1080	35	280	7176
997	S45x280-360x8x1080	360	360	8	1080	45	280	8312
998	S60x280-360x8x1080	360	360	8	1080	60	280	10061
999	S70x280-360x8x1080	360	360	8	1080	70	280	11253
1000	S25x350-360x8x1080	360	360	8	1080	25	350	6936
1001	S35x350-360x8x1080	360	360	8	1080	35	350	7952
1002	S45x350-360x8x1080	360	360	8	1080	45	350	9016
1003	S60x350-360x8x1080	360	360	8	1080	60	350	10713
1004	S70x350-360x8x1080	360	360	8	1080	70	350	11881
1005	S30x420-360x8x1080	360	360	8	1080	30	420	8248
1006	S40x420-360x8x1080	360	360	8	1080	40	420	9207
1007	S50x420-360x8x1080	360	360	8	1080	50	420	10280
1008	S60x420-360x8x1080	360	360	8	1080	60	420	11403
1009	S80x420-360x8x1080	360	360	8	1080	80	420	13709
1010	S30x500-360x8x1080	360	360	8	1080	30	500	9282
1011	S40x500-360x8x1080	360	360	8	1080	40	500	10114
1012	S50x500-360x8x1080	360	360	8	1080	50	500	11092
1013	S60x500-360x8x1080	360	360	8	1080	60	500	12155
1014	S80x500-360x8x1080	360	360	8	1080	80	500	14406

Nº	Name	B	D	t	L _e	f _{c'}	σ _{0.2}	P _n
1015	S20x300-50x3x150	50	50	3	150	20	300	265
1016	S25x300-50x3x150	50	50	3	150	25	300	272
1017	S30x300-50x3x150	50	50	3	150	30	300	279
1018	S35x300-50x3x150	50	50	3	150	35	300	286
1019	S40x300-50x3x150	50	50	3	150	40	300	292
1020	S20x450-50x3x150	50	50	3	150	20	450	380
1021	S25x450-50x3x150	50	50	3	150	25	450	388
1022	S30x450-50x3x150	50	50	3	150	30	450	396
1023	S35x450-50x3x150	50	50	3	150	35	450	403
1024	S40x450-50x3x150	50	50	3	150	40	450	411
1025	S20x300-50x2x150	50	50	2	150	20	300	183
1026	S25x300-50x2x150	50	50	2	150	25	300	189
1027	S30x300-50x2x150	50	50	2	150	30	300	195
1028	S35x300-50x2x150	50	50	2	150	35	300	201
1029	S40x300-50x2x150	50	50	2	150	40	300	209
1030	S20x350-50x2x150	50	50	2	150	20	350	208
1031	S25x350-50x2x150	50	50	2	150	25	350	215
1032	S30x350-50x2x150	50	50	2	150	30	350	221
1033	S35x350-50x2x150	50	50	2	150	35	350	226
1034	S40x350-50x2x150	50	50	2	150	40	350	233
1035	C25x200-120x5x3000	-	120	5	3000	25	200	369
1036	C30x200-120x5x3000	-	120	5	3000	30	200	387
1037	C35x200-120x5x3000	-	120	5	3000	35	200	402
1038	C25x300-120x5x3000	-	120	5	3000	25	300	471
1039	C30x300-120x5x3000	-	120	5	3000	30	300	492
1040	C25x400-120x5x3000	-	120	5	3000	25	400	537
1041	C35x400-120x5x3000	-	120	5	3000	35	400	576
1042	C40x400-120x5x3000	-	120	5	3000	40	400	601
1043	C50x400-120x5x3000	-	120	5	3000	50	400	633
1044	C60x400-120x5x3000	-	120	5	3000	60	400	662
1045	S30x320-580x10x8800	580	580	10	8800	30	320	14393
1046	S40x320-580x10x8800	580	580	10	8800	40	320	16831
1047	S50x320-580x10x8800	580	580	10	8800	50	320	19132
1048	S60x320-580x10x8800	580	580	10	8800	60	320	21494
1049	S70x320-580x10x8800	580	580	10	8800	70	320	23519
1050	S30x500-580x10x8800	580	580	10	8800	30	500	17254

Nº	Name	B	D	t	L _e	f' _c	σ _{0.2}	P _n
1051	S40x500-580x10x8800	580	580	10	8800	40	500	19731
1052	S50x500-580x10x8800	580	580	10	8800	50	500	22300
1053	S60x500-580x10x8800	580	580	10	8800	60	500	24663
1054	S70x500-580x10x8800	580	580	10	8800	70	500	27015
1055	S30x320-360x10x4700	360	360	10	4700	30	320	14393
1056	S40x320-360x10x4700	360	360	10	4700	40	320	16831
1057	S50x320-360x10x4700	360	360	10	4700	50	320	19132
1058	S60x320-360x10x4700	360	360	10	4700	60	320	21494
1059	S70x320-360x10x4700	360	360	10	4700	70	320	23519
1060	S30x500-360x10x4700	360	360	10	4700	30	500	17254
1061	S40x500-360x10x4700	360	360	10	4700	40	500	19731
1062	S50x500-360x10x4700	360	360	10	4700	50	500	22300
1063	S60x500-360x10x4700	360	360	10	4700	60	500	24663
1064	S70x500-360x10x4700	360	360	10	4700	70	500	27015
1065	R20x250-260x420x6x3000	260	420	6	3000	20	250	3754
1066	R30x250-260x420x6x3000	260	420	6	3000	30	250	4587
1067	R40x250-260x420x6x3000	260	420	6	3000	40	250	5536
1068	R50x250-260x420x6x3000	260	420	6	3000	50	250	6427
1069	R60x250-260x420x6x3000	260	420	6	3000	60	250	7236
1070	R25x320-260x420x6x3000	260	420	6	3000	25	320	4650
1071	R35x320-260x420x6x3000	260	420	6	3000	35	320	5607
1072	R45x320-260x420x6x3000	260	420	6	3000	45	320	6430
1073	R60x320-260x420x6x3000	260	420	6	3000	60	320	7612
1074	R70x320-260x420x6x3000	260	420	6	3000	70	320	8450
1075	R25x400-260x420x6x3000	260	420	6	3000	25	400	5236
1076	R40x400-260x420x6x3000	260	420	6	3000	40	400	6590
1077	R50x400-260x420x6x3000	260	420	6	3000	50	400	7495
1078	R60x400-260x420x6x3000	260	420	6	3000	60	400	8387
1079	R70x400-260x420x6x3000	260	420	6	3000	70	400	9219
1080	R25x540-260x420x6x3000	260	420	6	3000	25	540	6154
1081	R35x540-260x420x6x3000	260	420	6	3000	35	540	7011
1082	R45x540-260x420x6x3000	260	420	6	3000	45	540	7821
1083	R60x540-260x420x6x3000	260	420	6	3000	60	540	9062
1084	R70x540-260x420x6x3000	260	420	6	3000	70	540	10100
1085	S20x320-300x10x4800	300	300	10	4800	20	320	4653
1086	S30x320-300x10x4800	300	300	10	4800	30	320	5291

Nº	Name	B	D	t	L _e	f _{c'}	σ _{0.2}	P _n
1087	S40x320-300x10x4800	300	300	10	4800	40	320	5841
1088	S50x320-300x10x4800	300	300	10	4800	50	320	6494
1089	S60x320-300x10x4800	300	300	10	4800	60	320	6928
1090	S20x450-300x10x4800	300	300	10	4800	20	450	5779
1091	S30x450-300x10x4800	300	300	10	4800	30	450	6410
1092	S40x450-300x10x4800	300	300	10	4800	40	450	7009
1093	S50x450-300x10x4800	300	300	10	4800	50	450	7454
1094	S60x450-300x10x4800	300	300	10	4800	60	450	7957
1095	S30x500-300x10x4800	300	300	10	4800	30	500	6820
1096	S40x500-300x10x4800	300	300	10	4800	40	500	7378
1097	S50x500-300x10x4800	300	300	10	4800	50	500	7974
1098	S60x500-300x10x4800	300	300	10	4800	60	500	8586
1099	S70x500-300x10x4800	300	300	10	4800	70	500	8920
1100	S40x600-300x10x4800	300	300	10	4800	40	600	8318
1101	S50x600-300x10x4800	300	300	10	4800	50	600	8810
1102	S60x600-300x10x4800	300	300	10	4800	60	600	9347
1103	S70x600-300x10x4800	300	300	10	4800	70	600	9926
1104	S80x600-300x10x4800	300	300	10	4800	80	600	10492
1105	C20x280-50x1.2x150	-	50	1.2	150	20	280	110
1106	C30x280-50x1.2x150	-	50	1.2	150	30	280	128
1107	C40x280-50x1.2x150	-	50	1.2	150	40	280	143
1108	C20x320-50x1.2x150	-	50	1.2	150	20	320	119
1109	C30x320-50x1.2x150	-	50	1.2	150	30	320	138
1110	C40x320-50x1.2x150	-	50	1.2	150	40	320	154
1111	C20x280-50x1.6x150	-	50	1.6	150	20	280	130
1112	C30x280-50x1.6x150	-	50	1.6	150	30	280	149
1113	C40x280-50x1.6x150	-	50	1.6	150	40	280	166
1114	C20x320-50x1.6x150	-	50	1.6	150	20	320	142
1115	C30x320-50x1.6x150	-	50	1.6	150	30	320	161
1116	C40x320-50x1.6x150	-	50	1.6	150	40	320	179
1117	C25x250-310x10x930	-	310	10	930	25	250	5032
1118	C35x250-310x10x930	-	310	10	930	35	250	5705
1119	C45x250-310x10x930	-	310	10	930	45	250	6305
1120	C50x250-310x10x930	-	310	10	930	50	250	6578
1121	C25x560-310x10x930	-	310	10	930	25	560	8631
1122	C35x560-310x10x930	-	310	10	930	35	560	9389

Nº	Name	B	D	t	L _e	f _{c'}	σ _{0.2}	P _n
1123	C45x560-310x10x930	-	310	10	930	45	560	10114
1124	C50x560-310x10x930	-	310	10	930	50	560	10470
1125	C20x400-310x10x930	-	310	10	930	20	400	6399
1126	C30x400-310x10x930	-	310	10	930	30	400	7159
1127	C40x400-310x10x930	-	310	10	930	40	400	7870
1128	C50x500-125x1.5x375	-	125	1.5	375	50	500	931



จุฬาลงกรณ์มหาวิทยาลัย
CHULALONGKORN UNIVERSITY

APPENDIX B STANDARD SPECIFICATIONS PREDICTED COLUMN STRENGTHS

This section listed head-to-head predictions of both standard specifications discussed in section 3.5.of total 1128 columns data. Note that the numbering order is arranged from left to right, top to bottom.

Nº	P _{act}	P _{EC4}	P _{AISC}	Nº	P _{act}	P _{EC4}	P _{AISC}
1	534	400	572	2	687	498	720
3	836	671	866	4	1410	852	1080
5	1488	957	1224	6	1559	1071	1320
7	699	587	495	8	901	728	630
9	1133	854	749	10	1593	1227	787
11	1648	1375	927	12	1674	1506	1052
13	6134	5572	3866	14	7076	6181	4194
15	8088	6982	4636	16	5601	5806	4089
17	6848	6409	4410	18	8230	7203	4846
19	6171	5983	4257	20	7193	6581	4574
21	8432	7371	5005	22	10190	8807	6942
23	11032	12667	7904	24	12926	14379	8870
25	10304	9249	7362	26	10260	13098	8314
27	13499	14799	9269	28	10533	9489	7590
29	13240	13332	8536	30	13265	15026	9485
31	1293	1383	1198	32	1332	1499	1308
33	1625	2075	1382	34	1672	2301	1504
35	1498	1006	1556	36	1559	1106	1683
37	1985	1371	1746	38	2068	1576	2006
39	1708	1831	1325	40	1423	1620	1294
41	823	936	734	42	923	612	857
43	667	683	488	44	1137	823	689
45	1680	1211	1013	46	2181	1648	1377
47	109	140	89	48	132	158	107
49	136	173	108	50	165	190	124
51	424	461	305	52	477	537	378
53	675	431	401	54	746	552	516
55	809	549	544	56	897	724	710
57	1384	925	920	58	1536	1236	1216
59	239	131	167	60	271	151	192
61	361	219	279	62	394	238	302
63	711	439	559	64	754	519	660
65	1350	781	994	66	1448	855	1088
67	1049	597	847	68	1142	789	1091
69	1801	1027	1308	70	1962	1204	1533

Nº	P _{act}	P _{EC4}	P _{AISC}	Nº	P _{act}	P _{EC4}	P _{AISC}
71	525	556	537	72	504	515	497
73	481	487	470	74	498	493	470
75	429	468	446	76	424	440	418
77	737	691	659	78	670	639	607
79	639	601	570	80	575	634	601
81	555	585	555	82	540	551	523
83	2923	3236	2361	84	3164	2193	2792
85	791	924	898	86	842	968	949
87	889	1009	999	88	929	1047	1047
89	967	1081	1093	90	897	1048	961
91	1107	1273	1171	92	1278	1465	1365
93	1451	1629	1543	94	1612	1768	1708
95	1000	1092	1019	96	1036	1127	1056
97	1112	1163	1094	98	1212	1304	1243
99	1281	1376	1317	100	1033	1108	1042
101	1168	1211	1158	102	1387	1299	1267
103	1098	917	1114	104	1254	1000	1224
105	875	987	897	106	1033	1137	1049
107	1178	1263	1188	108	983	830	970
109	1150	950	1113	110	1421	1127	1364
111	1183	942	1108	112	1398	1027	1191
113	1547	1100	1292	114	1685	1162	1387
115	6136	5208	5884	116	7496	6544	7113
117	8841	7827	8315	118	9884	9074	9493
119	6812	5355	5932	120	2372	2537	2395
121	2620	2765	2641	122	2864	2968	2875
123	2585	2162	2583	124	2827	3017	2929
125	3082	3500	3301	126	3471	3942	3723
127	4228	4740	4520	128	4575	5097	4898
129	3355	3750	3540	130	3732	4174	3951
131	4531	4937	4730	132	4879	5278	5099
133	4388	4773	4558	134	5152	5448	5293
135	11366	11776	11379	136	12735	13384	12795
137	14104	14875	14189	138	15425	16338	15563
139	14715	15172	14511	140	16030	16627	15878
141	19644	20281	19355	142	20748	21638	20656
143	22303	22967	21940	144	23464	24268	23208
145	9417	10037	9555	146	10757	11551	10957
147	12057	13026	12332	148	13418	14465	13680
149	11033	11575	11015	150	12416	13047	12385
151	13775	14482	13728	152	16082	15880	15045
153	13931	14494	13762	154	17827	18564	17631
155	6434	7224	6767	156	7344	8223	7717

Nº	P _{act}	P _{EC4}	P _{AISC}	Nº	P _{act}	P _{EC4}	P _{AISC}
157	8297	9149	8626	158	9028	10004	9498
159	7428	8133	7634	160	8414	9058	8541
161	9324	9911	9410	162	10096	10695	10244
163	9189	8079	9305	164	12560	10635	12451
165	20299	21269	20247	166	22789	24019	22804
167	25393	26703	25313	168	27784	29322	27776
169	24428	25356	24077	170	29348	30588	28996
171	33996	35553	33746	172	33970	27627	30197
173	35623	32380	34900	174	44882	40893	43867
175	4763	4158	4577	176	5535	4849	5222
177	6933	6218	6492	178	5297	4239	4159
179	6006	4927	4645	180	10196	8938	7496
181	6448	4995	4980	182	6060	4342	4658
183	8066	6393	6095	184	10854	9019	7968
185	22564	19831	22345	186	24225	21298	23969
187	26401	22667	25554	188	27999	23942	27101
189	33366	26069	31205	190	24427	20023	23641
191	26430	21414	25226	192	29212	22729	26733
193	31302	23870	28112	194	34698	25916	30789
195	18738	15715	17294	196	20499	17310	18793
197	22277	18859	20271	198	24017	20361	21729
199	21569	17498	17099	200	25113	20501	19439
201	28510	23314	21735	202	24309	19174	19047
203	26090	20630	20203	204	29594	23397	22482
205	2333	2540	2419	206	2822	3119	2937
207	3579	3931	3687	208	4530	4955	4645
209	4219	3185	4105	210	4706	3684	4575
211	5388	4389	5257	212	7342	6018	6967
213	2982	3349	3156	214	3782	4150	3897
215	3683	4474	4187	216	4362	5231	4909
217	5147	6227	5916	218	5648	6218	5910
219	5982	6502	6219	220	5985	6768	6519
221	6489	7019	6811	222	7802	7881	7902
223	8330	8241	8406	224	9270	8851	9342
225	11048	8061	10538	226	12402	9465	11801
227	18314	14942	17124	228	21065	16947	19332
229	13314	9717	11841	230	19396	15033	16103
231	20732	16030	17009	232	21778	16965	17902
233	24619	18663	19651	234	9722	10685	9992
235	1276	1399	1302	236	1390	1538	1429
237	1521	1673	1553	238	1768	1931	1792
239	1879	2054	1908	240	1486	1611	1496
241	1603	1743	1618	242	1724	1872	1738

Nº	P _{act}	P _{EC4}	P _{AISC}	Nº	P _{act}	P _{EC4}	P _{AISC}
243	1947	2117	1969	244	2193	2346	2192
245	2879	3032	2869	246	3176	3371	3168
247	3438	3693	3463	248	3742	4010	3754
249	4046	4322	4041	250	3299	3538	3325
251	3642	3857	3617	252	3937	4171	3905
253	4237	4481	4190	254	5692	5957	5563
255	4996	5185	4911	256	6076	6321	5994
257	6658	6899	6528	258	7162	7489	7056
259	8776	9194	8612	260	6324	5156	6111
261	6862	5743	6642	262	7409	6312	7168
263	7825	6868	7689	264	11796	10560	11214
265	1861	1909	1787	266	2126	2169	2033
267	2387	2428	2275	268	2644	2688	2515
269	2902	2951	2751	270	2298	1773	2041
271	2543	2037	2254	272	2660	2297	2465
273	3052	2549	2674	274	3289	2797	2881
275	13076	10367	12771	276	12044	11754	14172
277	15541	12397	14852	278	17011	13589	16177
279	19994	15632	18690	280	11325	9974	11232
281	12840	11478	12721	282	15148	13493	14849
283	17970	15760	17507	284	20629	17622	19986
285	7247	7852	7323	286	8162	9150	8516
287	9627	10383	9667	288	10632	11550	10780
289	11883	12651	11856	290	8234	6932	8147
291	9418	8146	9306	292	10319	9275	10424
293	11523	10321	11506	294	11703	11286	12553
295	6980	5560	6547	296	8130	6650	7522
297	8618	7160	7996	298	10334	8550	9369
299	10862	9378	10479	300	6667	5497	6506
301	7771	6604	7560	302	8333	7122	8070
303	9637	8530	9306	304	10647	9388	10255
305	720	797	737	306	768	879	812
307	871	958	884	308	928	1035	955
309	991	1109	1025	310	689	766	710
311	765	850	785	312	837	930	858
313	912	1008	930	314	982	1083	1000
315	10557	10749	10237	316	12595	12898	12286
317	14486	15136	14298	318	20049	20436	19177
319	23431	24462	22943	320	12110	9323	11600
321	14123	11566	13620	322	16154	13692	15604
323	21461	18759	20420	324	25379	22577	24141
325	20790	16043	18073	326	24102	19163	20548
327	28498	23002	23759	328	32527	26478	26879

Nº	P _{act}	P _{EC4}	P _{AISC}	Nº	P _{act}	P _{EC4}	P _{AISC}
329	37061	29610	29914	330	19882	15840	18671
331	23195	18998	21592	332	27256	22892	25355
333	31717	26428	28983	334	35972	29620	32488
335	6632	5767	6417	336	8511	7581	8125
337	9413	8489	8966	338	10333	9388	9798
339	14534	13685	13846	340	7198	5877	6722
341	9055	7688	8350	342	9978	8595	9152
343	10898	9489	9946	344	13847	13756	13819
345	1261	1147	1273	346	1528	1426	1537
347	1644	1555	1663	348	1791	1677	1787
349	1913	1792	1907	350	1432	1183	1413
351	1688	1450	1668	352	1840	1573	1790
353	1972	1688	1909	354	2080	1797	2026
355	3202	2706	3197	356	4345	3818	4268
357	5116	4530	5016	358	5672	4950	5491
359	6539	5675	6392	360	3350	2746	3334
361	4507	3840	4392	362	5277	4537	5131
363	5848	4947	5601	364	6629	5653	6492
365	4604	3899	4780	366	5675	4660	5711
367	5795	4817	5927	368	7374	5565	7107
369	7719	5761	7461	370	4162	4563	4288
371	5242	5476	5282	372	5479	5670	5513
373	6862	6613	6774	374	7199	6861	7151
375	21248	18024	21281	376	24941	21476	24594
377	28546	24692	27791	378	32604	28614	31895
379	36153	32127	35834	380	27555	29053	27515
381	29570	31174	29605	382	30265	33208	31651
383	34066	35158	33656	384	37636	38803	37549
385	3650	3961	3812	386	4328	4692	4528
387	5008	5452	5231	388	5672	6225	5922
389	6367	6952	6603	390	4167	4401	4272
391	4834	5146	4979	392	5479	5932	5674
393	6125	6676	6357	394	8139	8785	8345
395	911	1005	985	396	967	1067	1045
397	1234	1398	1341	398	1327	1521	1457
399	1446	1643	1571	400	1306	1424	1375
401	1363	1485	1433	402	1600	1786	1716
403	1736	1903	1827	404	1835	2018	1936
405	3487	3844	3551	406	4264	4740	4362
407	5081	5570	5129	408	5831	6333	5857
409	6499	7030	6549	410	5755	4304	5156
411	6562	4977	5711	412	7166	5568	6246
413	8103	6086	6764	414	10264	7309	8229

Nº	P _{act}	P _{EC4}	P _{AISC}	Nº	P _{act}	P _{EC4}	P _{AISC}
415	1009	1078	998	416	1069	1157	1073
417	1144	1232	1145	418	1284	1373	1285
419	1122	976	1121	420	1482	1157	1475
421	1708	1281	1617	422	2053	1470	1877
423	2359	1612	2110	424	2641	1725	2319
425	963	1224	1164	426	1004	1290	1228
427	1136	1472	1409	428	1207	1581	1523
429	1303	1926	1932	430	1671	1892	1886
431	1720	1926	1933	432	1860	2018	2065
433	2032	2122	2225	434	2229	2246	2439
435	519	589	557	436	552	622	595
437	586	651	631	438	646	703	698
439	585	635	611	440	816	921	836
441	854	956	874	442	889	991	912
443	952	1062	988	444	1102	1205	1138
445	3176	3685	3548	446	3572	3983	3893
447	3824	4243	4217	448	4162	4472	4522
449	4394	4672	4811	450	4632	4850	5085
451	4839	5007	5344	452	5030	5148	5591
453	5216	5275	5825	454	5547	5495	6258
455	437	487	451	456	585	632	594
457	718	746	721	458	827	834	835
459	937	905	937	460	494	413	509
461	646	539	644	462	765	631	765
463	894	700	872	464	1011	755	970
465	286	349	330	466	305	372	355
467	323	392	379	468	347	390	377
469	366	408	399	470	904	1022	1013
471	954	1058	1060	472	1003	1091	1106
473	1048	1121	1149	474	1088	1148	1190
475	4736	3500	4528	476	5042	3688	4796
477	5335	3872	5060	478	5629	4051	5322
479	6126	4393	5838	480	5883	4307	5649
481	6196	4474	5905	482	6445	4636	6157
483	7074	4944	6655	484	7646	5232	7142
485	6937	5012	6699	486	7247	5157	6944
487	7698	5432	7425	488	8242	5688	7897
489	8975	5925	8005	490	7862	5615	7215
491	8514	5859	7691	492	9119	6085	8158
493	9665	6295	8616	494	10792	6668	9506
495	7610	5583	7102	496	8956	6458	8236
497	10233	7323	9363	498	11520	8180	10482
499	12770	9027	11358	500	8597	6263	7973

Nº	P _{act}	P _{EC4}	P _{AISC}	Nº	P _{act}	P _{EC4}	P _{AISC}
501	9979	7130	9100	502	11267	7989	10220
503	12546	8839	11334	504	13752	9680	12112
505	12389	8912	11410	506	13793	9753	12515
507	15075	10585	13143	508	5493	5315	3388
509	6384	6308	4021	510	15385	11996	14327
511	16482	12806	15414	512	18838	13608	16495
513	5560	5330	3388	514	6439	6322	4021
515	1780	1085	1248	516	2041	1264	1444
517	2337	1441	1638	518	2612	1614	1831
519	2877	1785	2023	520	1860	1100	1248
521	2709	1627	1831	522	3263	1965	2213
523	3707	2292	2590	524	4832	2914	4002
525	2594	1484	1638	526	3177	1824	2023
527	3424	1990	2213	528	3992	2314	2590
529	4528	2626	3666	530	4242	2335	2590
531	5286	2943	4175	532	5874	3231	4599
533	6393	3507	5018	534	7473	4028	5842
535	7601	5643	7198	536	9764	7094	9130
537	11153	8020	10388	538	13259	9345	12233
539	14587	10184	13024	540	9601	7016	8982
541	11108	7945	10241	542	12563	8840	11476
543	14728	10117	13290	544	16112	10924	13885
545	13006	8092	12063	546	14565	8920	13265
547	15990	9705	14447	548	18803	11152	15967
549	21364	12437	18237	550	15954	9283	13536
551	17359	10022	14713	552	19973	11373	17014
553	23008	12562	19247	554	25698	13604	21419
555	3204	2402	3129	556	3855	2811	3750
557	4186	2995	4050	558	5130	3602	5179
559	6245	4046	6116	560	3690	2373	3552
561	4445	2726	4149	562	4694	2880	4437
563	6399	3569	5873	564	7863	4006	7305
565	4229	2468	4044	566	5870	3140	5421
567	7047	3502	6178	568	8072	3774	7121
569	8543	3888	7566	570	5045	2678	4821
571	6398	3119	5837	572	7599	3435	6507
573	8579	3678	7417	574	10095	3963	8658
575	1524	922	1065	576	2066	1298	1469
577	2667	1667	1869	578	3173	2030	2265
579	3804	2386	2659	580	1689	953	1065
581	2263	1328	1469	582	2850	1695	1869
583	3415	2056	2265	584	3984	2410	2659
585	1783	970	1065	586	2360	1344	1469

Nº	P _{act}	P _{EC4}	P _{AISC}	Nº	P _{act}	P _{EC4}	P _{AISC}
587	2904	1710	1869	588	3509	2070	2265
589	4085	2423	2659	590	1865	985	1065
591	2443	1358	1469	592	3039	1724	1869
593	3525	2083	2265	594	4191	2436	2659
595	2820	2236	1452	596	3276	3256	2104
597	4180	4266	2749	598	5044	5268	3388
599	6037	6263	4021	600	2562	2269	1452
601	3482	3288	2104	602	2820	4298	2749
603	5328	5299	3388	604	6208	6292	4021
605	2670	2287	1452	606	3614	3305	2104
607	4557	4314	2749	608	18882	13031	16412
609	21406	14620	18563	610	2772	2303	1452
611	3724	3321	2104	612	4650	4330	2749
613	22855	15962	19703	614	23303	17489	21815
615	2239	2183	1413	616	3061	3163	2029
617	3920	4124	2630	618	4755	5070	3218
619	5618	6000	3794	620	2466	2215	1413
621	3329	3192	2029	622	4191	4152	2630
623	5034	5095	3218	624	5831	6023	3794
625	2601	2231	1413	626	3484	3208	2029
627	4344	4167	2630	628	5128	5109	3218
629	6014	6036	3794	630	2706	2246	1413
631	3611	3223	2029	632	4471	4181	2630
633	5307	5122	3218	634	6175	6049	3794
635	1423	1141	1325	636	1740	1412	1602
637	2047	1677	1874	638	2361	1935	2141
639	2669	2187	2341	640	1615	1195	1458
641	1928	1463	1722	642	2231	1724	1982
643	2547	1978	2238	644	2847	2226	2451
645	1756	1236	1521	646	2073	1501	1759
647	2385	1760	1993	648	2708	2011	2224
649	3018	2256	2541	650	1878	1273	1534
651	2197	1536	1760	652	2541	1792	1983
653	2824	2041	2203	654	3173	2283	2625
655	1179	978	1125	656	1374	1157	1326
657	1550	1309	1514	658	1890	1549	1821
659	2197	1726	2129	660	1353	1002	1216
661	1563	1166	1404	662	1751	1305	1580
663	2086	1522	1881	664	2393	1683	2181
665	1415	1017	1258	666	1682	1172	1426
667	1884	1301	1586	668	2241	1504	1929
669	2552	1656	2221	670	1535	1030	1267
671	1755	1176	1427	672	1973	1298	1580

Nº	P _{act}	P _{EC4}	P _{AISC}	Nº	P _{act}	P _{EC4}	P _{AISC}
673	2340	1490	1972	674	2249	1634	2258
675	2690	2407	1990	676	3347	3096	2472
677	4702	4472	3435	678	5409	5160	3917
679	6737	6536	4880	680	3041	2491	2199
681	3693	3179	2681	682	5017	4555	3644
683	5696	5244	4126	684	7077	6620	5089
685	1413	1255	1287	686	1852	1730	1735
687	2765	2681	2633	688	3730	3631	3530
689	4650	4582	4427	690	1565	1299	1161
691	1991	1775	1493	692	2922	2725	2159
693	3874	3676	2824	694	4820	4626	3490
695	7112	8731	5585	696	9265	10999	7740
697	10877	13268	9895	698	13018	15536	12050
699	15244	17804	14205	700	10786	14271	8526
701	13271	16539	10681	702	15488	18807	12836
703	17432	21076	14990	704	19019	23344	17145
705	8200	6967	4474	706	10072	8783	6199
707	11354	10599	7924	708	12889	12414	9649
709	14526	14230	11374	710	9083	12118	7223
711	11101	13934	8948	712	12929	15750	10673
713	14560	17566	12398	714	15917	19381	14123
715	13273	15969	10699	716	16163	19588	14137
717	19076	23207	17575	718	22430	26826	21013
719	27703	32255	26171	720	14512	17726	11623
721	17746	21345	15061	722	20195	24964	18499
723	23607	28583	21937	724	28814	34012	27094
725	450	413	420	726	611	585	584
727	763	757	747	728	927	929	911
729	1133	1101	1074	730	516	430	377
731	673	602	498	732	837	774	618
733	1004	946	738	734	1176	1118	859
735	2023	1834	1773	736	2538	2424	2333
737	3063	3014	2893	738	3640	3603	3453
739	4223	4193	4014	740	2508	1986	2000
741	2920	2576	2531	742	3429	3165	3061
743	4002	3755	3591	744	4570	4345	4122
745	615	738	479	746	667	787	526
747	716	836	572	748	760	885	619
749	801	935	666	750	791	1008	624
751	846	1057	671	752	900	1106	718
753	951	1156	765	754	1002	1205	812
755	324	379	261	756	352	415	295
757	376	451	329	758	401	488	364

Nº	P _{act}	P _{EC4}	P _{AISC}	Nº	P _{act}	P _{EC4}	P _{AISC}
759	433	524	398	760	409	496	322
761	445	532	357	762	478	568	391
763	507	605	425	764	533	641	460
765	2342	3203	2064	766	2618	3477	2325
767	2889	3751	2585	768	3153	4025	2845
769	3407	4299	3106	770	2903	4170	2586
771	3186	4444	2846	772	3460	4718	3106
773	3728	4992	3367	774	4001	5266	3627
775	2640	3270	2109	776	2920	3536	2362
777	3186	3802	2614	778	3431	4068	2867
779	3658	4334	3119	780	3632	4772	2929
781	3929	5037	3182	782	4215	5303	3435
783	4493	5569	3687	784	4763	5835	3940
785	3144	2916	2794	786	3674	3535	3383
787	4283	4154	3971	788	4893	4774	4559
789	5469	5393	5147	790	4114	3224	2898
791	4586	3843	3332	792	5004	4463	3765
793	5548	5082	4199	794	6131	5701	4632
795	732	864	593	796	852	1030	750
797	989	1196	907	798	1073	1278	986
799	1148	1361	1065	800	905	809	715
801	1058	975	873	802	1177	1140	1030
803	1237	1223	1109	804	1298	1306	1187
805	2869	2498	2509	806	4350	4141	4070
807	5936	5784	5630	808	6805	6606	6411
809	8310	8248	7972	810	4066	2826	2759
811	5304	4469	3909	812	6800	6111	5059
813	7543	6933	5634	814	9149	8576	6784
815	8569	7629	7307	816	11015	10643	10170
817	13907	13656	13033	818	16850	16669	15896
819	21380	21190	20190	820	10661	8362	7509
821	12963	11375	9619	822	15455	14389	11728
823	18353	17402	13838	824	22754	21922	17002
825	2665	1626	2071	826	2751	1735	2209
827	2828	1843	2346	828	3253	2167	2759
829	3339	2275	2897	830	3733	2223	2831
831	3843	2331	2969	832	3944	2440	3106
833	4198	2764	3519	834	4319	2872	3657
835	4800	2820	3591	836	5038	3037	3866
837	5242	3253	4142	838	5423	3469	4417
839	5610	3685	4692	840	5717	3417	4351
841	5969	3633	4626	842	6189	3850	4902
843	6385	4066	5177	844	6584	4282	5452

Nº	P _{act}	P _{EC4}	P _{AISC}	Nº	P _{act}	P _{EC4}	P _{AISC}
845	1801	1576	1505	846	1819	1750	1648
847	2104	1923	1792	848	2451	2444	2222
849	2610	2617	2365	850	2315	2017	1970
851	2395	2191	2114	852	2503	2364	2257
853	2938	2885	2688	854	3107	3058	2831
855	2943	2458	2436	856	3121	2805	2723
857	3327	3152	3010	858	3593	3500	3297
859	3883	3847	3583	860	3513	2479	2902
861	3709	2827	3188	862	3898	3174	3475
863	4119	3521	3762	864	4370	3868	4049
865	1200	811	1032	866	1262	876	1116
867	1336	942	1200	868	1504	1074	1367
869	1689	1205	1535	870	1772	1139	1450
871	1829	1205	1534	872	1880	1271	1618
873	1999	1402	1785	874	2161	1534	1953
875	5022	4292	4279	876	5527	5064	4944
877	6171	5836	5609	878	6930	6608	6274
879	7589	7379	6938	880	6170	5062	5105
881	6548	5834	5770	882	7180	6606	6435
883	7647	7377	7100	884	8399	8149	7764
885	6804	5502	5577	886	7208	6274	6242
887	7680	7045	6907	888	8335	7817	7572
889	9035	8589	8236	890	8235	6491	6639
891	8690	7263	7304	892	9077	8035	7969
893	9749	8807	8634	894	10191	9578	9298
895	5467	3796	4833	896	6093	4326	5509
897	6821	4857	6185	898	7942	5654	7199
899	8709	6185	7607	900	7626	5030	6404
901	8028	5561	7080	902	8539	6092	7756
903	9715	6888	8770	904	10401	7419	8954
905	199	226	211	906	213	243	229
907	226	258	246	908	230	251	238
909	246	265	254	910	1234	1436	1367
911	1250	1537	1462	912	1311	1636	1555
913	1544	1782	1698	914	1637	1873	1787
915	696	630	700	916	890	821	883
917	1068	980	1050	918	1236	1111	1204
919	1393	1220	1347	920	829	650	720
921	1028	828	859	922	1217	974	991
923	1391	1094	1116	924	1556	1194	1234
925	411	426	410	926	467	487	469
927	493	517	498	928	522	549	527
929	550	581	556	930	573	613	585

Nº	P _{act}	P _{EC4}	P _{AISC}	Nº	P _{act}	P _{EC4}	P _{AISC}
931	576	596	566	932	657	684	654
933	693	728	697	934	734	772	740
935	776	817	783	936	815	861	825
937	2310	1430	1821	938	2411	1550	1974
939	2520	1670	2126	940	2626	1609	2048
941	2738	1729	2201	942	2825	1848	2354
943	2938	1968	2506	944	3276	2208	2738
945	2900	1787	2275	946	3037	1907	2428
947	3108	2027	2581	948	3204	2147	2733
949	3305	2387	2949	950	3409	2144	2730
951	3534	2264	2883	952	3646	2384	3035
953	3762	2504	3188	954	4011	2743	3367
955	1253	1138	1108	956	1336	1272	1219
957	1435	1407	1330	958	1544	1542	1441
959	1792	1811	1576	960	1490	1321	1301
961	1566	1456	1412	962	1656	1590	1523
963	1751	1725	1634	964	1974	1994	1735
965	774	622	646	966	898	764	744
967	1040	907	842	968	1190	1049	940
969	1483	1334	1253	970	845	649	646
971	986	791	744	972	1117	933	842
973	1257	1076	940	974	1551	1360	1314
975	1885	1505	1771	976	2268	1864	2110
977	2658	2223	2449	978	3264	2762	2958
979	3668	3121	3152	980	2124	1594	2000
981	2472	1953	2338	982	2851	2313	2677
983	3440	2852	3184	984	3847	3211	3325
985	2513	1855	2371	986	2865	2214	2700
987	3240	2574	3029	988	3626	2933	3358
989	4427	3651	3831	990	2755	1940	2570
991	3103	2299	2877	992	3455	2658	3185
993	3826	3018	3492	994	4608	3736	4015
995	6067	4452	5669	996	7176	5242	6674
997	8312	6032	7680	998	10061	7217	9189
999	11253	8007	9832	1000	6936	5071	6457
1001	7952	5861	7463	1002	9016	6651	8469
1003	10713	7836	9978	1004	11881	8626	10476
1005	8248	5292	7748	1006	9207	6082	8754
1007	10280	6872	9760	1008	11403	7662	10766
1009	13709	9242	12111	1010	9282	5635	8650
1011	10114	6425	9655	1012	11092	7215	10661
1013	12155	8005	11667	1014	14406	9585	12813
1015	265	159	202	1016	272	165	210

Nº	P _{act}	P _{EC4}	P _{AISC}	Nº	P _{act}	P _{EC4}	P _{AISC}
1017	279	172	219	1018	286	178	227
1019	292	185	235	1020	380	225	287
1021	388	232	295	1022	396	238	303
1023	403	245	311	1024	411	251	320
1025	183	119	151	1026	189	126	160
1027	195	133	169	1028	201	140	178
1029	209	147	187	1030	208	134	170
1031	215	141	179	1032	221	148	188
1033	226	155	197	1034	233	162	206
1035	369	454	435	1036	387	478	461
1037	402	499	486	1038	471	528	519
1039	492	545	542	1040	537	577	585
1041	576	603	624	1042	601	614	642
1043	633	635	677	1044	662	653	709
1045	14393	8906	13422	1046	16831	10374	15531
1047	19132	11729	17585	1048	21494	12972	19588
1049	23519	14108	20738	1050	17254	9613	16083
1051	19731	10944	17998	1052	22300	12156	19867
1053	24663	13254	21694	1054	27015	14246	22739
1055	14393	5302	6805	1056	16831	5928	7647
1057	19132	6536	8478	1058	21494	7126	9298
1059	23519	7698	9767	1060	17254	6867	8846
1061	19731	7449	9659	1062	22300	8012	10461
1063	24663	8555	11252	1064	27015	9080	11402
1065	3754	3477	3528	1066	4587	4531	4305
1067	5536	5573	5071	1068	6427	6603	5825
1069	7236	7622	6569	1070	4650	4199	4329
1071	5607	5242	5060	1072	6430	6272	5781
1073	7612	7797	6845	1074	8450	8799	7357
1075	5236	4394	4686	1076	6590	5946	5653
1077	7495	6966	6288	1078	8387	7974	6917
1079	9219	8971	7718	1080	6154	4692	4980
1081	7011	5723	5735	1082	7821	6741	6480
1083	9062	8247	7579	1084	10100	9236	8299
1085	4653	3484	4481	1086	5291	3873	5025
1087	5841	4244	5558	1088	6494	4597	6081
1089	6928	4931	6594	1090	5779	4335	5617
1091	6410	4686	6141	1092	7009	5017	6652
1093	7454	5329	7154	1094	7957	5623	7646
1095	6820	4972	6548	1096	7378	5288	7053
1097	7974	5585	7547	1098	8586	5863	8032
1099	8920	6124	8139	1100	8318	5785	7334
1101	8810	6053	7823	1102	9347	6303	8303

Nº	P _{act}	P _{EC4}	P _{AISC}	Nº	P _{act}	P _{EC4}	P _{AISC}
1103	9926	6536	8775	1104	10492	6754	9239
1105	110	133	85	1106	128	151	102
1107	143	168	119	1108	119	147	93
1109	138	165	110	1110	154	182	126
1111	130	161	101	1112	149	178	117
1113	166	195	133	1114	142	179	111
1115	161	196	127	1116	179	214	143
1117	5032	6029	3925	1118	5705	6689	4552
1119	6305	7350	5180	1120	6578	7680	5494
1121	8631	11456	6847	1122	9389	12117	7474
1123	10114	12777	8102	1124	10470	13108	8415
1125	6399	8325	5025	1126	7159	8985	5652
1127	7870	9646	6280	1128	931	823	696



จุฬาลงกรณ์มหาวิทยาลัย
CHULALONGKORN UNIVERSITY

REFERENCES



- [1] Fernando, D., Teng, J., Quach, W., & De Waal, L. (2020). Full-range stress-strain model for stainless steel alloys. *Journal of Constructional Steel Research*, 173, 106266.
- [2] Tao, Z., Wang, Z.-B., & Yu, Q. (2013). Finite element modelling of concrete-filled steel stub columns under axial compression. *Journal of Constructional Steel Research*, 89, 121-131.
- [3] Lam, D., & Gardner, L. (2008). Structural design of stainless steel concrete filled columns. *Journal of Constructional Steel Research*, 64(11), 1275-1282.
- [4] Peng, D., Lu, Y., Xuan, W., & Yu-hang, Z. (2019). Experimental studies on the behavior and capacity of concrete filled stainless steel tube short columns. *工程力学*, 36(S1), 298-305.
- [5] Liao, F.-Y., Hou, C., Zhang, W.-J., & Ren, J. (2019). Experimental investigation on sea sand concrete-filled stainless steel tubular stub columns. *Journal of Constructional Steel Research*, 155, 46-61.
- [6] Tam, V. W., Wang, Z.-B., & Tao, Z. (2014). Behaviour of recycled aggregate concrete filled stainless steel stub columns. *Materials and structures*, 47, 293-310.
- [7] Yang, Y.-F., & Ma, G.-L. (2013). Experimental behaviour of recycled aggregate concrete filled stainless steel tube stub columns and beams. *Thin-Walled Structures*, 66, 62-75.
- [8] Ellobody, E., & Ghazy, M. F. (2012). Experimental investigation of eccentrically loaded fibre reinforced concrete-filled stainless steel tubular columns. *Journal of Constructional Steel Research*, 76, 167-176.
- [9] Guo, L., Liu, Y., Fu, F., & Huang, H. (2019). Behavior of axially loaded circular stainless steel tube confined concrete stub columns. *Thin-Walled Structures*, 139, 66-76.
- [10] Uy, B., Tao, Z., & Han, L.-H. (2011). Behaviour of short and slender concrete-filled stainless steel tubular columns. *Journal of Constructional Steel Research*, 67(3), 360-378.
- [11] He, A., Su, A., Liang, Y., & Zhao, O. (2021). Experimental and numerical investigations of circular recycled aggregate concrete-filled stainless steel tube columns. *Journal of Constructional Steel Research*, 179, 106566.
- [12] Han, L.-H., Xu, C.-Y., & Hou, C. (2022). Axial compression and bond behaviour of recycled aggregate concrete-filled stainless steel tubular stub columns. *Engineering Structures*, 262, 114306.
- [13] Dai, P., Yang, L., Wang, J., & Zhou, Y. (2020). Compressive strength of concrete-filled stainless steel tube stub columns. *Engineering Structures*, 205, 110106.
- [14] Yu, C., Fengxia, L., & Jiang, W. (2013). Experimental study on axial compressive behavior of concrete-filled thermoforming stainless steel tubular stub columns. *Journal of Building Structures*, 34(2), 106.

- [15] Li, Y., Zhao, X., Singh, R. R., & Al-Saadi, S. (2016). Tests on seawater and sea sand concrete-filled CFRP, BFRP and stainless steel tubular stub columns. *Thin-Walled Structures*, 108, 163-184.
- [16] Li, Y., Zhao, X. L., Raman, R. S., & Yu, X. (2018). Axial compression tests on seawater and sea sand concrete-filled double-skin stainless steel circular tubes. *Engineering Structures*, 176, 426-438.
- [17] Tao, Z., Song, T.-Y., Uy, B., & Han, L.-H. (2016). Bond behavior in concrete-filled steel tubes. *Journal of Constructional Steel Research*, 120, 81-93.
- [18] Naser, M., Thai, S., & Thai, H.-T. (2021). Evaluating structural response of concrete-filled steel tubular columns through machine learning. *Journal of Building Engineering*, 34, 101888.
- [19] Truong, V.-H., Pham, H.-A., Van, T. H., & Tangaramvong, S. (2022). Evaluation of machine learning models for load-carrying capacity assessment of semi-rigid steel structures. *Engineering Structures*, 273, 115001.
- [20] Xu, Y., Zheng, B., & Zhang, M. (2021). Capacity prediction of cold-formed stainless steel tubular columns using machine learning methods. *Journal of Constructional Steel Research*, 182, 106682.
- [21] Nguyen, T.-A., Trinh, S. H., Nguyen, M. H., & Ly, H.-B. (2023). Novel ensemble approach to predict the ultimate axial load of CFST columns with different cross-sections. *Structures*,
- [22] Tran, V. L., Ahmed, M., & Gohari, S. (2023). Prediction of the ultimate axial load of circular concrete-filled stainless steel tubular columns using machine learning approaches. *Structural Concrete*.
- [23] Samani, A. K., & Attard, M. M. (2012). A stress-strain model for uniaxial and confined concrete under compression. *Engineering Structures*, 41, 335-349.
- [24] Han, L.-H., Xu, C.-Y., & Tao, Z. (2019). Performance of concrete filled stainless steel tubular (CFSST) columns and joints: Summary of recent research. *Journal of Constructional Steel Research*, 152, 117-131.
- [25] Tao, Z., Uy, B., Liao, F.-Y., & Han, L.-H. (2011). Nonlinear analysis of concrete-filled square stainless steel stub columns under axial compression. *Journal of Constructional Steel Research*, 67(11), 1719-1732.
- [26] Arrayago, I., Real, E., & Gardner, L. (2015). Description of stress-strain curves for stainless steel alloys. *Materials & Design*, 87, 540-552.
- [27] Liu, X., Zheng, S., Xu, Z., Wang, S., & Yuan, B. (2022). Size effect of square concrete-filled stainless steel tubular short columns under axial compression. *Structures*,
- [28] Cruise, R., & Gardner, L. (2008). Residual stress analysis of structural stainless steel sections. *Journal of Constructional Steel Research*, 64(3), 352-366.

- [29] Committee, A. C. I. A. (2019). Building Code Requirements for Structural Concrete ACI 318-19 and Commentary 318R-19. *American Concrete Institute ACI Committee: Farmington Hills, MI, USA.*
- [30] Hafezolghorani, M., Hejazi, F., Vaghei, R., Jaafar, M. S. B., & Karimzade, K. (2017). Simplified damage plasticity model for concrete. *Structural Engineering International*, 27(1), 68-78.
- [31] Hassanein, M., Elchalakani, M., & Patel, V. (2017). Overall buckling behaviour of circular concrete-filled dual steel tubular columns with stainless steel external tubes. *Thin-Walled Structures*, 115, 336-348.
- [32] Committee, A. (2022). Specification for structural steel buildings (ANSI/AISC 360-22).
- [33] Azad, S. K., & Uy, B. (2020). Effect of concrete infill on local buckling capacity of circular tubes. *Journal of Constructional Steel Research*, 165, 105899.
- [34] Wang, J. (2020). An intuitive tutorial to Gaussian processes regression. *arXiv preprint arXiv:2009.10862*.
- [35] CEN. (2004). Eurocode 4 EN 1994-1-1: 2004. Design of composite steel and concrete structures. Part 1-1: General rules and rules for buildings. In: European Committee for Normalization Brussels
- [36] Standardization, E. C. f. (2005). Eurocode 2: design of concrete structures-part 1-1: general rules and rules for buildings. *British Standard Institution, London.*
- [37] Standardization, E. C. f. (2006). EN 1993-1-5: 2006, Eurocode 3-Design of steel structures-Part 1-5: Plated structural elements.

VITA

NAME	Ly Ith
DATE OF BIRTH	06 October 1997
PLACE OF BIRTH	Takeo Province, Cambodia
INSTITUTIONS ATTENDED	The author, Ly Ith, completed his bachelor's degree in civil engineering from Norton University in 2021. Later in early 2022, he pursued his master's degree in civil engineering at Chulalongkorn University under the supervision of Associate Professor Dr. Sawekchai Tangaramvong with the support of Chulalongkorn University's Graduate Scholarship Programme for ASEAN or Non-ASEAN Countries.
HOME ADDRESS	Phnom Penh, Cambodia

